Projet d'étude d'un Régulateur MPPT pour éoliennes en injection directe

Autheur : Association P'TIWATT

avec Philippe de Craene dcphilippe@yahoo.fr
et Dominique Boucherie ptiwatt@mailoo.org

Date : septembre – octobre 2018

Version 0.1

Un régulateur est un dispositif qui adapte l'énergie disponible d'un générateur d'électricité – un panneau photovoltaïque ou une éolienne – à une charge – une batterie ou un onduleur, un injecteur –

Il existe une multitude de régulateurs, mais peu sont spécifiques aux éoliennes domestiques, encore moins sont MPPT, et quand ils le sont c'est pour charger une batterie. Or dans notre cas nous ne voulons pas de batterie, mais injecter directement la puissance disponible sur le réseau électrique. En outre plusieurs questions sont posées et restent sans réponse quant au mode de fonctionnement de ces régulateurs, que nous allons passer en revu ci-dessous. Enfin ces appareils sont forts chers, alors qu'une fabrication artisanale s'avère aussi efficace et à moins de 30€.

Ce document décrit comment réaliser cet appareil en 3 étapes :

1- Réalisation d'une sécurité contre l'absence de charge en électronique analogique auto-alimentée,
2- Réalisation d'un banc de mesure des tensions et courants avec les données sauvegardées sur carte SD,
3- Réalisation d'un régulateur MPPT.

A noter : la réalisation de ce programme a demandé plusieurs dizaines d'heures de développement, apprendre à utiliser l'Arduino, comprendre son comportement, en cramer deux… apprendre son langage, faire des tests sur différents composants, tester différents algorithmes, et imaginer tous les tests possibles pour fiabiliser au maximum l'appareil. Toute contribution en vue de l'amélioration de l'appareil est la bienvenue ! Il vous est juste demandé de conserver mon nom et mon email dans l'entête du programme, et bien sûr de partager avec moi cette amélioration. Merci.

Table des matières

Introduction à la régulation MPPT

Nous n'allons pas revenir en détail sur la théorie ou l'avantage de faire appel au MPPT, tout est très bien expliqué en Annexe A.

Quand nous sommes en possession d'une éolienne, parfois elle tourne vite, parfois elle tourne peu, et parfois pas du tout. ET tout cela en un temps très court, bien plus court que le nuage qui va gêner le soleil qui éclaire le panneau photovoltaïque. Donc on imagine qu'il faut un appareil de course pour courir et adapter le ratio courant/tension afin d'obtenir la meilleure puissance possible avec ce qui est disponible. Et en effet en lisant des articles sur les algorithmes MPPT, on tombe sur des équations incroyables.

De plus, avec notre éolienne on nous fait presque peur du risque d'emballement de celle-ci en cas de tempête ou bien en cas de déconnection de la charge : l'absence de courant supprime la force qui résiste à la rotation des pales, d'où risque d'emballement. Ce phénomène peut se produire notamment lorsqu'il se met à y avoir du vent, le temps que l'onduleur-injecteur se mette en état de fonctionnement – soit plusieurs secondes, jusqu'à 5s pour le Winmaster 500 de MasterVolt – l'éolienne n'est pas chargée. Il faut donc un dispositif de détection d'une tension au-delà d'une valeur qui connecte une résistance de puissance au moins équivalente à la puissance de l'éolienne. Ce dispositif est spécifique à l'éolienne et n'existe pas pour le photovoltaïque, ce qui limite à priori drastiquement le choix d'un régulateur.

Nous verrons par la suite que nous pouvons aisément mettre en place cette sécurité, et un montage pratique sera proposé à cette fin, pour peu que l'on soit en possessions d'une « dump load resistor »

Bref, chez les professionnels, que nous est-il proposé comme régulateur éolien ?

Il y a le régulateur Tristar de Morningstar, normalement prévu pour le photovoltaïque mais adaptable à l'éolien. Seulement voilà il n'est pas MPPT. Ça veut dire quoi ? Ça veut dire que si la tension disponible au niveau du générateur est inférieure à la tension de service de la charge, il n'y a pas transfert de charge. Cette (faible) puissance est perdue.

Il y a les régulateurs pour la navigation de plaisance.

Il y a les régulateurs, souvent hybrides PV/éolien, disponibles sur le marché chinois – qui est le premier marché mondial de l'éolien domestique.

Or ces régulateurs sont spécifiquement dédiés à la charge d'une batterie. Et sauf cas d'un site isolé il est désastreux au niveau du rendement de faire appel à une batterie.

De plus quand on s'aperçoit de la versatilité du vent, quelle est l'efficacité du régulateur s'il lui faut quelques centaines de millisecondes – ou plus ! - pour s'initialiser ?

Le MPPT existe depuis les années 80, mais il y a un tel voile de mystère que même Wikipédia https://fr.wikipedia.org/wiki/Maximum_power_point_tracker est d'une désolante pauvreté.

Il existe une bonne douzaine d'algorithmes de calcul, mais aucun n'indique le choix retenu.

Parfois lorsqu'on a accès à quelques informations la surprise peut être incroyable. Par exemple avec le montage ci-dessous tout à fait paradoxal : si la tension de batterie est supérieure à la tension de PV, il ne se passe rien, l'énergie est perdue ! A quoi sert le MPPT ?

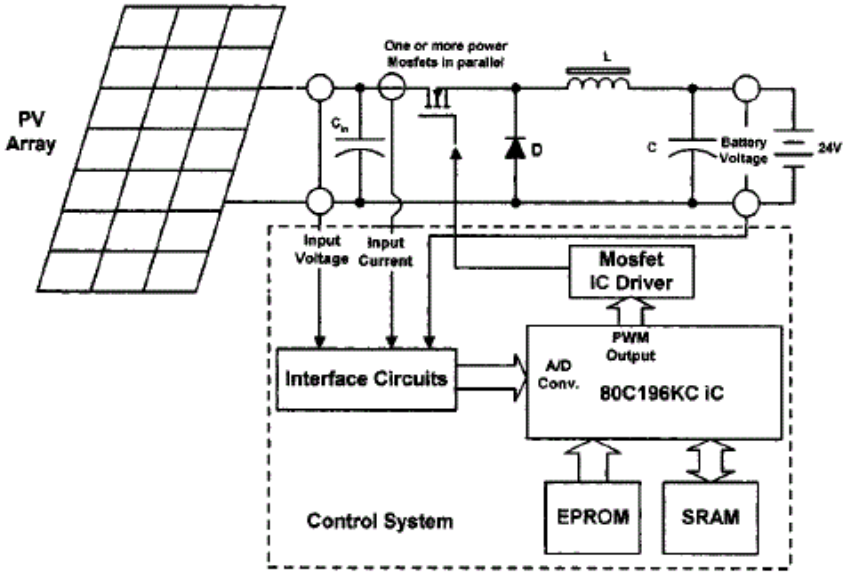

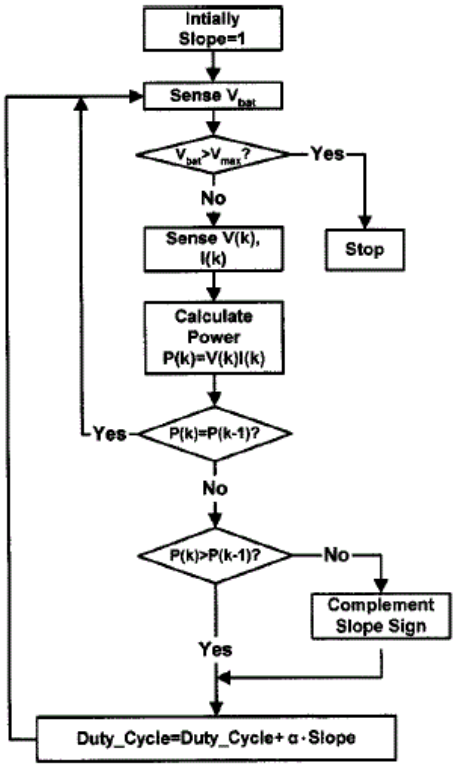

Cahier des charges et contraintes

Le régulateur devra répondre aux besoins suivants :

- S'adapter aux éoliennes de 24 à 48V,
- Ne pas utiliser les paramètres constructeurs propres au modèle utilisé (à part les données de tension et puissance).
- Le dimensionnement permet un courant de travail jusqu'à 30A.
- Pouvoir alimenter un injecteur réseau standard : tension d'entrée de 22V à 60V pour une éolienne 24V,
- Pouvoir de captation du MPPT ultra rapide pour s'adapter au mieux aux variations du vent,
- Très faible consommation interne.

Choix de l'algorithme

Comme expliqué en Annexes, la courbe de puissance d'un panneau photovoltaïque, comme pour une éolienne, n'est pas linéaire, mais croit jusqu'à une valeur de tension, puis décroit. L'appareil doit être capable de déterminer l'asymptote, et ce quelque soit la puissance disponible à l'instant t

Courbes de puissance correspondante à une vitesse de vent donnée (éolienne) ou 1 éclairement donné (photovoltaïque) :

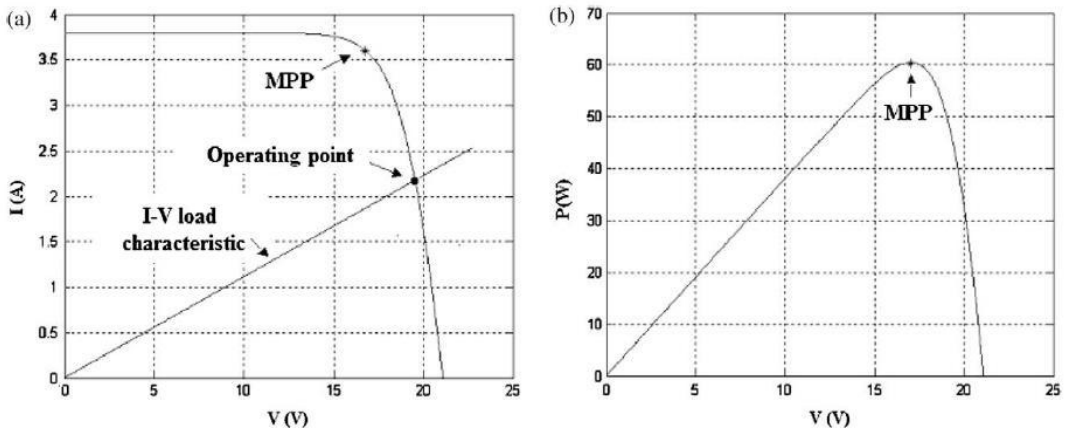

Courbes pour 3 vitesses de vent V1, V2 et V3 :

Nous voyons que le MPP (Maximum Power Point) B, F et D diffèrent et expriment la non-linéarité du générateur, comme montré par la courbe en pointillés ci-dessous :

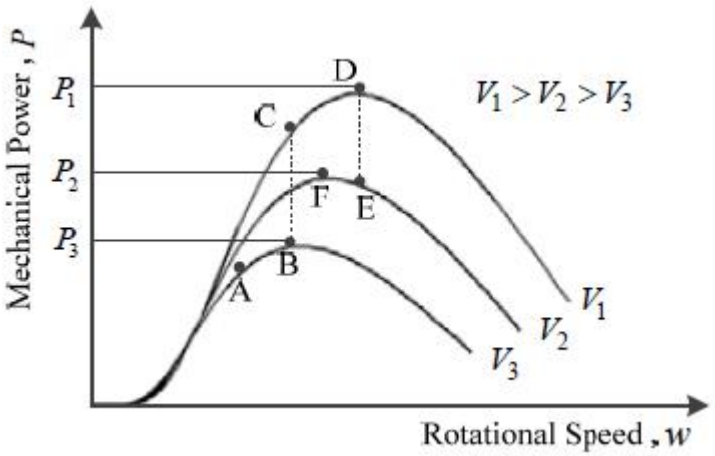

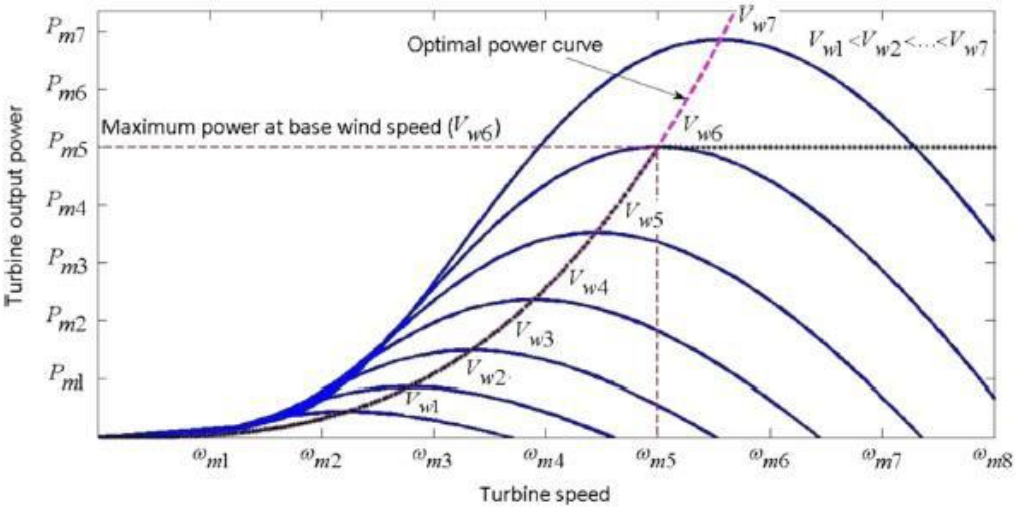

La qualité de l'algorithme sera jugée par la rapidité du dispositif à retrouver le MPP lorsque le vent évolue.

En écartant tous les algorithmes qui utilisent des paramètres dépendant du matériel, sachant que dans ce cas nous utiliserons que des paramètres mesurables immédiatement – la tension, le courant, la vitesse de rotation (traduite par la fréquence du signal), les algorithmes les plus communs sont le PO (Perturb & Observe) ou le INC (Incremental Conductance).

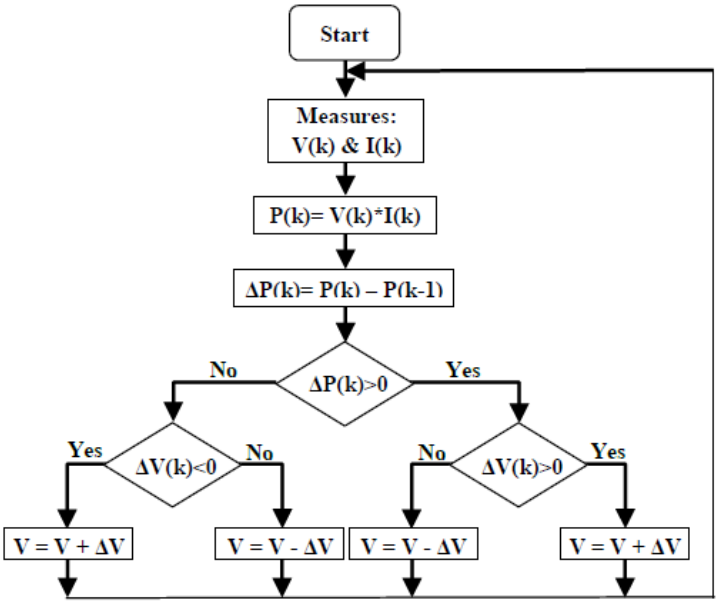

Algorithme PO

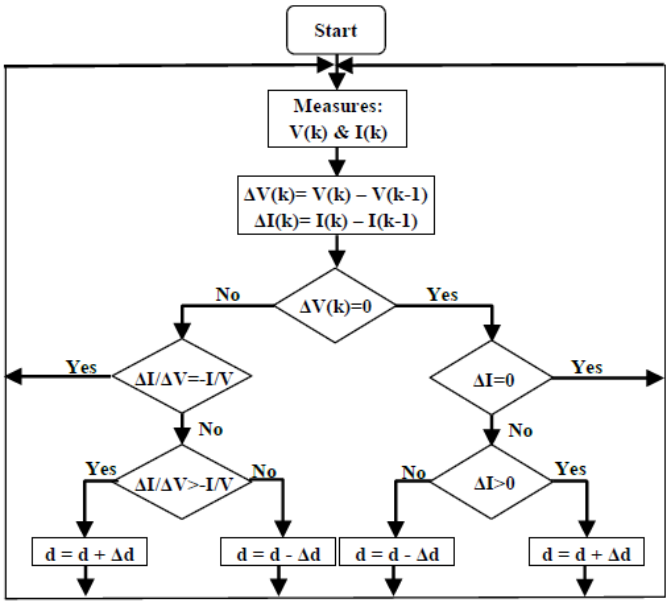

Algorithme INC

Ces deux algorithmes sont basés sur le principe d'incrémenter ou de décrémenter le rapport cyclique du convertisseur de tension suivant le résultat de mesures qui est comparé au résultat des mesures précédent.

Nous imaginons que ce signal de commande du rapport cyclique « court » après le sommet de la courbe correspondant au MPP, d'où le terme HCS pour Hill Climbing Search.

Tel quel, avec un pas fixe, ces algorithmes présentes 3 inconvénients, cf annexe 2 :

- Au niveau du MPP, le signal « passe son temps » à se décrémenter et à s'incrémenter pour chevaucher continuellement le MPP : nous avons donc une petite perte de puissance, d'autant moindre que le pas sera faible.
- La vitesse pour atteindre le MPP lorsque le vent change est dépendant de la hauteur du pas : plus il est faible plus il faudra de boucles d'incrémentation ou de décrémentation pour l'atteindre, et plus la durée de gestion du changement sera importante.
- En cas de brusque baisse de vent, la faible puissance disponible qui en résulta fait que l'algorithme peut « perdre les pédales » et s'incrémenter jusqu'en butée alors qu'il devrait se décrémenter.

La proposition en annexe 3 permet de résoudre ces problèmes :

- Utilisation d'un pas variable en fonction du résultat des mesures : plus l'écart de données entre la mesure actuelle et la mesure précédente est grand, plus le pas sera élevé. Atteindre le MPP est désormais bien plus rapide. En outre au niveau du MPP le pas est réduit, ce qui évite la perte d'énergie quand le signal oscille autour du MPP.
- La mesure de la vitesse de rotation de l'hélice permet une mesure plus fine des variations que la mesure de la puissance qui est le résultat de la mesure de la tension et du courant, et empêche ainsi la perte du MPP aux faibles niveaux de puissance.

L'algorithme est donc le suivant :

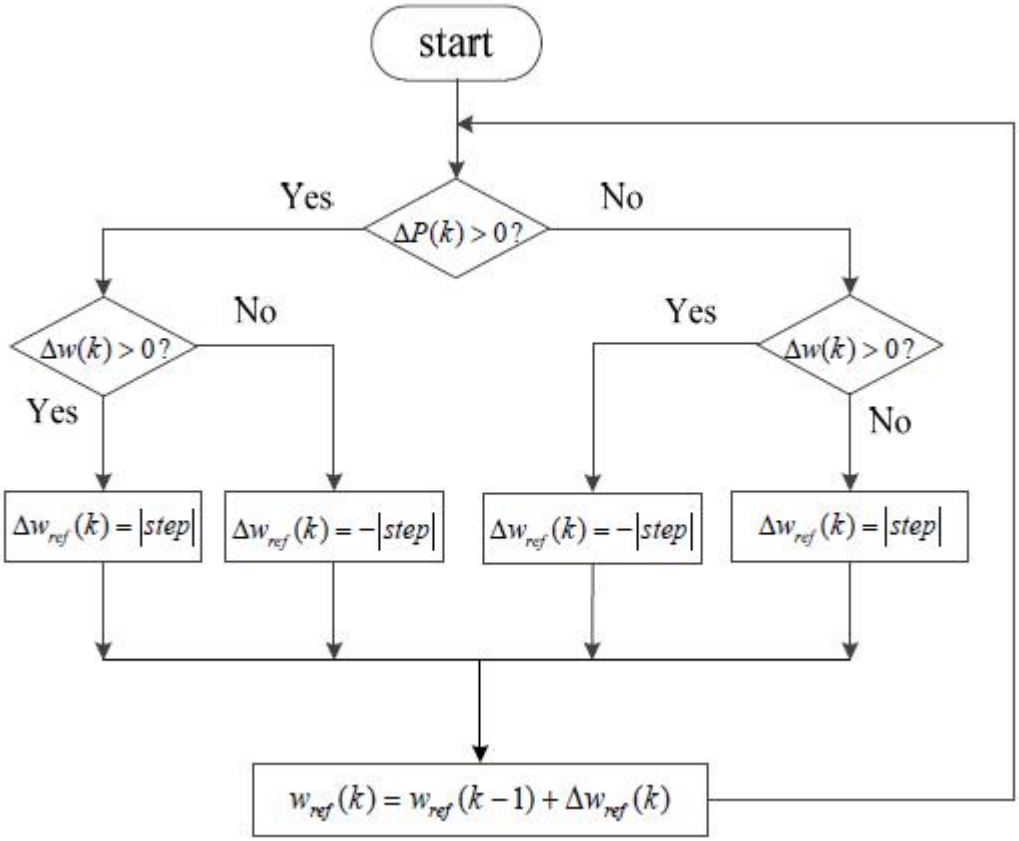

La valeur du pas est proportionnelle à la différence de vitesse de rotation entre 2 mesures.

Liste des courses

Commun aux 3 parties du projet :

1- Un pont de diode de redressement triphasé, dont le courant est largement surdimensionné à la puissance de l'éolienne, par exemple ce modèle tient 150A : https://fr.aliexpress.com/item/1PC-MDS150A-3-Phase-Diode-Bridge-Rectifier-150A-Amp-1600V-Copper-150-Celsius-80x40x33mm-Metal-Case/32827227402.html?spm=a2g0s.9042311.0.0.5e286c37aR2fHw

2- La résistance de « Dump Load », adaptée à la puissance admissible

Pour la partie protection en circuit analogique :

1- 3 transistors NPN haute tension, par exemple des 2SC4382 qui tiennent 200V et que l'on peut trouver ici : https://fr.aliexpress.com/item/Free-shipping-10pcs-lot-2SC4382-C4382-NPN-TO-220F-new-original/32823025012.html?spm=a2g0s.9042311.0.0.27426c37fml1w1

2- 1 Amplificateur Opérationnel de type UA741. Eviter les TL0xx qui ne peuvent suivre la demande en courant de commande : https://fr.aliexpress.com/item/10PCS-LOT-UA741CN-UA741-741CN-741-DIP8-op-amp-compensation-type/32808572254.html?spm=a2g0w.search0104.3.2.15de5c61MAl9rX&ws_ab_test=searchweb0_0,searchweb201602_5_10065_10068_10843_5015215_10059_5015315_10696_100031_10084_10083_10103_451_10618_452_10304_10307_10820_10821_5015915_5016015_10302,searchweb201603_16,ppcSwitch_5&algo_expid=d7a65203-3b97-4831-8477-a9f8fb381be0-0&algo_pvid=d7a65203-3b97-4831-8477-a9f8fb381be0&transAbTest=ae803_2&priceBeautifyAB=0

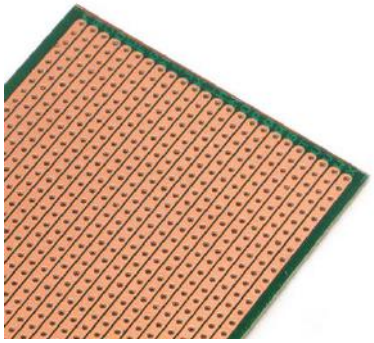

3- 2 transistors de puissance C-MOS, par exemple le IRFB4110 qui tient 100V 180A pour 370W de dissipation, ou encore des IRFP4227 qui tiennent 200V et sont spécialisés à la commutation.

4- Une plaquette de montage à bandes de cuivre et perforée : https://fr.aliexpress.com/item/5-Pcs-6-5x14-5-cm-Stripboard-Veroboard-Uncut-PCB-Platine-Seul-C-t-Circuit-Conseil/32844204108.html?spm=a2g0s.13010208.99999999.259.4bf23c00bUTsM4

5- 2 zeners 15V, 1 zener 4,7V, 1 condensateur électrochimique de tension de service de 200V, 2 condensateurs entre 10 et 22uF, quelques résistances, support de circuit intégré 8 broches, etc…

Pour la partie acquisition de données :

1- Un arduino Uno R3 : https://fr.aliexpress.com/item/One-set-New-2016-UNO-R3-ATmega328P-CH340G-MicroUSB-Compatible-for-Arduino-UNO-Rev-3-0/32696412561.html?spm=a2g0s.9042311.0.0.27426c37rrsgNO

2- Une carte d'extension : https://fr.aliexpress.com/item/Free-Shipping-UNO-Proto-Shield-prototype-expansion-board-with-SYB-170-mini-bread-board-based-For/32502867722.html?spm=a2g0s.9042311.0.0.27426c37rrsgNO

3- Un capteur de courant à base de l' ACS712, il en existe 3 modèles : 5A, 20A et 30A. Le choix se portera sur le modèle 20A si l'éolienne ne peut pas fournir plus : https://fr.aliexpress.com/item/WAVGAT-Hot-Sale-ACS712-20A-Range-Hall-Current-Sensor-Module-ACS712-Module-For-Arduino-20A/32827933262.html?spm=a2g0s.13010208.99999999.258.16fd3c00mx02AD

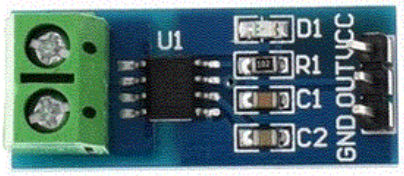

4- Un capteur de courant alternatif sensible : https://fr.aliexpress.com/item/Free-shipping-0-30A-sensor-split-core-current-transformer-SCT006/32579590465.html?spm=a2g0s.9042311.0.0.27426c37zd6RJS

Le capteur de courant est une sorte de mini transformateur ne comportant qu'un secondaire qui doit être chargé sur une résistance (dite de Burden) de l'ordre de 100Ω. Inutile d'augmenter la valeur de cette résistance pour tenter d'obtenir un meilleur taux de transformation, ça sature très vite ces petits capteurs.
Ce modèle possède sa propre résistance de Burden : https://fr.aliexpress.com/item/5A-Range-of-Single-Phase-AC-Current-Sensor-Module-for-Arduino-Free-Shipping/32713284483.html?spm=a2g0s.9042311.0.0.27426c37TNdWoA

5- Un afficheur LCD 1602 avec I2C : https://fr.aliexpress.com/item/1602-LCD-Module-Bleu-Jaune-Vert-cran-avec-IIC-I2C-16x2-LCD-R-tro-clairage-Module/32891917063.html?spm=a2g0s.9042311.0.0.458d6c37pXdIJP

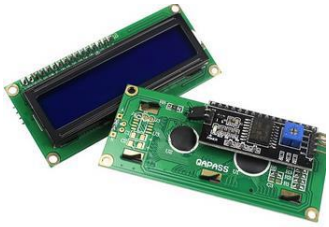

6- Un module de lecteur de carte SD pour le cas où vous souhaitez conserver les données de mesure et vérifier le fonctionnement et le rendement du montage : https://fr.aliexpress.com/item/New-Data-Module-Logging-Shield-SD-Card-Data-Recorder-Shield-V1-0-UNO-SD-Card-Hot/32815793580.html?spm=a2g0s.9042311.0.0.27426c377SIMdS

7- Quelques zeners 4,7V, résistances, condensateurs dont les valeurs sont données dans le circuit électrique…

8- Une alimentation 5V pour l'Arduino, c'est-à-dire un chargeur de téléphone portable de récupération, du câble Dupont (bof bof c'est plein de mauvais contacts, rien de vaut mieux que la soudure), une toute petite poignée de composants électriques dont la liste est un peu plus bas.

En plus pour la partie régulateur MPPT :

9- Une jolie boite pour intégrer durablement le montage (c'est d'ailleurs l'élément le très loin le plus cher)

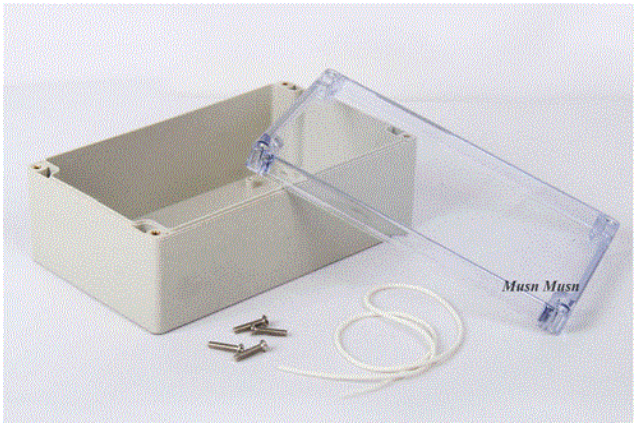

Circuit électrique autour de la protection analogique :

Sur certains sites cet appareil est nommé un régulateur. En fait il n'a de régulateur que le fait que sa présence empêche l'emballement de l'éolienne et ainsi sa détérioration. Cet emballement n'étant possible qu'en absence de charge, la tension va grimper au-delà de la valeur usuelle de fonctionnement. Le dispositif de sécurité va donc connecter une charge résistive lorsque la tension générée dépasse le double de la tension de service : une cinquantaine de volt pour une éolienne de 24V, une centaine de volt pour la version 48V.

Aussi au lieu de parler de régulation il est plus judicieux de parler de sécurité, à l'image du fusible qui protège une installation électrique des courts-circuits, la sécurité connecte automatiquement une charge qui transforme en Joules la surtension. Cette charge est appelée résistance de Dump Load, sa taille dépend de la puissance qu'elle doit pouvoir absorber – au moins égale à la puissance nominale de l'éolienne – et dont la valeur ohmique dépend de la tension nominale, par la formule $R= U^2/P$ (R en ohms, U en Volts, P en Watt).
Pour une éolienne de 350W sous 24V, nous avons R=1,5 ohms

Il se raconte également sur un certain forum que cette sécurité n'est pas nécessaire sur les éoliennes Piggott, puisque la construction du safran permet la mise en drapeau de l'hélice, c'est-à-dire que celle-ci se place à la quasi perpendiculaire du sens du vent, ce qui empêcherait son emballement. C'est une idée fausse et très dangereuse pour ceux qui la suivraient : en effet le safran reste dans le sens du vent, c'est la force du vent qui « pousse » l'hélice jusqu'à ce qu'elle pivote pour offrir moins de prise au vent. Or pour que le vent puisse pousser l'hélice, il faut bien que celle-ci offre une résistance. Or pour offrir une résistance elle doit être chargée. En roue libre la résistance n'est rien d'autre que les pertes de l'axe de rotation, elle peut tourner à une vitesse vertigineuse sans jamais se placer autrement que face au vent.

Montage comparateur

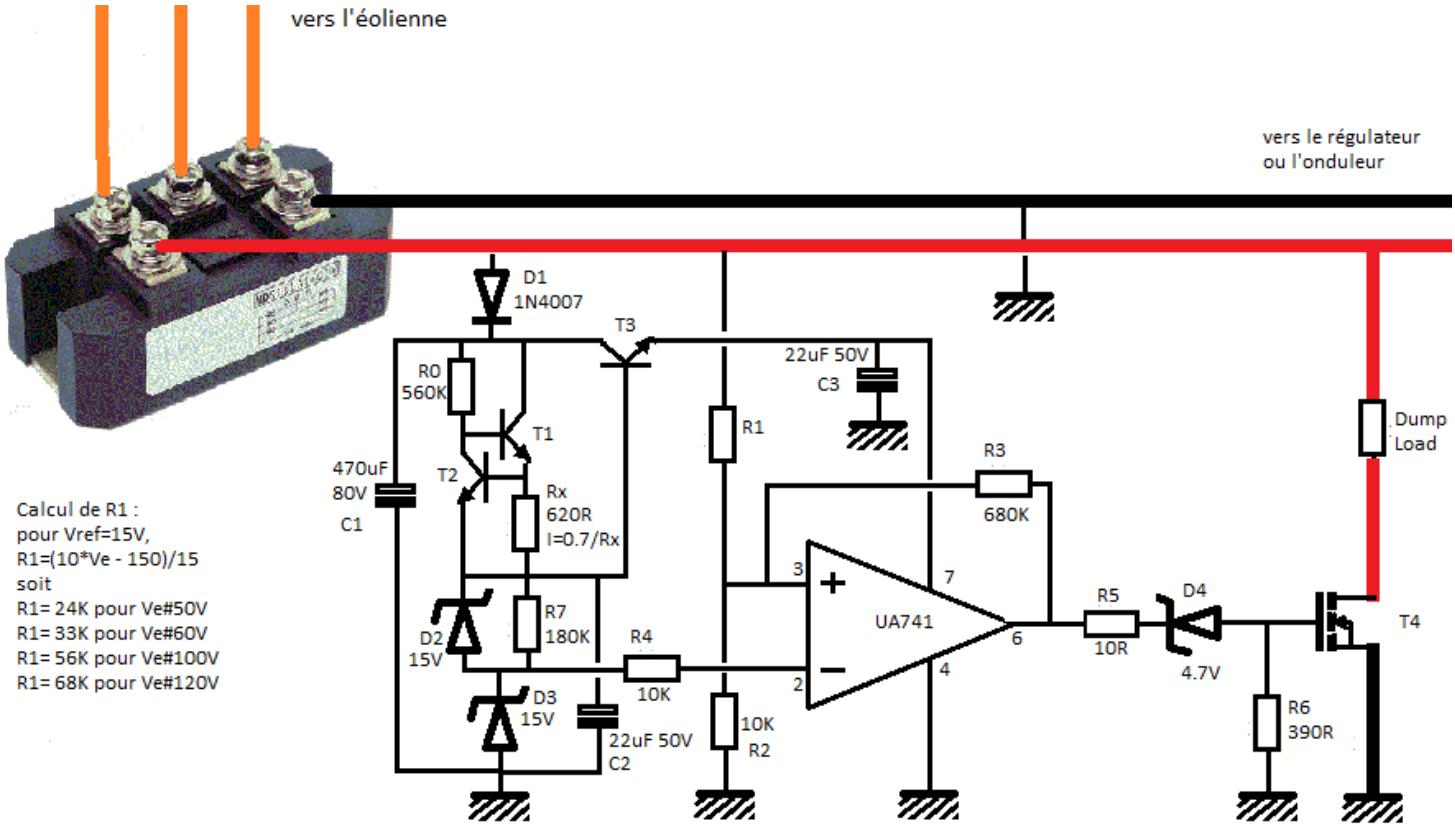

Le montage comparateur est construit autour de l'ampli opérationnel uA741 ou LM741, un grand classique (des années 70 et toujours fabriqué !) qui offre l'avantage de fonctionner sous des tensions de l'ordre de 2x20V et fournir un courant de sortie d'une dizaine de milliampère, ce qui est suffisant pour commander les 2 MOSFET de puissance T4 montés en parallèle. La zéner D4 soustrait la tension résiduelle en sortie d'AOP au niveau bas, afin de garantir 0V sur la grille de T4 quand ce dernier doit être au repos (T4 en état bloqué).

L'alimentation de l'AOP est confiée à 2 zéners de 15V à travers le balastre T3, ces 2 zéners elles-mêmes alimentées par un générateur de courant construit autour de T1 et T2. Cette configuration offre l'avantage d'un courant constant quel que soit la tension disponible fournie par l'éolienne, à partir du moment où cette tension est supérieure à 30V. De plus la consommation globale du montage n'est même pas 1 Watt.

Le diviseur de tension autour de R1 et R2 fournie une mesure proportionnelle à la tension disponible, elle est comparée à la tension de référence de 15V – aux bornes de la zéner D3 – ; dès que la tension en R2 dépasse 15V, l'AOP bascule et T4 devient passant (T4 en état saturé). R3 offre une hystérésis de quelques volts pour éviter les oscillations autour du point de bascule de changement d'état, ce qui surchaufferait inutilement le MOSFET.

Les valeurs de R1 sont données pour 2 cas possibles :

Cas éolienne de 24V => tension maxi de 50V => R1 = 24K

Cas éolienne de 48V => tension maxi de 100V => R1 = 56K

Implantation des composants

A partir d'une plaquette à bandes de cuivres, l'implantation proposée est la suivante :

Pour des soucis de visibilité, les pistes sont en jaunes, ou en rouge qui correspond à l'arrivée électrique, en rose l'alimentation du circuit intégré, en bleu la masse.

Attention ! Vue côté composants

Montage et illustration

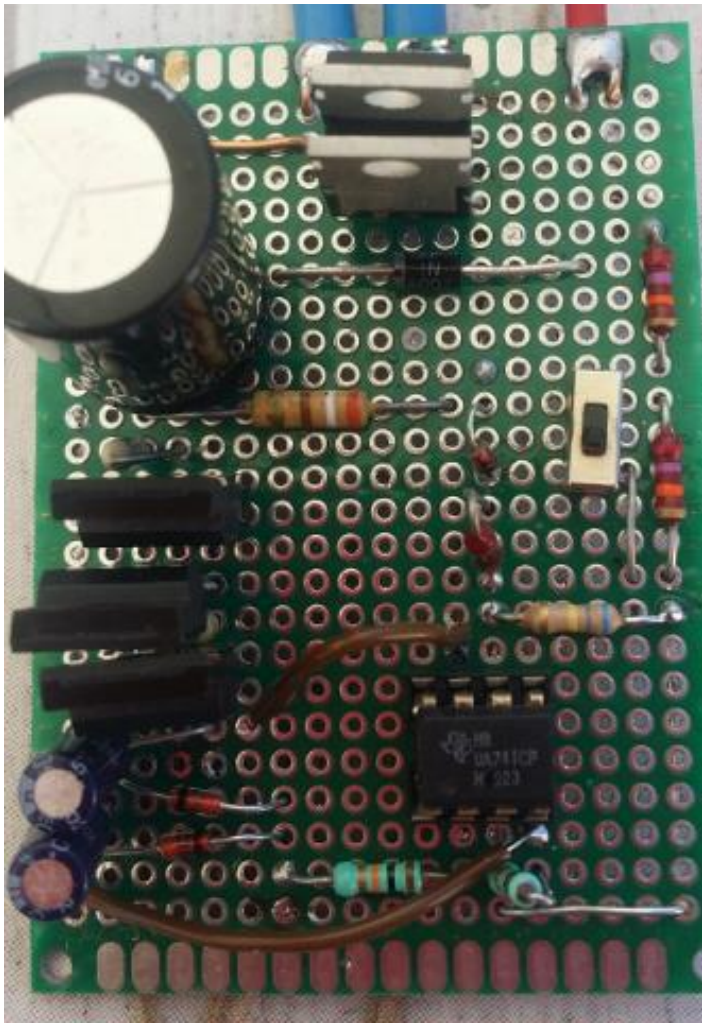

Recto

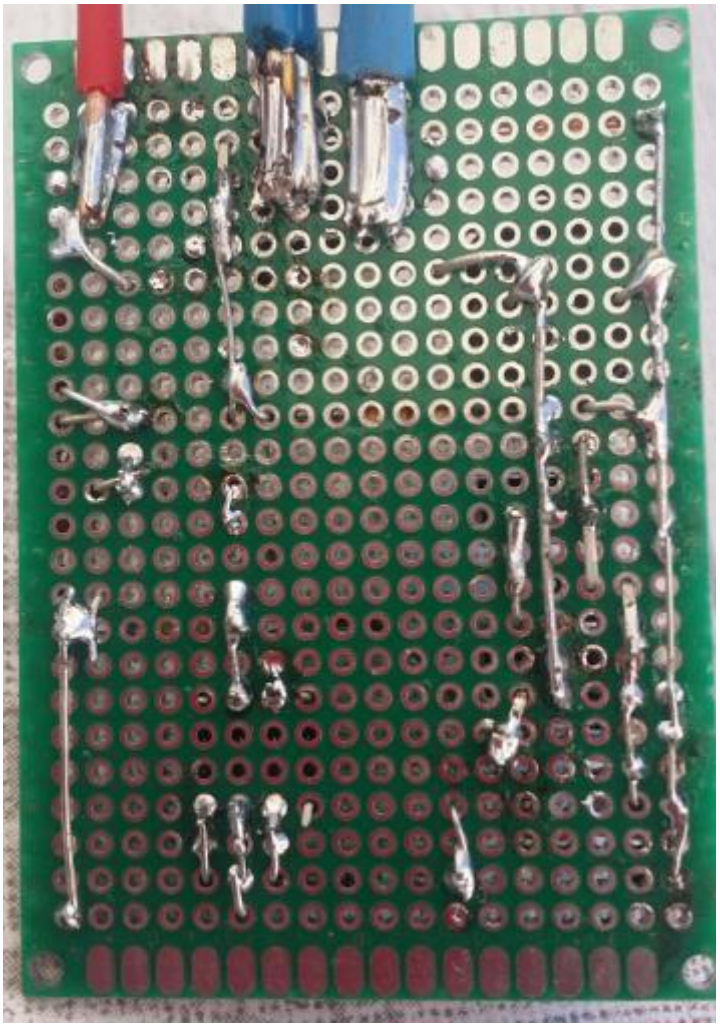

Verso

Il faut juste être méticuleux et aimer le jeu des 7 erreurs pour réaliser ce montage.

Une attention particulière sera portée au sens des 3 transistors, chacun est inversé de son voisin. Attention aussi au sens des diodes, et des condensateurs chimiques.

Quelques remarques :

Ne disposant pas de plaquette à bandes, ce sont les queues des composants qui ont servi de pistes.

Et puis la plaquette n'était pas assez longue, du coup au lieu de placer l'AOP dans la continuité de l'émetteur du transistor T3, celui-ci est mis sur le côté avec un strap non prévu au départ pour son alimentation électrique (broche 7).

A noter que sur cette illustration R1 est composé de 2 résistances de 27K en série, dont l'une peut être court-circuitée par un petit inverseur : ainsi ce montage est utilisable pour toute éolienne en 24V ou 48V.

Enfin je ne suis pas du tout fan des contacts à vis lorsqu'il y a des ampères qui circulent. Ce montage ayant vocation d'être mis dans une boite, je n'ai pas l'intention de l'ouvrir pour y vérifier le serrage des vis ! Alors les contacts sont soudés et le problème du vieillissement est résolu.

ATTENTION : Sur les photos il n'y a pas R7, qui a été rajouté après la mise en place définitive du montage. R7 assure une meilleure stabilité du montage, lorsque l'éolienne démarre la tension monte, cependant l'AOP se met à fonctionner avant l'atteinte des 30V, et dans ce cas il faut s'assurer que la tension de référence du comparateur aux bornes de la zéner D3 atteigne sa valeur en premier, au risque que la sécurité se déclenche aux faibles tensions. Cette résistance assure un courant dans D3 même lorsque D2 est bloquée faute d'une tension suffisante.

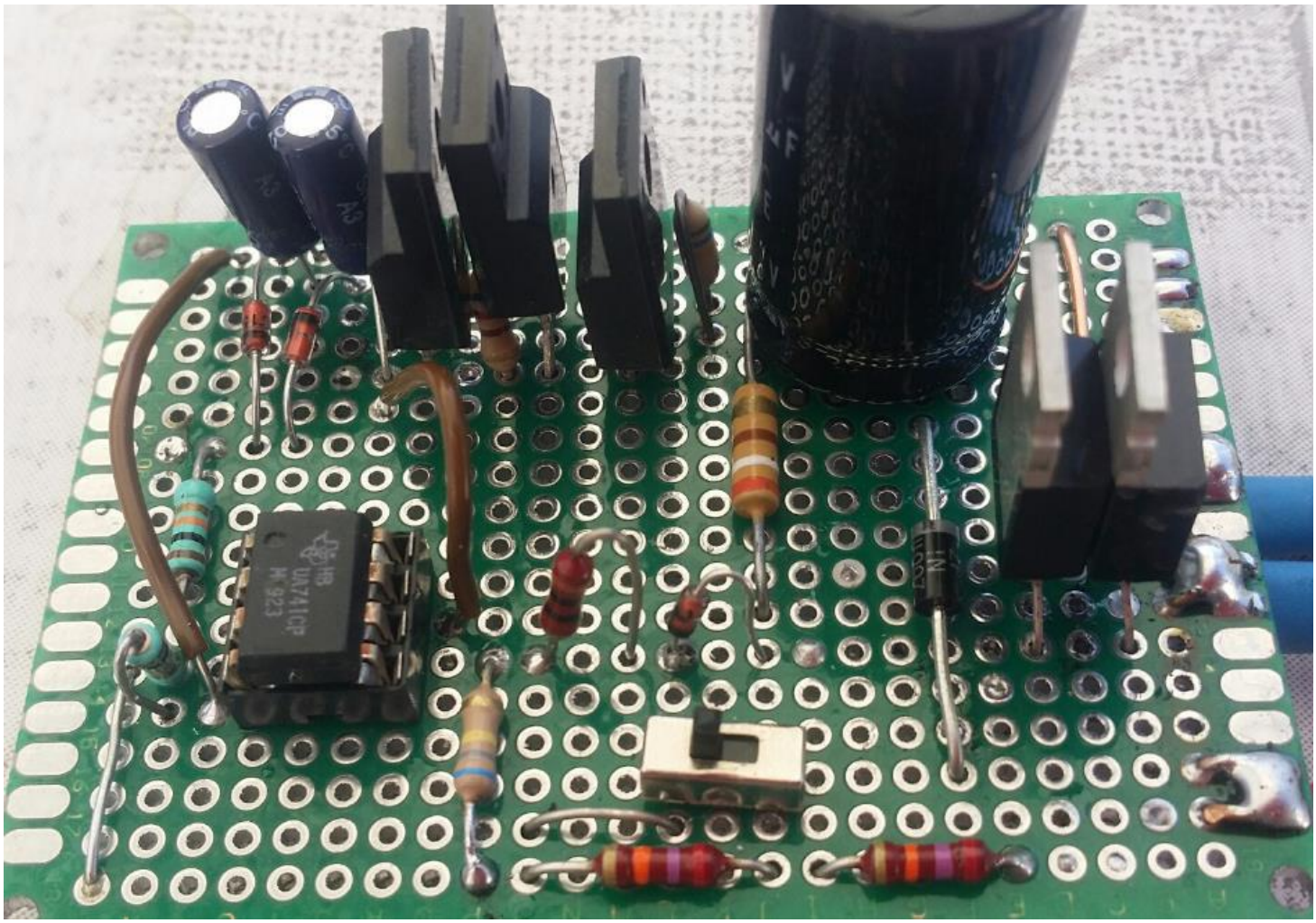

Test de fonctionnement

Pour tester le montage, il faut disposer d'une alimentation capable de fournir une tension sinusoïdale ou continue pouvant monter jusqu'à 60V pour une éolienne 24V et 120V pour une éolienne de 48V.

On commence par tester le montage sans l'AOP ni la résistance de Dump Load : il s'agit de vérifier qu'il y a bien 30V en broche 7, 15V en broche 2, et quelque chose proportionnelle à l'alimentation en broche 3.

Lors des essais la résistance de Dump Load sera remplacée par une résistance adaptée à la puissance de l'alimentation, dans notre exemple il s'agit d'une résistance de puissance de 3K.

A gauche : La tension disponible est en dessous du seuil, la tension mesurée au niveau de la Dump Load vaut zéro.

Ci-dessous à gauche : cas du montage pour éolienne 24V. On monte progressivement la tension d'alimentation, vers 55V la sécurité se déclenche.

Ci-dessous à droite : cas du montage pour éolienne 48V. La tension de sécurité est de 99V.

Mise en place définitive

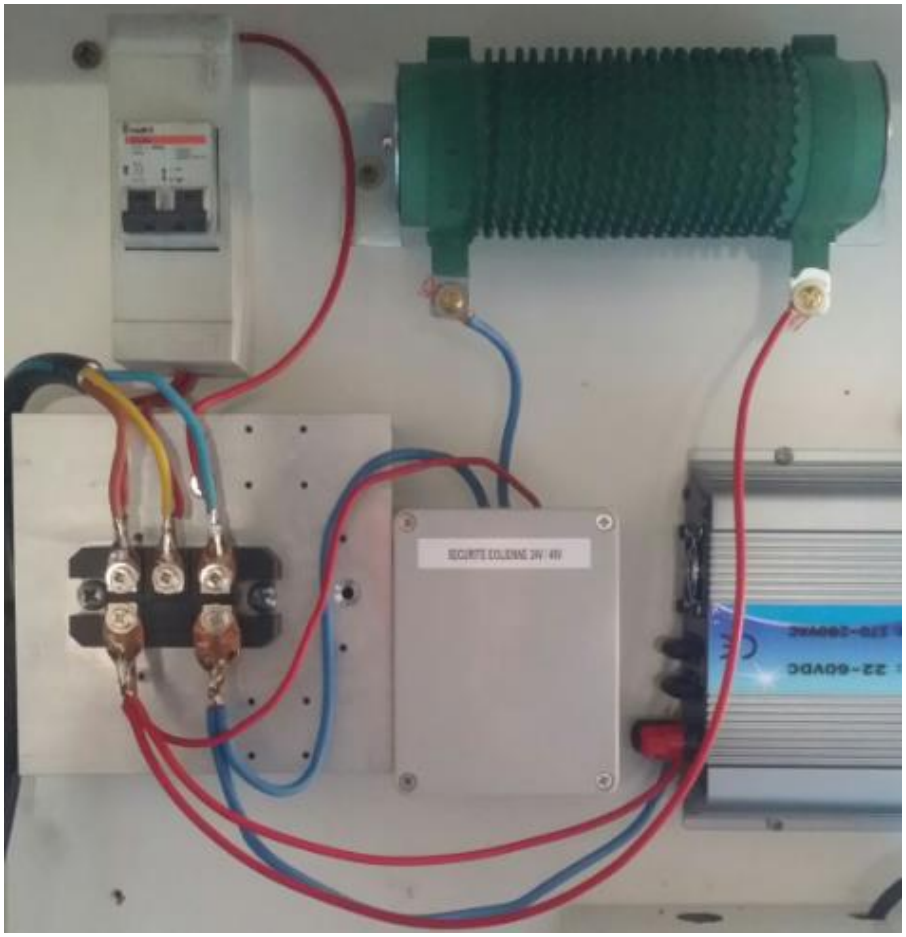

Circuit électrique autour du banc de mesures :

Le banc de mesure va collecter les informations suivantes :

Si l'éolienne tourne, et dans ce cas à intervalles réguliers :

- Date et l'heure,
- Vitesse de rotation Fprimaire
- Tension délivrée au pont de diode Vprimaire
- Courant délivré au pont de diode Iprimaire
- Courant injecté sur le réseau Isortie
  On suppose que la tension du réseau est stable à 230V.

Vprimaire * Iprimare = Pprimaire

230 * Isortie = Psortie

D'où calcul du rendement Psortie/Pprimaire, mesure de la courbe Iprimaire et Vprimaire en fonction de la vitesse de rotation, mesure du temps de recherche du MPPT du régulateur/injecteur, etc….

Mesure de la tension, des courants et de la fréquence

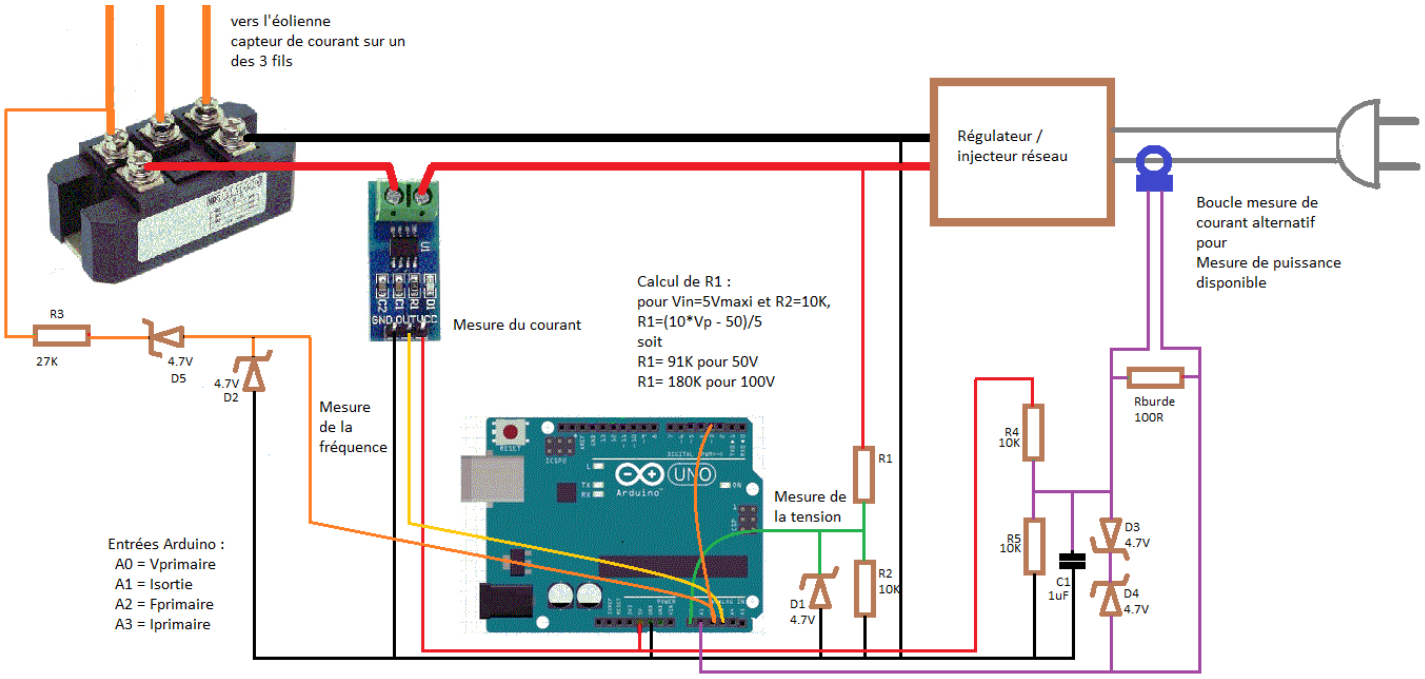

Le capteur de vitesse de rotation de l'hélice est construit autour de R3, D2 et D5. Le signal alternatif est récupéré sur l'une des 3 entrées du pont de diode. Entre chacune de ces 3 entrées le signal est sinusoïdal, mais par rapport à la masse le signal n'est plus que la demie-alternance positive. R3 limite le courant à moins de 5 milliampères, D5 sécurise qu'il n'y est aucun signal négatif et crée par la même occasion un offset à 4,7V, car ça ne sert pas à grand-chose d'effectuer des relevés de mesure quand l'hélice tourne si doucement qu'aucun courant récupérable n'est produit. Enfin D2 limite le signal à 4,7V compatible avec l'Arduino. Pour les tests du circuit le capteur est branché sur l'entrée analogique A2 pour vérifier l'amplitude du signal, et l'entrée numérique 3 pour calculer la fréquence.

Le capteur de tension primaire est un simple pont diviseur construit autour de R1 et R2. La mesure s'effectue aux bornes de R2, la tension recueillie est V = Vprimaire * R2 / (R1+R2). D1 est une sécurité qui protège l'Arduino en cas de surtension.

Le capteur de courant primaire est constitué du module ACS712, qui fournit une tension de mesure comprise entre 0 et 5V, et proportionnelle au courant qui le traverse.

Le capteur de courant d'injection est constitué d'un capteur à effet Hall, c'est une sorte de bobinage traversé par le fil dont on veut effectuer la mesure. Cette méthode préserve de manipuler la haute tension du secteur…
Pour fonctionner correctement ce bobinage doit être connecté à une résistance de Burden, qui peut être dans le capteur lui-même. Aux bornes de cette résistance il y aura une tension (alternative) proportionnelle au courant alternatif parcouru dans le fil. Pour ramener cette tension tantôt négative tantôt positive sur une fourchette de 0 à 5V, un côté de Rburden est branché au pont diviseur R4 et R5 où le potentiel vaut 2,5V. C1 découple le pont diviseur pour éliminer tout résidu alternatif. 2 zéners tête-bêche de 4,7V aux bornes de Rburden limitent l'amplitude de la tension à 5V.

Quelques photos du circuit autour des capteurs

Comme déjà fait pour le montage de sécurité étudié précédemment, R1 est composée de 2 résistance en série de 91K avec un interrupteur miniature permettant le shunt de l'une des 2. Cette configuration permet les essais aussi bien sur des éoliennes de 24V que de 48V.

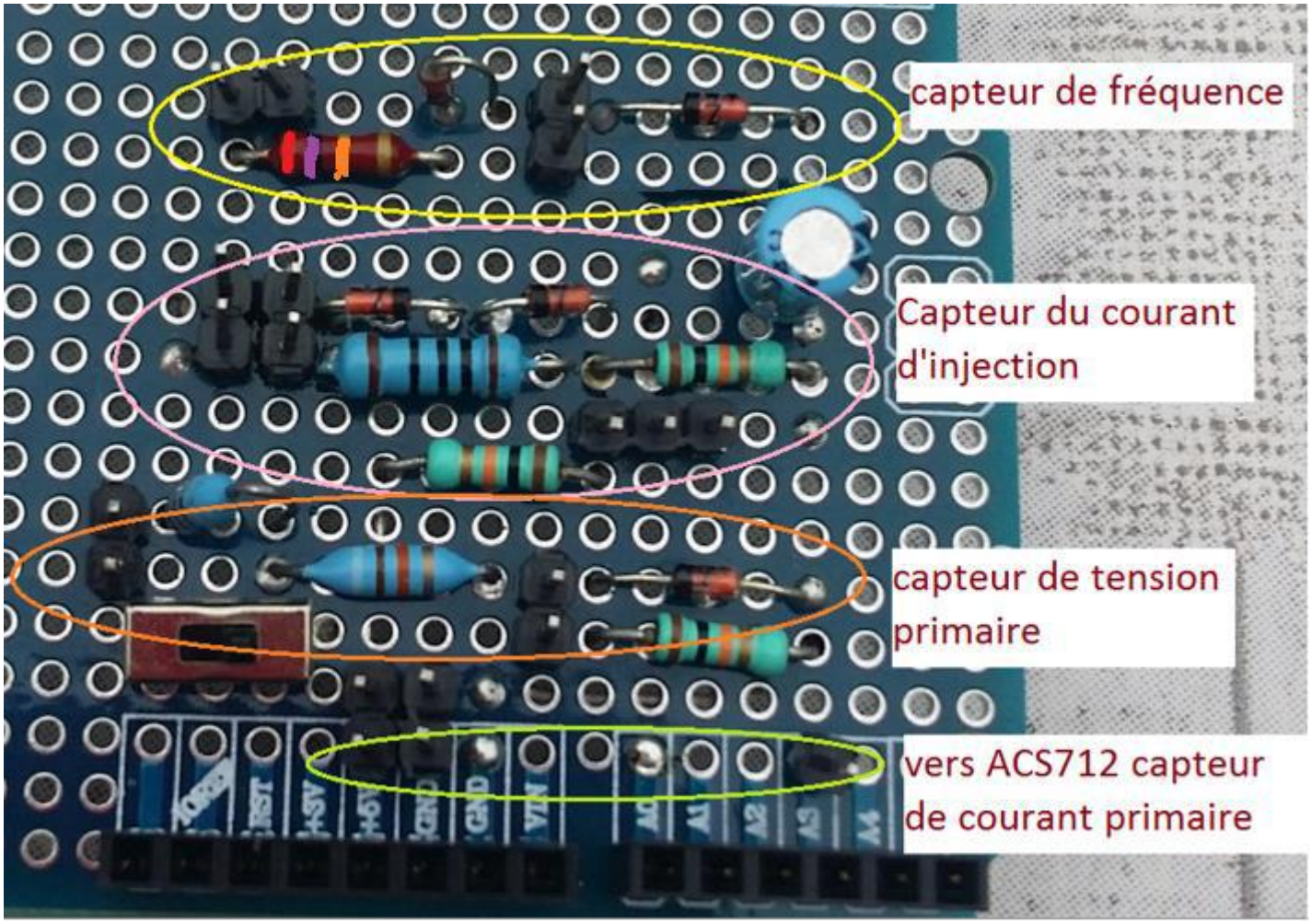

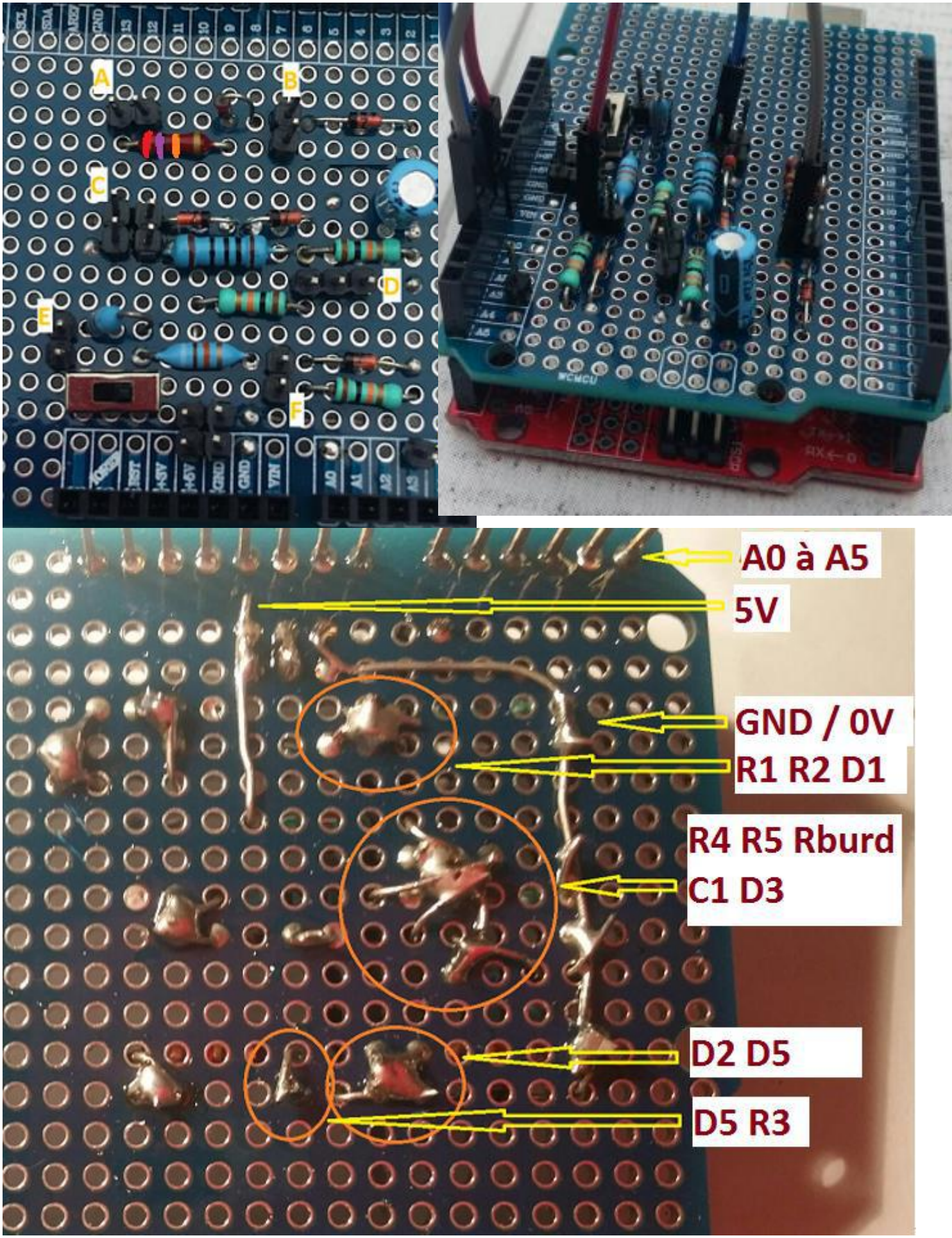

Liste des lettres :

A- Vers une des 3 phases de l'éolienne pour mesure de la fréquence du signal alternatif,

B- Vers A2 et 3 pour mesure de la vitesse de rotation de l'éolienne Fprimaire,
C- Vers A1 + Sonde de courant alternatif de mesure du courant d'injection Isortie,
D- Vers sonde de courant alternatif de mesure du courant d'injection,
E- Vers le pôle + du pont de diode pour mesure de la tension primaire,
F- Vers A0 pour mesure de la tension Vprimaire
G- (=broche A3) Vers module ACS712 pour mesure du courant primaire Iprimaire.

Premier test de mesures des capteurs

1- Sans enficher la carte d'extension dans l'Arduino, brancher l'Arduino sur le port USB du PC
2- Si ce n'est déjà fait, Installer l'interface de programmation, le programme est téléchargeable ici : https://www.arduino.cc/en/Main/OldSoftwareReleases
3- On installe les drivers pour l'arduino UNO : http://283.mytrademe.info/ch340.html
4- On lance le programme Arduino :
1- Menu outils-> type de carte-> UNO
2- Menu outils-> PORT-> ComX ou X représente le port sur lequel est installé votre arduino.
3- On efface ce qu'il y a dans la fenêtre d'édition
4- On y colle le code ci-dessous :

```
// minMaxAndRangeChecker
// A simple tool to investigate the ADC values that are seen at the
// first four analogue inputs of an Atmega chip, as used on an emonTx
//
// Robin Emley (calypso_rae on the Open Energy Monitor forum)
//
// 20th April 2013
//

int val_a0, val_a1, val_a2, val_a3;
int minVal_a0, minVal_a1, minVal_a2, minVal_a3;
int maxVal_a0, maxVal_a1, maxVal_a2, maxVal_a3;

int loopCount = 0;
unsigned long timeAtLastDisplay = 0;
byte displayLineCounter = 0;

void setup(void) {
  Serial.begin(9600);
  Serial.print("ready ...");
  delay(700);
  Serial.println ();
  Serial.println(" The Min, Max and Range ADC values for analog inputs 0 to 3:");
}

void loop(void) {
  val_a0 = analogRead(0);
  val_a1 = analogRead(1);
  val_a2 = analogRead(2);
  val_a3 = analogRead(3);

  if (val_a0 < minVal_a0) { minVal_a0 = val_a0;}
  if (val_a0 > maxVal_a0) { maxVal_a0 = val_a0;}
  if (val_a1 < minVal_a1) { minVal_a1 = val_a1;}
  if (val_a1 > maxVal_a1) { maxVal_a1 = val_a1;}
  if (val_a2 < minVal_a2) { minVal_a2 = val_a2;}
  if (val_a2 > maxVal_a2) { maxVal_a2 = val_a2;}
  if (val_a3 < minVal_a3) { minVal_a3 = val_a3;}
  if (val_a3 > maxVal_a3) { maxVal_a3 = val_a3;}

  unsigned long timeNow = millis();
  if ((timeNow - timeAtLastDisplay) >= 3000) {
    timeAtLastDisplay = timeNow;
    displayVal(minVal_a0);
    displayVal(maxVal_a0);
    displayVal(maxVal_a0 - minVal_a0);
    Serial.print(";  ");

    displayVal(minVal_a1);
    displayVal(maxVal_a1);
    displayVal(maxVal_a1 - minVal_a1);
    Serial.print(";  ");

    displayVal(minVal_a2);
```

```
    displayVal(maxVal_a2);
    displayVal(maxVal_a2 - minVal_a2);
    Serial.print(";  ");

    displayVal(minVal_a3);
    displayVal(maxVal_a3);
    displayVal(maxVal_a3 - minVal_a3);
    Serial.println();

    resetMinAndMaxValues();
    displayLineCounter++;

    if (displayLineCounter >= 5) {
      Serial.println();
      displayLineCounter = 0;
      delay(2000); // to allow time for data to be accessed
    }
  }
}

void resetMinAndMaxValues() {
  minVal_a0 = 1023, minVal_a1 = 1023, minVal_a2 = 1023, minVal_a3 = 1023;
  maxVal_a0 = 0, maxVal_a1 = 0, maxVal_a2 = 0, maxVal_a3 = 0;
}
void displayVal(int intVal){
  char strVal[4];
  byte lenOfStrVal;
  itoa(intVal, strVal, 10); // decimal conversion to string
  lenOfStrVal = strlen(strVal); // determine length of string

  for (int i = 0; i < (4 - lenOfStrVal); i++)  {
    Serial.print(' ');
  }

  Serial.print(strVal);
}
```

5- Enregistrer ce programme sur le PC sous le nom de testminmax.ino par exemple.

6- Puis : Menu croquis -> téléverser.

7- Ouvrir le moniteur série : Menu outils -> moniteur série : une autre fenêtre s'ouvre. Régler le débit (baud rate à 9600 si ce n'est pas le réglage par défaut)

Nous devons obtenir les résultats suivants :

Les entrées sont en l'air, c'est proche de zéro mais pas tout à fait.

```
The Min, Max and Range ADC values for analog inputs 0 to 3:
  0 340 340;     0 334 334;     0 326 326;     0 318 318
  0  65  65;     0  62  62;     0  59  59;     0  68  68
  0  66  66;     0  62  62;     0  60  60;     0  68  68
  0  68  68;     0  64  64;     0  60  60;     0  70  70
```

8- Débrancher la carte Arduino, insérer la carte d'extension sans brancher les capteurs.

9- Rebrancher la carte Arduino, et réouvrir le moniteur série.

Nous devons obtenir les résultats suivants :

La première ligne n'est pas significative, il faut laisser le temps au programme d'effectuer les calculs après initialisation des variables.

```
The Min, Max and Range ADC values for analog inputs 0 to 3:
  0   0   0;     0 513 513;     0 102 102;     0 511 511;
  0   2   2;   509 514   5;    55 145  90;   508 514   6;
  0   2   2;   509 514   5;    55 145  90;   507 515   8;
  0   2   2;   508 514   6;    55 145  90;   508 515   7;
```

Les entrées analogiques passent par un convertisseur numérique qui fournit 0 à 1024 bits pour une valeur lue de 0 à 5V.

A vérifier : A0 = 0 avec un bruit de l'ordre de 2 bits, A1 = 512 (soit 2,5V ce qui correspond au 5V divisé par R4 et R5) avec un bruit de 6 bits, A2 est branché sur une diode sans courant, c'est comme si elle n'était pas connectée, et enfin A3 donne 512 (soit 2,5V délivrée par l'ACS712) avec un bruit de 6 bits. Décidément ces CAN ont une mauvaise précision à bas niveau, ce qui ne nous arrange pas pour les mesures de petites puissances.

10- Brancher les capteurs :

Nous pouvons fabriquer un environnement d'essais à partir d'une alimentation expérimentale avec un transformateur 230V/20V suivi d'un pont de diode, d'un condensateur de filtrage – ce qui permet d'avoir une tension continue et non

pas une succession de demie-alternances positives - et une charge constituée de 2 ampoules halogènes 12V/20W branchées en série. Ainsi nous avons des grandeurs continue et alternatives pour effectuer les essais.

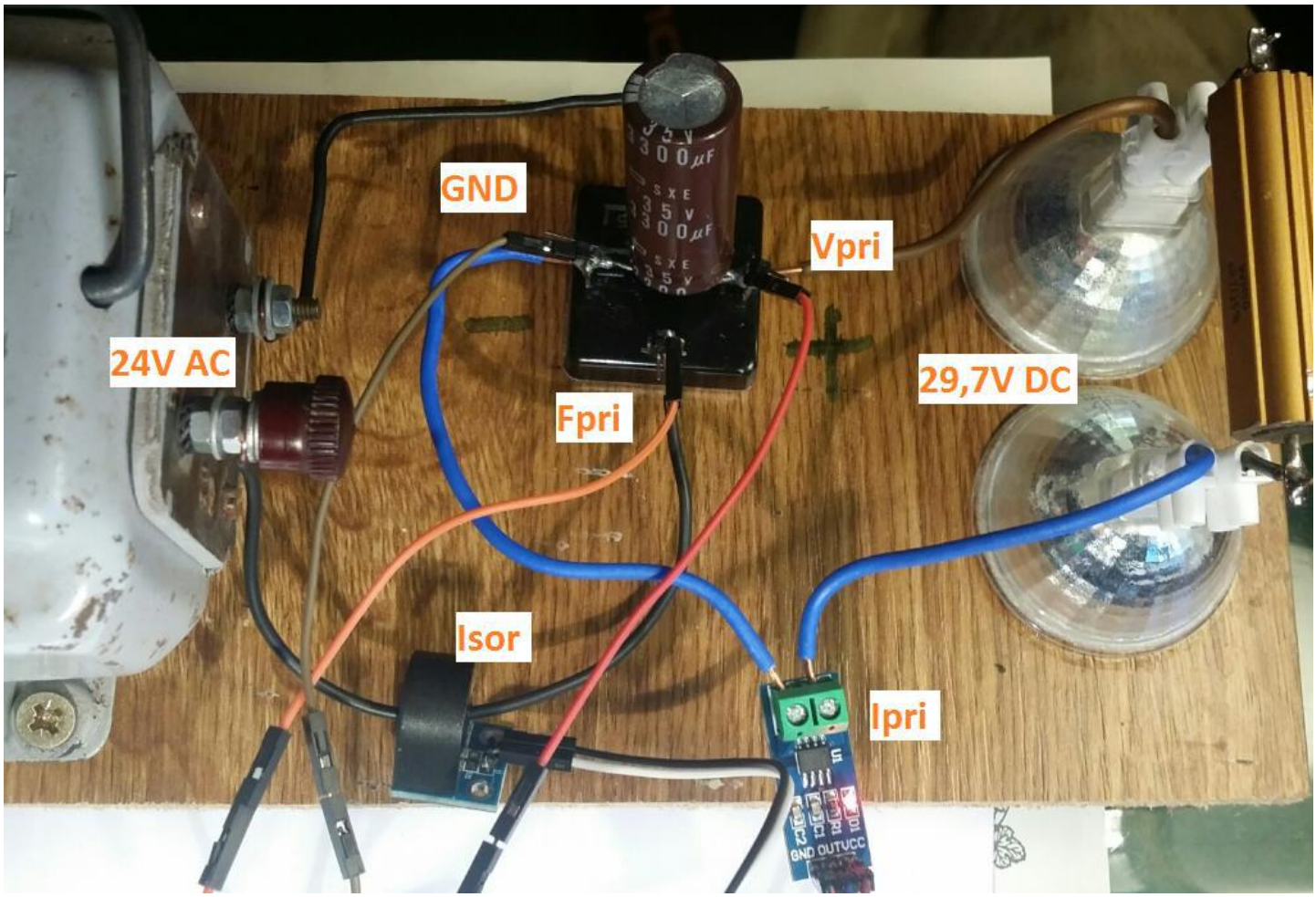

Nous obtenons le résultat suivant sur la console :

```
The Min, Max and Range ADC values for analog inputs 0 to 3: +ms +Hz
  0 594 594;      0 351 351;      0 874 874;      0 545 545;  19.74 50.66
570 627  57;    350 673 323;      0 878 878;    539 549  10;  19.73 50.67
571 628  57;    349 672 323;      0 878 878;    539 549  10;  19.73 50.69
571 628  57;    349 673 324;      0 878 878;    539 549  10;  19.73 50.68
```

Les mesures au multimètre donnent les informations : Vac = 24V / 50Hz, Vprimaire = 29,7V, Isortie = 2,55A

- A0 indique 571 à 628, un tel delta est dû à l'ondulation du signal. Une mesure charge débranchée (sans les ampoules halogènes) donne 636 à 642 pour 34V.
- A1 indique Isortie, qui oscille de 349 à 673, c'est normal puisque le courant est alternatif, la grandeur à mesurer est le delta 324.
- A2 indique Fpri, la mesure est une oscillation qui va de 0 à 878.
- A3 indique Ipri, la sortie de l'ACS712 va de 539 à 549, par rapport à 512. L'écart de 10 est lié à l'ondulation résiduelle en plus du bruit.

Vous obtenez grosso-modo les mêmes résultats ? Alors on continue.

Passer des bits à des valeurs normalisées

Vpri : il suffit d'appliquer une règle de 3. Si « 639 » (moyenne de 636 à 642) indique 34V, il y a donc 18,8 bits par volt.

Ipri : le module ACS712 envoie « 512 » pour 0A, « 0 » pour -20A et « 1023 » pour +20A. Déjà on remarquera que si la mesure est négative il suffit d'inverser le sens de la sonde. Il s'agit donc de convertir les bits en tension, puis d'appliquer la conversion courant/tension suivante :

- Module ACS712 de 5A => 185mV/A
- Module ACS712 de 20A => 100mV/A
- Module ACS712 de 30A => 66mV/A

Fpri : l'instruction `pulseln(pin, HIGH)` permet de calculer le nombre de microseconde entre 2 instants où le signal est à l'état haut. De même `pulseln(pin, LOW)` fait la même chose pour l'état bas. La somme de ces 2 mesures de temps donne la période du signal. Cette instruction ne fonctionne que sur une entrée numérique, d'où le choix de l'entrée 3.

Isor : Il est plus compliqué de mesurer un courant ou une tension alternative, parce que justement elle n'est pas statique. Un procédé consiste à prendre un échantillonnage de mesures sur un temps donné, de déterminer la valeur min et max, et d'en tirer la valeur efficace. Il est possible de réaliser cette programmation qui est la base de fonctionnement de testminmax.ino. Cependant il existe une librairie qui fait le job : *EmonLib.h*
A voir ici : https://learn.openenergymonitor.org/electricity-monitoring/ctac/how-to-build-an-arduino-energy-monitor

Utiliser un afficheur LCD 1602

A terme les données seront stockées sur une carte SD, néanmoins il est intéressant d'avoir une vue globale que les mesures sans nécessiter le branchement d'un PC sur le port USB et d'ouvrir le moniteur série.

Nous allons utiliser l'afficheur le plus classique qui soit : le LCD 1602 pour 16 caractères sur 2 lignes, avec l'extension I2C qui réduit considérablement la complexité du montage qui se résume à 2 fils de data. Toutes les infos sont décrites là : https://andrologiciels.wordpress.com/arduino/lcd/lcd-1602-i2c/

La bibliothèque est ici : https://app.box.com/s/czde88f5b9vpulhf8z56

Attention ! L'installation de la bibliothèque met à disposition une nouvelle bibliothèque *LiquidChrystal.h* ; il faut donc absolument supprimer – ou renommer – tous les fichiers de même nom : *LiquidCrystal.h* et *LiquidCrystal.cpp*, qui se trouvent quelque part sous le répertoire *C:\Program Files (x86)\Arduino\librairies*. Heureusement il n'y a rien de destructifs, les nouvelles librairies apportant les fonctionnalités compatibles avec les LCD classiques.

Programme initial de banc de test

1- Télécharger la librairie *emonLib.h* : https://github.com/openenergymonitor/EmonLib/archive/master.zip
2- Télécharger la librairie *LiquidCrystal_I2C.h* : https://app.box.com/s/czde88f5b9vpulhf8z56
3- Les déclarer : (In the Arduino IDE) Sketch > Include Library > Add .ZIP Library > select the downloaded file > Open
4- Ajouter l'extension *.orig* à *LiquidCrystal.h* et *LiquidCrystal.cpp*, qui se trouvent quelque part sous le répertoire *C:\Program Files (x86)\Arduino\librairies*
5- Créer un nouveau programme avec le code ci-dessous :

```
/*
Banc de mesures pour éoliennes 24 ou 48V
_____________________________________________________________
|                                                            |
|       auteur : Philippe de Craene <dcphilippe@yahoo.fr     |
|             pour l' Association PTIWATT                    |
_____________________________________________________________

*/

#include <Wire.h>
#include <LiquidCrystal_I2C.h> // https://app.box.com/s/czde88f5b9vpulhf8z56
```

```
// Attention ! Renomer la librairie d'origine de l'IDE LiquidCrystal.h et LiquidCrystal.cpp
#include <EmonLib.h>           // https://github.com/openenergymonitor/EmonLib
EnergyMonitor injection;       // Création de l'instance injection

// Brochage des entrées des capteurs et paramétrage

const byte broche_Vpri = A0;   // broche lecture tension pont de diodes
const byte broche_Isor = A1;   // broche lecture courant d'injection
const byte broche_Ipri = A3;   // broche lecture courant pont de diodes
const byte broche_Fpri = 3;    // broche numérique calcul fréquence

// choisir le modèle d'éolienne 24V ou 48V à vérifier expérimentalement :
// éolienne 24V avec maxi à 54V => conv_Vpri = 20.2
// éolienne 48V avec maxi à 95V => conv Vpri = 11.2
const float conv_Vpri = 20.2;  // conversion bytes/tension pour éolienne 24V

// Choisir le modèle de sonde ACS712 :
// Module ACS712 de 5A => 0.185V/A
// Module ACS712 de 20A => 0.1V/A
// Module ACS712 de 30A => 0.066mV/A
const float conv_Ipri = 0.1;   //  pour modèle 20A

// Calibration de Isor à définir expérimentalement suivant la sonde utilisée
// => valeur à saisir dans le setup()
// offset pour supprimer le bruit pour avoir 0 en absence de courant
const float Isor_offset = 0.06;

// Variables de traitement

float Vpri;                 // Tension au pont de diode
float Ipri;                 // Courant délivré au pont de diode
float Fpri;                 // Vitesse de rotation
int Vsor = 230;             // Tension du réseau
float Isor;                 // Courant injecté sur le réseau
unsigned long duree_H;      // durée de la demie période état haut
unsigned long duree_L;      // durée de la demie période état bas

int B_Vpri, B_Ipri;         // lecture des capteurs en bytes

// Déclaration du LCD en mode I2C :
// toutes les infos ici : http://arduino-info.wikispaces.com/LCD-Blue-I2C
// Set the pins on the I2C chip used for LCD connections:
//                    addr, en,rw,rs,d4,d5,d6,d7,bl,blpol
LiquidCrystal_I2C lcd(0x27, 2, 1, 0, 4, 5, 6, 7, 3, POSITIVE);
// => connexion des 2 broches I2C sur l'Arduino Uno R3 : SDA en A4, SCL en A5

//
// SETUP
//_____________________________________________________________________________________________

void setup() {

  pinMode(broche_Fpri, INPUT);

// Calibration de Isor à définir expérimentalement suivant la sonde utilisée
  injection.current(broche_Isor, 9.85);    // Current: input pin, calibration.

// initialisation de l'affichage et du mode console
  Serial.begin(9600);            // préparation du moniteur série
  Serial.println ();
  Serial.println("ready ...");
  Serial.println ();

// initialisation du LCD
  lcd.begin(16,2);               // initialize the lcd for 16 chars 2 lines
  lcd.clear();
  lcd.setCursor(0, 0);
  lcd.print("*** BONJOUR ***");
  lcd.setCursor(0, 1);
  lcd.print("    *******");

  delay(1500);

}                                 // fin de setup

//
// LOOP
//_____________________________________________________________________________________________

void loop() {

// Calcul de Vprimaire
  B_Vpri = analogRead( broche_Vpri );
  Vpri = B_Vpri / conv_Vpri;

// Calcul de Iprimaire
  B_Ipri = analogRead( broche_Ipri );
```

```
  Ipri = abs(( B_Ipri * 5.0 / 1023.0 ) - 2.5 ) / conv_Ipri;

// Calcul de Isortie    //initialement Isor = injection.calcIrms(1480);
// https://openenergymonitor.org/forum-archive/node/846.html
//  Isor donne 0.06mA en l'absence de courant, dû au bruit des 2 derniers bits du CAN
//  donc on soustrait 0.06 à la lecture et on coupe la résolution à 0.01
  Isor = 0.01 * ( abs( int( 100 * (injection.calcIrms(1172) - Isor_offset))));

// Calcul de la vitesse de rotation Fpri
  duree_H = pulseIn(broche_Fpri, HIGH);
  duree_L = pulseIn(broche_Fpri, LOW);
  if( duree_H + duree_L > 1 ) { Fpri = 1000000.0/(duree_H + duree_L);}
  else { Fpri = 0;}

// Affichage des résultats sur le moniteur série
  Serial.println(" Vpri  | Ipri  || Isor  | Fpri ");
  Serial.print(Vpri);
  Serial.print("V | ");
  Serial.print(Ipri);
  Serial.print("A || ");
  Serial.print(Isor);
  Serial.print("A | ");
  Serial.print(Fpri);
  Serial.println("Hz ");

// Affichage du résultat sur le LCD
  lcd.setCursor(0, 0);
  lcd.print(String(Vpri,1));
  lcd.print("V ");
  if( Vpri < 10) { lcd.print(" ");}
  lcd.print("Pe=");
  if( Vpri*Ipri < 100) { lcd.print(" ");}
  if( Vpri*Ipri < 10) { lcd.print(" ");}
  lcd.print(String(Vpri*Ipri,1));
  lcd.print("W ");
  lcd.setCursor(0, 1);
  lcd.print(String(Fpri,0));
  lcd.print("Hz ");
  lcd.print(" Ps=");
  if( Vsor*Isor < 100) { lcd.print(" ");}
  if( Vsor*Isor < 10) { lcd.print(" ");}
  lcd.print(String(Vsor*Isor,1));
  lcd.print("VA");

}
```

6- Enregistrer ce programme sur le PC sous le nom de mesures_eolienne.ino par exemple.

7- Puis : Menu croquis -> téléverser.

8- Ouvrir le moniteur série :

Montage d'essai éteint :

```
 Vpri  | Ipri  || Isor  | Fpri
0.00V | 0.07A || -0.01A | 0.00Hz
 Vpri  | Ipri  || Isor  | Fpri
0.00V | 0.07A || 0.00A | 0.00Hz
 Vpri  | Ipri  || Isor  | Fpri
0.00V | 0.07A || 0.00A | 0.00Hz
```

Montage d'essai allumé :

```
 Vpri  | Ipri  || Isor  | Fpri
30.35V | 1.69A || 3.02A | 50.32Hz
 Vpri  | Ipri  || Isor  | Fpri
30.35V | 1.69A || 3.02A | 50.33Hz
 Vpri  | Ipri  || Isor  | Fpri
30.40V | 1.69A || 3.02A | 50.32Hz
```

Le montage d'essai éteint, ajuster :

- `const float Isor_offset = 0.06;` => pour obtenir Isor =0 (c'est au 1/100ème près !)

Le montage d'essai allumé, ajuster :

- `const float conv_Vpri = 20.2;` => pour Vpri = valeur du multimètre
- `injection.current(broche_Isor, 9.85);` => pour Isor = valeur du multimètre

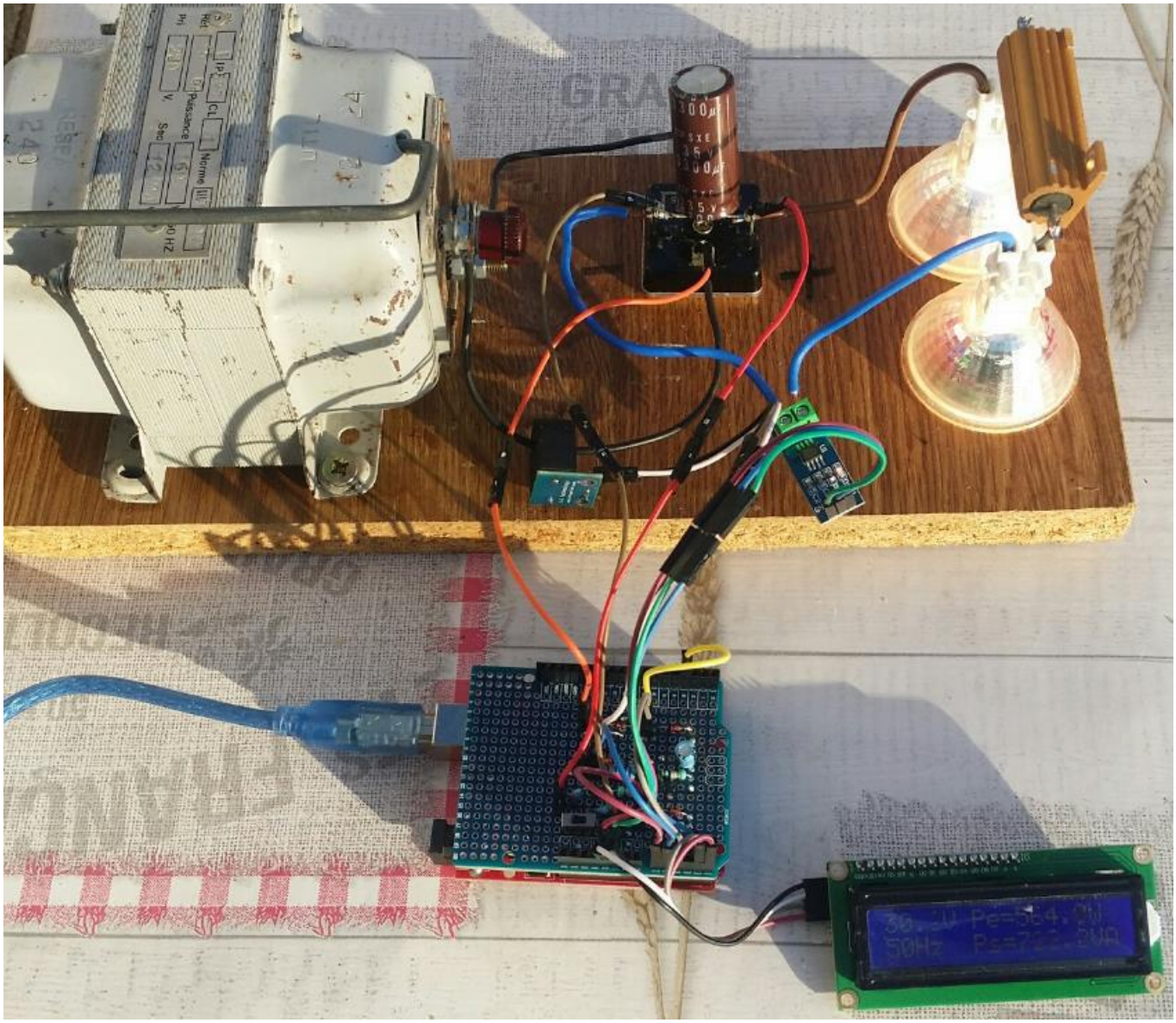

Mise en œuvre du module de carte SD et mesure du temps

Il eut été trop simple qu'il n'exista qu'une seule version de module de carte SD. Il en existe 2 ! La nouvelle qui utilise les librairies déjà installées sur le programme PC, et l'ancienne version … ET la carte dont j'ai donné le lien dans la liste des courses est l'ancienne version.

Il faut donc installer les bonnes librairies, et surtout retrouver *SD.h* et *SD.cpp* quelque part dans *C:\Program Files (x86)\Arduino\librairies\SD\src* et les renommer pour les rendre inutilisables, par exemple en leur ajoutant l'extension *.orig*.

Toutes les informations sont disponibles ici : https://learn.adafruit.com/adafruit-data-logger-shield/overview

La procédure pour installer la librairie : https://learn.adafruit.com/adafruit-data-logger-shield/for-the-mega-and-leonardo

Et le lien de téléchargement de la bibliothèque : https://github.com/adafruit/SD

Ensuite il faudra installer la librairie pour utiliser la partie RTC du module. Toutes les information sont disponibles ici : https://learn.adafruit.com/adafruit-data-logger-shield/using-the-real-time-clock

Et le lien de téléchargement de la bibliothèque : https://github.com/adafruit/RTClib/archive/master.zip

A l'aide d'une loupe il faudra regarder la référence du circuit de gestion du temps : *PCF8523* ou *DS1307.* Celui du lien donné en liste des courses est l'ancien modèle DS1307.

Ensuite à la 1ère utilisation du module, ou bien à chaque fois qu'elle n'est plus alimentée en énergie – il parait que la pile possède une durée de vie de 5 ans – il faudra programmer l'heure avec l'instruction :
`rtc.adjust(DateTime(2018, 10, 14, 14, 51, 0));` pour 14 octobre 2018 à 14h51. Sinon `rtc.isrunning()` ne se lance pas.

Test d'écriture de la date et l'heure sur la carte SD

1- Télécharger la librairie *SD.h* : https://github.com/adafruit/SD
2- Télécharger la librairie *RTClib.h* : https://app.box.com/s/czde88f5b9vpulhf8z56
3- Les déclarer : (In the Arduino IDE) Sketch > Include Library > Add .ZIP Library > select the downloaded file > Open
4- Ajouter l'extension *.orig* à *SD.h* et *SD.cpp* dans *C:\Program Files (x86)\Arduino\librairies\SD\src* et les renommer pour les rendre inutilisables.
5- Créer un nouveau programme avec le code ci-dessous :

```
// Date et l'heure enregistées sur carte SD

#include <Wire.h>
#include <RTClib.h>
#include <SPI.h>
#include <SD.h>

// On the Ethernet Shield, CS is pin 4. Note that even if it's not
// used as the CS pin, the hardware CS pin (10 on most Arduino boards,
// 53 on the Mega) must be left as an output or the SD library
// functions will not work.
const int chipSelect = 4;

File dataFile;

// Choix du modèle de RTC
RTC_DS1307 rtc;
//RTC_PCF8523 rtc;

char daysOfTheWeek[7][12] = {"Sunday", "Monday", "Tuesday", "Wednesday", "Thursday", "Friday",
"Saturday"};

void setup () {
  Serial.begin(9600);
  if(! rtc.begin()) { Serial.println("Couldn't find RTC"); while (1);}
//  if(! rtc.isrunning()) { Serial.println("RTC is NOT running!");

// Mise à l'heure du module qui ne sera fait qu'une seule fois :
// suivant le modèle suivant :
// pour 14 octobre 2018 à 15h30 :
  rtc.adjust(DateTime(2018, 10, 14, 15, 30, 0));
//  }

  Serial.print("Initializing SD card...");
  // make sure that the default chip select pin is set to
  // output, even if you don't use it:
  pinMode(SS, OUTPUT);

  // see if the card is present and can be initialized:
  if (!SD.begin(chipSelect)) {
    Serial.println("Card failed, or not present");
    // don't do anything more:
    while (1) ;
  }
  Serial.println("card initialized.");

  // Open up the file we're going to log to!
  dataFile = SD.open("datalog.txt", FILE_WRITE);
  if (! dataFile) {
    Serial.println("error opening datalog.txt");
    // Wait forever since we cant write data
    while (1) ;
  }
}

void loop () {
```

```
  // make a string for assembling the data to log:
  String dataString = "";

  DateTime now = rtc.now();

  dataString += String(daysOfTheWeek[now.dayOfTheWeek()]);
  dataString += ";";
  dataString += String(now.day(), DEC);
  dataString += ";";
  dataString += String(now.month(), DEC);
  dataString += ";";
  dataString += String(now.year(), DEC);
  dataString += ";";
  dataString += String(now.hour(), DEC);
  dataString += ";";
  dataString += String(now.minute(), DEC);
  dataString += ";";
  dataString += String(now.second(), DEC);

  dataFile.println(dataString);     // enregistre la ligne
  Serial.println(dataString);       // et l'affiche à la console

// The following line will 'save' the file to the SD card after every line of data
// this will use more power and slow down how much data you can read but it's safer!
// If you want to speed up the system, remove the call to flush() and it will save
// the file only every 512 bytes - every time a sector on the SD card is filled.
  dataFile.flush();

  delay(3000);
}
```

6- Effectuer la mise à jour de la ligne correspondante à la déclaration de la date et l'heure

7- Enregistrer ce programme sur le PC sous le nom de test_module_SD_RTC.ino par exemple.

8- Puis : Menu croquis -> téléverser.

9- Ouvrir le moniteur série, si les données sont bonnes insérer la pile dans son compartiment.

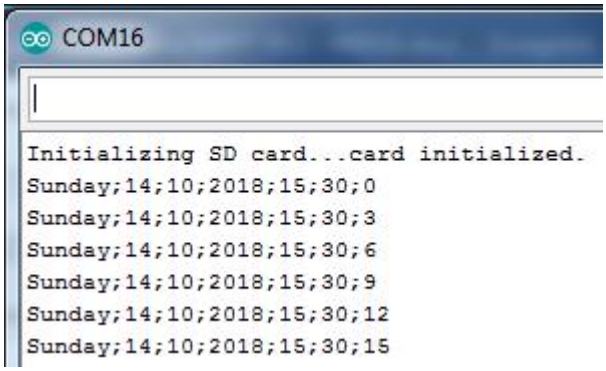

A noter : en principe ce programme n'est à exécuter qu'une fois, sinon la date et l'heure seront systématiquement réinitialisées à la valeur saisie.

Ensuite nous devons retrouver le même résultat dans le fichier *datafile.txt* présent sur la carte SD.

Programme final du banc de mesures avec enregistrement sur carte SD

```
/*

Banc de mesures pour éoliennes 24 ou 48V avec enregistrement sur carte SD
_____________________________________________________________________
|                                                                    |
|       auteur : Philippe de Craene <dcphilippe@yahoo.fr             |
|           pour l' Association P'TIWATT                             |
_____________________________________________________________________

Toute contribution en vue de l'amélioration de l'appareil est la bienvenue ! Il vous est juste
demandé de conserver mon nom et mon email dans l'entête du programme, et bien sûr de partager
avec moi cette amélioration. Merci.

*/

#include <Wire.h>
#include <LiquidCrystal_I2C.h> // https://app.box.com/s/czde88f5b9vpulhf8z56
// Attention ! Renomer la librairie d'origine de l'IDE LiquidCrystal.h et LiquidCrystal.cpp
#include <SD.h>                // https://github.com/adafruit/SD
// Attention ! Renomer la librairie d'origine de l'IDE SD.h et SD.cpp
#include <EmonLib.h>           // https://github.com/openenergymonitor/EmonLib
#include <RTClib.h>            // https://github.com/adafruit/RTClib/archive/master.zip
#include <SPI.h>

EnergyMonitor injection;       // Création de l'instance injection pour EmonLib.h
File dataFile;                 // Création de l'instance pour gérer le fichier sur SD

// Brochage des entrées des capteurs et paramétrage

const byte broche_Vpri = A0;   // broche lecture tension pont de diodes
const byte broche_Isor = A1;   // broche lecture courant d'injection
const byte broche_Ipri = A3;   // broche lecture courant pont de diodes
const byte broche_Fpri = 3;    // broche numérique calcul fréquence
// On the Ethernet Shield, CS is pin 4. Note that even if it's not used as the CS pin, the
// hardware CS pin must be left as an output or the SD library functions will not work.
const byte chipSelect  = 4;

// choisir le modèle d'éolienne 24V ou 48V à vérifier expérimentalement :
// éolienne 24V avec maxi à 54V => conv_Vpri = 20.2
// éolienne 48V avec maxi à 95V => conv Vpri = 11.2
const float conv_Vpri = 20.2;  // conversion bytes/tension pour éolienne 24V

// Choisir le modèle de sonde ACS712 :
// Module ACS712 de 5A => 0.185V/A
// Module ACS712 de 20A => 0.1V/A
// Module ACS712 de 30A => 0.066mV/A
const float conv_Ipri = 0.1;   //  pour modèle 20A

// Calibration de Isor à définir expérimentalement suivant la sonde utilisée
// => valeur à saisir dans le setup()
// offset pour supprimer le bruit pour avoir 0 en absence de courant
const float Isor_offset = 0.059;

// Choisir le modèle de RTC sur le module carte SD :
RTC_DS1307 rtc;
//RTC_PCF8523 rtc;

// Variables de traitement

float Vpri;                 // Tension au pont de diode
float Ipri;                 // Courant délivré au pont de diode
float Fpri;                 // Vitesse de rotation
int Vsor = 230;             // Tension du réseau
float Isor;                 // Courant injecté sur le réseau
unsigned long duree_H;      // durée de la demie période état haut
unsigned long duree_L;      // durée de la demie période état bas
int B_Vpri, B_Ipri;         // lecture des capteurs en bytes
byte prev_second = 0;       // pour le compteur

char daysOfTheWeek[7][12] = {"Sunday", "Monday", "Tuesday", "Wednesday", "Thursday", "Friday",
"Saturday"};

// Déclaration du LCD en mode I2C :
// toutes les infos ici : http://arduino-info.wikispaces.com/LCD-Blue-I2C
// Set the pins on the I2C chip used for LCD connections:
//                    addr, en,rw,rs,d4,d5,d6,d7,bl,blpol
LiquidCrystal_I2C lcd(0x27, 2, 1, 0, 4, 5, 6, 7, 3, POSITIVE);
// => connexion des 2 broches I2C sur l'Arduino Uno R3 : SDA en A4, SCL en A5

//
// SETUP
//_____________________________________________________________________________________________
```

```
void setup() {

  pinMode(broche_Fpri, INPUT);

// Calibration de Isor à définir expérimentalement suivant la sonde utilisée
  injection.current(broche_Isor, 8.35);    // Current: input pin, calibration.

// initialisation de l'affichage et du mode console
  Serial.begin(9600);            // préparation du moniteur série
  Serial.println ();
  if(! rtc.begin()) { Serial.println("RTC introuvable");}
  if(! rtc.isrunning()) { Serial.println("Date et heure à programmer sur le RTC");}
  Serial.print("Initializing SD card...");
// make sure that the default chip select pin is set to output, even if you don't use it:
  pinMode(SS, OUTPUT);
// see if the card is present and can be initialized:
  if (!SD.begin(chipSelect)) {  Serial.println("Card failed, or not present"); }
  else { Serial.println("card initialized."); }
// Open up the file we're going to log to!
  dataFile = SD.open("datalog.txt", FILE_WRITE);
  if (! dataFile) { Serial.println("erreur sur fichier datalog.txt"); }
  Serial.println("ready ...");
  Serial.println ();

// initialisation du LCD
  lcd.begin(16,2);               // initialize the lcd for 16 chars 2 lines
  lcd.clear();
  lcd.setCursor(0, 0);
  lcd.print("*** BONJOUR ***");
  lcd.setCursor(0, 1);
  lcd.print("    *******");

  delay(1500);

}                                  // fin de setup

//
// LOOP
//_____________________________________________________________________________________________

void loop() {

// Calcul de Vprimaire
  B_Vpri = analogRead( broche_Vpri );
  Vpri = B_Vpri / conv_Vpri;

// Calcul de Iprimaire
  B_Ipri = analogRead( broche_Ipri );
  Ipri = abs(( B_Ipri * 5.0 / 1023.0 ) - 2.5 ) / conv_Ipri;

// Calcul de Isortie    //initialement Isor = injection.calcIrms(1480);
// https://openenergymonitor.org/forum-archive/node/846.html
//  Isor donne 0.06mA en l'absence de courant, dû au bruit des 2 derniers bits du CAN
//  donc on soustrait 0.06 à la lecture et on coupe la résolution à 0.01
  Isor = 0.01 * ( abs( int( 100 * (injection.calcIrms(1172) - Isor_offset))));

// Calcul de la vitesse de rotation Fpri
  duree_H = pulseIn(broche_Fpri, HIGH);
  duree_L = pulseIn(broche_Fpri, LOW);
  if( duree_H + duree_L > 1 ) { Fpri = 1000000.0/(duree_H + duree_L);}
  else { Fpri = 0;}

  DateTime now = rtc.now();        // récupération de la date et l'heure
  if( now.second() != prev_second ) {    // toutes les secondes

// Affichage du résultat sur le LCD

    lcd.setCursor(0, 0);
    lcd.print(String(Vpri,1));
    lcd.print("V ");
    if( Vpri < 10) { lcd.print(" ");}
    lcd.print("Pe=");
    if( Vpri*Ipri < 100) { lcd.print(" ");}
    if( Vpri*Ipri < 10) { lcd.print(" ");}
    lcd.print(String(Vpri*Ipri,1));
    lcd.print("W ");
    lcd.setCursor(0, 1);
    lcd.print(String(Fpri,0));
    lcd.print("Hz ");
    lcd.print(" Ps=");
    if( Vsor*Isor < 100) { lcd.print(" ");}
    if( Vsor*Isor < 10) { lcd.print(" ");}
    lcd.print(String(Vsor*Isor,1));
    lcd.print("VA");

// Affichage du résultat sur carte SD
```

```
    if( Fpri > 0 ) {                // dès que l'éolienne tourne
      String dataString = "";       // initialisation d'une chaine de caractères
      dataString += String(daysOfTheWeek[now.dayOfTheWeek()]);
      dataString += ";";
      dataString += String(now.day(), DEC);
      dataString += ";";
      dataString += String(now.month(), DEC);
      dataString += ";";
      dataString += String(now.year(), DEC);
      dataString += ";";
      dataString += String(now.hour(), DEC);
      dataString += ";";
      dataString += String(now.minute(), DEC);
      dataString += ";";
      dataString += String(now.second(), DEC);
      dataString += ";";
      dataString += ";";
      dataString += String(Vpri);
      dataString += ";";
      dataString += String(Ipri);
      dataString += ";";
      dataString += String(Isor);
      dataString += ";";
      dataString += String(Fpri);
      dataFile.println(dataString);     // enregistre la ligne
      dataFile.flush();                 // l'enregistre sur SD
      Serial.println(dataString);       // et l'affiche à la console
    }      // fin test Fpri
    prev_second = now.second();
  }        // fin compteur de seconde
}          // fin de loop()
```

Analyse des mesures sur carte SD

Annexe A

Energy comparison of MPPT techniques for PV Systems

ROBERTO FARANDA, SONIA LEVA
Department of Energy
Politecnico di Milano
Piazza Leonardo da Vinci, 32 – 20133 Milano
ITALY
roberto.faranda, sonia.leva@polimi.it

Abstract: - Many maximum power point tracking techniques for photovoltaic systems have been developed to maximize the produced energy and a lot of these are well established in the literature. These techniques vary in many aspects as: simplicity, convergence speed, digital or analogical implementation, sensors required, cost, range of effectiveness, and in other aspects. This paper presents a comparative study of ten widely-adopted MPPT algorithms; their performance is evaluated on the energy point of view, by using the simulation tool Simulink®, considering different solar irradiance variations.

Key-Words: - Maximum power point (MPP), maximum power point tracking (MPPT), photovoltaic (PV), comparative study, PV Converter.

1 Introduction

Solar energy is one of the most important renewable energy sources. As opposed to conventional unrenewable resources such as gasoline, coal, etc..., solar energy is clean, inexhaustible and free. The main applications of photovoltaic (PV) systems are in either stand-alone (water pumping, domestic and street lighting, electric vehicles, military and space applications) [1-2] or grid-connected configurations (hybrid systems, power plants) [3].

Unfortunately, PV generation systems have two major problems: the conversion efficiency of electric power generation is very low (9÷17%), especially under low irradiation conditions, and the amount of electric power generated by solar arrays changes continuously with weather conditions.

Moreover, the solar cell V-I characteristic is nonlinear and varies with irradiation and temperature. In general, there is a unique point on the V-I or V-P curve, called the Maximum Power Point (MPP), at which the entire PV system (array, converter, etc…) operates with maximum efficiency and produces its maximum output power. The location of the MPP is not known, but can be located, either through calculation models or by search algorithms. Therefore Maximum Power Point Tracking (MPPT) techniques are needed to maintain the PV array's operating point at its MPP.

Many MPPT techniques have been proposed in the literature; examples are the Perturb and Observe (P&O) methods [4-7], the Incremental Conductance (IC) methods [4-8], the Artificial Neural Network method [9], the Fuzzy Logic method [10], etc... These techniques vary between them in many aspects, including simplicity, convergence speed, hardware implementation, sensors required, cost, range of effectiveness and need for parameterization.

The P&O and IC techniques, as well as variants thereof, are the most widely used.

In this paper, ten MPPT algorithms are compared under the energy production point of view: P&O, modified P&O, Three Point Weight Comparison [12], Constant Voltage (CV) [13], IC, IC and CV combined [13], Short Current Pulse [14], Open Circuit Voltage [15], the Temperature Method [16] and methods derived from it [16]. These techniques are easily implemented and have been widely adopted for low-cost applications. Algorithms such as Fuzzy Logic, Sliding Mode [11], etc…, are beyond the scope of this paper, because they are more complex and less often used.

The MPPT techniques will be compared, by using Matlab tool Simulink®, created by MathWorks, considering different types of insulation and solar irradiance variations. The partially shaded condition will not be considered: the irradiation is assumed to be uniformly spread over the PV array.

The PV system implementation takes into account the mathematical model of each component, as well as actual component specifications. In particular, without lack of generality, we will focus our attention on a stand-alone photovoltaic system constructed by connecting the dc/dc Single Ended Primary Inductor Converter (SEPIC) [17-18]

between the solar panel and the dc load as reported in Fig.1.

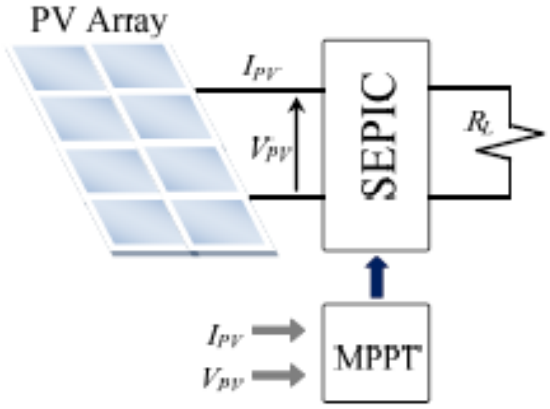

Fig. 1. Stand-alone PV system analyzed.

2 PV Array

A mathematical model is developed in order to simulate the PV array. Fig. 2 gives the equivalent circuit of a single solar cell, where I_{PV} and V_{PV} are the PV array's current and voltage, respectively, I_{ph} is the cell's photocurrent, R_j represents the nonlinear resistance of the p-n junction, and R_{sh} and R_s are the intrinsic shunt and series resistances of the cell.

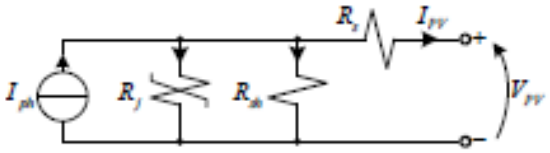

Fig. 2. Equivalent circuit of PV cell

Since R_{sh} is very large and R_s is very small, these terms can be neglected in order to simplify the electrical model. The following equation then describes the PV panel [8]:

$$I_{PV} = n_p \cdot I_{ph} - n_p \cdot I_{rs} \cdot \left[\exp\left(\frac{q}{k \cdot T \cdot A} \cdot \frac{V_{PV}}{n_s} \right) - 1 \right] \quad (1)$$

where n_s and n_p are the number of cells connected in series and the in parallel, q=1.602·10^{-19} C is the electron charge, k=1.3806·10^{-23} J·K^{-1} is Boltzman's constant, A=2 is the p-n junction's ideality factor, T is the cell's temperature (K), I_{ph} is the cell's photocurrent (it depends on the solar irradiation and temperature), and I_{rs} is the cell's reverse saturation current (it depends on temperature).

The PV panel here considered is a typical 50W PV module composed by n_s=36 series-connected polycrystalline cells (n_p=1). Its main specifications are shown in Table 1 while Fig. 2 and Fig. 3 show the power output characteristics of the PV panel as functions of irradiance and temperature, respectively. These curves are nonlinear and are crucially influenced by solar radiation and temperature.

The PV array is composed of three strings in parallel, each string consisting of 31 PV panels in series. The total power is 4650W.

Table 1. Electrical characteristics of PV panel with an irradiance level of 1000 W/m^2

Symbol	Quantity	Value
P_{MPP}	Maximum Power	50 W
V_{MPP}	Voltage at P_{MPP}	17.3 V
I_{MPP}	Voltage at I_{MPP}	2.89 A
I_{SC}	Short-Circuit Current	3.17 A
V_{OV}	Open-Circuit Voltage	21.8 V
T_{SC}	Temperature coefficient of I_{SC}	(0.065±0.015)%/°C
T_{OC}	Temperature coefficient of V_{OC}	-(80±10) mV/°C

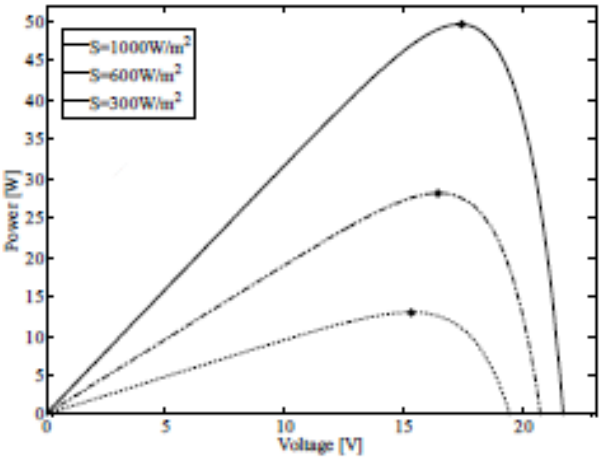

Fig. 3. V-P panel characteristics for three different irradiance levels. Each point represents the MPP of related curve.

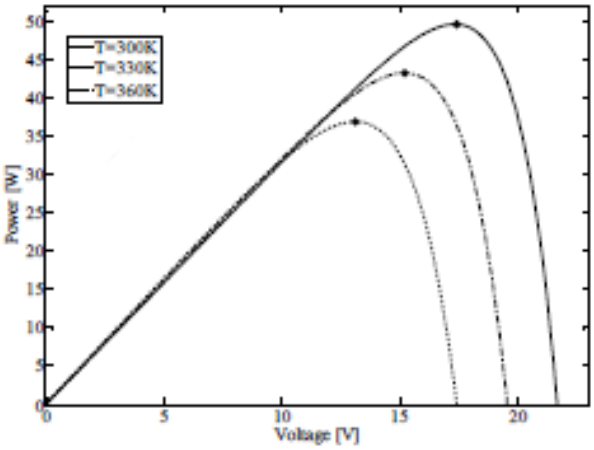

Fig. 4. V-P panel characteristics for three different temperature levels. Each point represents the MPP of related curve.

3 MPPT Control Algorithm

As known the output power characteristics of the PV system as functions of irradiance and temperature curves are nonlinear and are crucially influenced by solar irradiation and temperature. Furthermore, the daily solar irradiation diagram has abrupt variations during the day, as shown in Fig. 5. Under these conditions, the MPP of the PV array changes continuously; consequently the PV system's operating point must change to maximize the energy produced. An MPPT technique is therefore used to maintain the PV array's operating point at its MPP.

There are many MPPT methods available in the literature; the most widely-used techniques are described in the following sections, starting with the simplest method.

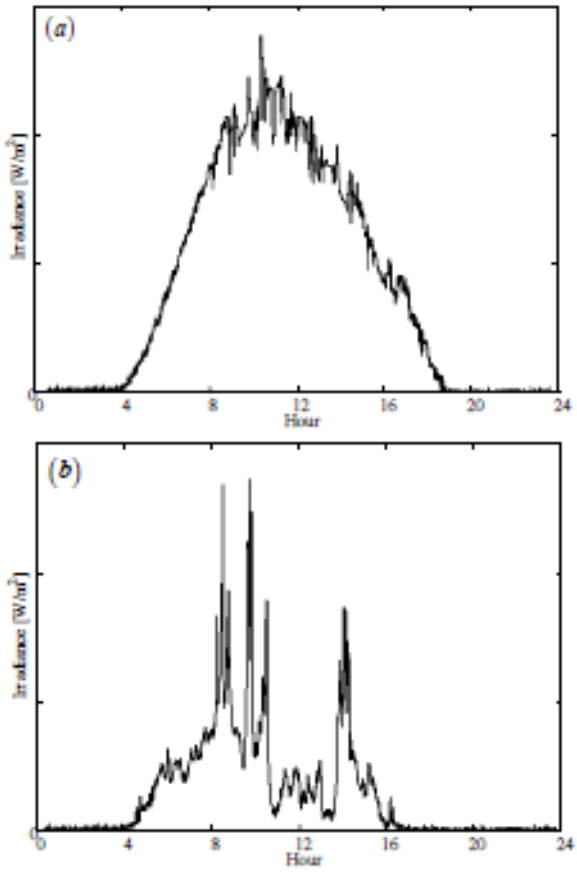

Fig. 5. Daily solar irradiation diagram: (a) sunny day (b) cloudy day.

3.1 Constant Voltage Method

The Constant Voltage (CV) algorithm is the simplest MPPT control method. The operating point of the PV array is kept near the MPP by regulating the array voltage and matching it to a fixed reference voltage V_{ref}. The V_{ref} value is set equal to the V_{MPP} of the characteristic PV module (see Table 1) or to another calculated best fixed voltage. This method assumes that individual insulation and temperature variations on the array are insignificant, and that the constant reference voltage is an adequate approximation of the true MPP. Operation is therefore never exactly at the MPP and different data has to be collected for different geographical regions.

The CV method does not require any input. However, measurement of the voltage V_{PV} is necessary in order to set up the duty-cycle of the dc/dc SEPIC by PI regulator, as shown in the block diagram of Fig. 6.

It is important to observe that when the PV panel is in low insulation conditions, the CV technique is more effective than either the P&O method or the IC method (analyzed below) [13]. Thanks to this characteristic, CV is sometime combined together with other MPPT techniques.

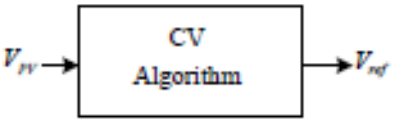

Fig. 6. CV block diagram.

3.2 Short-Current Pulse Method

The Short-Current Pulse (SC) method achieves the MPP by giving the operating current I_{op} to a current-controlled power converter. In fact, the optimum operating current I_{op} for maximum output power is proportional to the short-circuit current I_{SC} under various conditions of irradiance level S as follows:

$$I_{op}(S) = k \cdot I_{SC}(S) \qquad (2)$$

where k is a proportional constant. Eq. (2) shows that I_{op} can be determined instantaneously by detecting I_{SC}. The relationship between I_{op} and I_{SC} is still proportional, even though the temperature varies from 0°C to 60°C. The proportional parameter is estimated to be approximately 92% [14].

Therefore, this control algorithm requires measurements of the current I_{SC}. To obtain this measurement, it is necessary to introduce a static switch in parallel with the PV array, in order to create the short-circuit condition. It is important to note that during the short-circuit V_{PV}=0 consequently no power is supplied by the PV system and no energy is generated. As in the previous technique, measurement of the PV array voltage V_{PV} is required for the PI regulator (see Fig. 7) in order to obtain the V_{ref} value able to generate the current I_{op}.

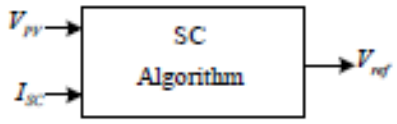

Fig. 7. SC block diagram.

3.3 Open Voltage Method

The Open Voltage (OV) method is based on the observation that the voltage of the maximum power point is always close to a fixed percentage of the open-circuit voltage. Temperature and solar insulation levels change the position of the maximum power point within a 2% tolerance band.

In general, the OV technique uses 76% of the open-circuit voltage V_{OV} as the optimum operating voltage V_{op} (at which the maximum output power can be obtained).

This control algorithm requires measurements of the voltage V_{OV} (see Fig. 8). Here again it is necessary to introduce a static switch into the PV array; for the OV method, the switch must be connected in series to open the circuit. When I_{PV}=0 no power is supplied by the PV system and consequently the total energy generated by the PV system is reduced. Also in this method measurement of the voltage V_{PV} is required for the PI regulator.

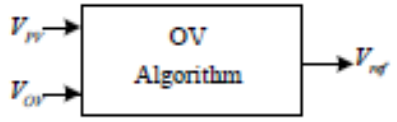

Fig. 8. OV block diagram.

3.4 Perturb and Observe Methods

The P&O algorithms operate by periodically perturbing (i.e. incrementing or decrementing) the array terminal voltage or current and comparing the PV output power with that of the previous perturbation cycle. If the PV array operating voltage changes and power increases ($dP/dV_{PV}>0$), the control system moves the PV array operating point in that direction; otherwise the operating point is moved in the opposite direction. In the next perturbation cycle the algorithm continues in the same way.

A common problem in P&O algorithms is that the array terminal voltage is perturbed every MPPT cycle; therefore when the MPP is reached, the output power oscillates around the maximum, resulting in power loss in the PV system. This is especially true in constant or slowly-varying atmospheric conditions.

Furthermore, P&O methods can fail under rapidly changing atmospheric conditions (see Fig. 9). Starting from an operating point A, if atmospheric conditions stay approximately constant, a perturbation ΔV the voltage V will bring the operating point to B and the perturbation will be reversed due to a decrease in power. However, if the irradiance increases and shifts the power curve from P_1 to P_2 within one sampling period, the operating point will move from A to C. This represents an increase in power and the perturbation is kept the same. Consequently, the operating point diverges from the MPP and will keep diverging if the irradiance steadily increases.

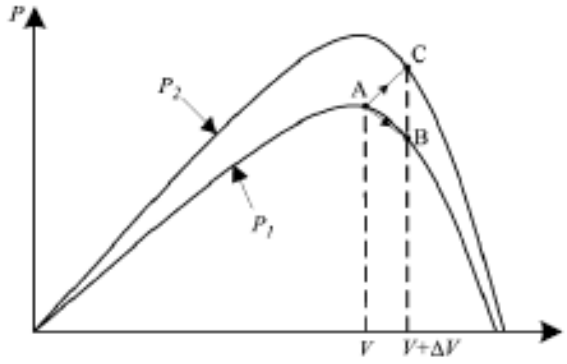

Fig. 9. Divergence of P&O from MPP [19].

There are many different P&O methods available in the literature. In this paper we consider the classic, the optimized and the three-points weight comparison algorithms.

In the classic P&O technique (P&Oa), the perturbations of the PV operating point have a fixed magnitude. In our analysis, the magnitude of perturbation is 0.37% of the PV array V_{OV} (around 2V)

In the optimized P&O technique (P&Ob), an average of several samples of the array power is used to dynamically adjust the perturbation magnitude of the PV operating point.

In the three-point weight comparison method (P&Oc), the perturbation direction is decided by comparing the PV output power on three points of the P-V curve. These three points are the current operation point (A), a point B perturbed from point A, and a point C doubly perturbed in the opposite direction from point B.

All three algorithms require two measurements: a measurement of the voltage V_{PV} and a measurement of the current I_{PV} (see Fig. 10).

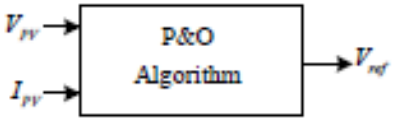

Fig. 10. P&O block diagram.

3.5 Incremental Conductance Methods

The Incremental Conductance (IC) algorithm is based on the observation that the following equation holds at the MPP [4]:

$$\left(\frac{dI_{PV}}{dV_{PV}}\right)+\left(\frac{I_{PV}}{V_{PV}}\right)=0 \qquad (3)$$

where I_{PV} and V_{PV} are the PV array current and voltage, respectively.

When the optimum operating point in the P-V plane is to the right of the MPP, we have $(dI_{PV}/dV_{PV})+(I_{PV}/V_{PV})<0$, whereas when the optimum operating point is to the left of the MPP, we have $(dI_{PV}/dV_{PV})+(I_{PV}/V_{PV})>0$.

The MPP can thus be tracked by comparing the instantaneous conductance I_{PV}/V_{PV} to the incremental conductance dI_{PV}/dV_{PV}. Therefore the sign of the quantity $(dI_{PV}/dV_{PV})+(I_{PV}/V_{PV})$ indicates the correct direction of perturbation leading to the MPP. Once MPP has been reached, the operation of PV array is maintained at this point and the perturbation stopped unless a change in dI_{PV} is noted. In this case, the algorithm decrements or increments V_{ref} to track the new MPP. The increment size determines how fast the MPP is tracked.

Through the IC algorithm it is therefore theoretically possible to know when the MPP has been reached, and thus when the perturbation can be stopped. The IC method offers good performance under rapidly changing atmospheric conditions.

There are two main different IC methods available in the literature.

The classic IC algorithm (ICa) requires the same measurements shown in Fig.10, in order to determine the perturbation direction: a measurement of the voltage V_{PV} and a measurement of the current I_{PV}.

The Two-Model MPPT Control (ICb) algorithm combines the CV and the ICa methods: if the irradiation is lower than 30% of the nominal irradiance level the CV method is used, other way the ICa method is adopted. Therefore this method requires the additional measurement of solar irradiation S as shown in Fig. 11.

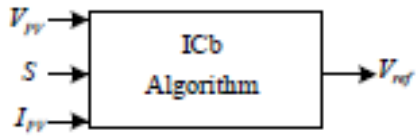

Fig. 11. ICb block diagram.

3.6 Temperature Methods

The open-circuit voltage V_{OV} of the solar cell varies mainly with the cell temperature, whereas the short-circuit current is directly proportional to the irradiance level (Fig. 12), and is relatively steady over cell temperature changes (Fig. 13).

The open-circuit voltage V_{OV} can be described through the following equation [16]:

$$V_{OV} \cong V_{OVSTC}+\frac{dV_{OV}}{dT}\cdot\left(T-T_{STC}\right) \qquad (4)$$

where V_{OVSTC}=21.8V is the open-circuit voltage under Standard Test Conditions (STC), (dV_{OV}/dT)=-0.08V/K is the temperature gradient, and T_{STC} is the cell temperature under STC. On the other hand, the MPP voltage, V_{MPP}, in any operating condition can be described through the following equation:

$$V_{MPP} \cong \left[\left(u+S\cdot v\right)-T\cdot\left(w+S\cdot y\right)\right]\cdot V_{MPP\_STC} \qquad (5)$$

where V_{MPP_STC} is the MPP voltage under STC. Table 2 shows the parameters of the optimal voltage equation (5) in relation to the irradiance level S.

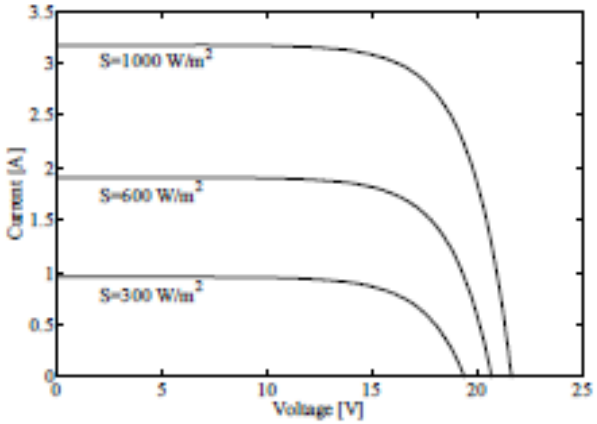

Fig. 12. V-I characteristics for three different irradiance levels.

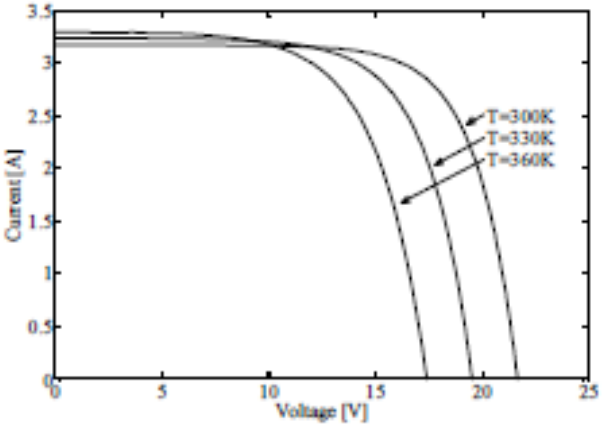

Fig. 13. V-I characteristics for three different temperatures.

There are two different temperature methods available in the literature.

The Temperature Gradient (TG) algorithm uses

the temperature T to determine the open-circuit voltage V_{OV} from equation (4). The MPP voltage V_{MPP} is then determined as in the OV technique, avoiding power losses. TG requires the measurement of the temperature T and a measurement of the voltage V_{PV} for the PI regulator (see Fig. 14 a).

Table 2. Parameters of the optimal voltage equation

S (kW/m^2)	$u(S)$	$v(S)$	$w(S)$	$y(S)$
0.1÷0.2	0.43404	0.1621	0.00235	-6e-4
0.2÷0.3	0.45404	0.0621	0.00237	-7e-4
0.3÷0.4	0.46604	0.0221	0.00228	-4e-4
0.4÷0.5	0.46964	0.0131	0.00224	-3e-4
0.5÷0.6	0.47969	-0.0070	0.00224	-3e-4
0.6÷0.7	0.48563	-0.0169	0.00218	-2e-4
0.7÷0.8	0.49270	-0.0270	0.00239	-5e-4
0.8÷0.9	0.49190	-0.0260	0.00223	-3e-4
0.9÷1.0	0.49073	-0.0247	0.00205	-1e-4

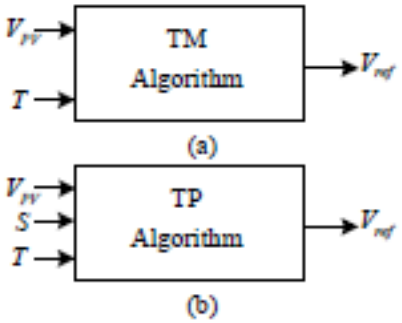

Fig. 14. (a) TM block diagram; (b) TP block diagram.

The Temperature Parametric equation method (TP) adopts equation (5) and determines the MPP voltage instantaneously by measuring T and S. TP requires, in general, also the measurement of solar irradiance S (see Fig. 13 b).

4 Simulation and Numerical Results

Fig. 4 shows that abrupt variations of solar irradiation can occur over short time intervals. For this reason, the analysis presented in this paper assumes that solar irradiation changes according to the diagrams show in Fig. 15.

The following different type of solar insulation are used to test the MPPT techniques at different operating conditions: step inputs (Fig. 15 a-d), ramp inputs (Fig. 15 e-h), rectangular impulse inputs (Fig. 15 i-l), triangular impulse input (Fig. 15 m), and two-step input (Fig. 15 n). The inputs in Fig. 15 simulate the time variation of irradiance on a PV array, for example, on a train roof during its run or on a house roof on a cloudy day, and so on.

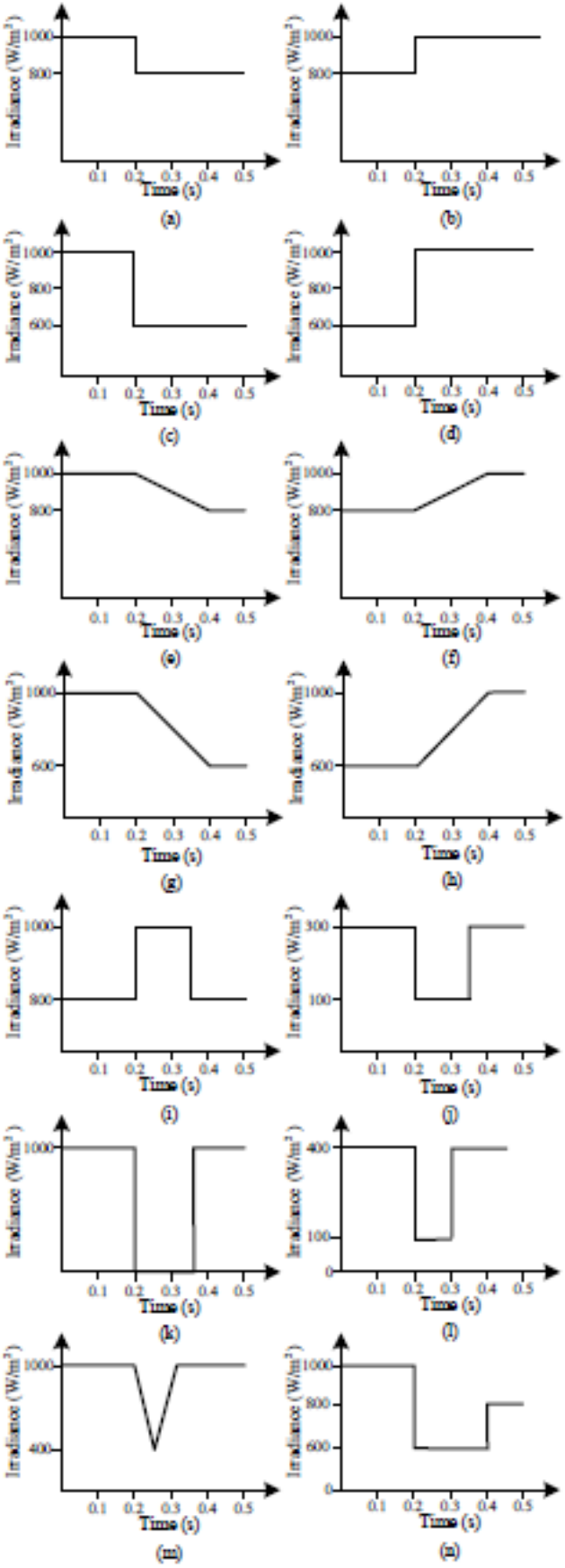

Fig. 15. Solar irradiance variations.

In order to analyze the temperature methods, we describe the variation of temperature on a PV array

Table 3. Energy generated as function of MPPT technique and irradiance input

Input	Theoretical Energy [J]	CV [J]	SC [J]	OV [J]	P&Oa [J]	P&Ob [J]	P&Oc [J]	ICa [J]	ICb [J]	TG [J]	TP [J]
(a)	1711	1359	1539	1627	1695	1707	1490	**1708**	**1708**	1562	1681
(b)	1785	1410	1687	1700	1774	1781	1558	**1782**	**1782**	1643	1761
(c)	1481	1192	1337	1403	1465	1476	1301	**1478**	**1478**	1311	1424
(d)	1633	1290	1492	1552	1625	**1628**	1416	**1628**	**1628**	1476	1589
(e)	1785	1403	1659	1699	1769	1780	1543	**1782**	**1782**	1643	1762
(f)	1711	1363	1636	1630	1692	1697	1508	**1709**	**1709**	1563	1683
(g)	1633	1298	1351	1552	1617	1627	1432	**1630**	**1630**	1477	1593
(h)	1482	1204	1397	1409	1441	1431	1311	**1479**	**1479**	1314	1429
(i)	1674	1339	1562	1595	1664	1671	1480	**1672**	**1672**	1522	1642
(j)	457	386.2	398.4	401.1	445.2	**446.3**	437.5	411.6	**446.3**	354.8	354.8
(k)	1354	1036	1247	1245	1332	**1343**	1153	1250	1333	1259	1338
(l)	540	459	427	479	524	**525**	515	469	503	397	444
(m)	1819	1410	1589	1730	1801	**1812**	1567	1808	1810	1681	1795
(n)	1558	1248	1388	1478	1542	1553	1370	**1555**	**1555**	1395	1510
Total	20623	16397	18709	19500	20386	20477	18081	20361	20515	18597	20005
%	100	79.51	90.72	94.56	98.85	99.29	87.68	98.73	99.48	90.18	97.01
Ranking		10	7	6	3	2	9	4	1	8	5

accordingly to the equivalent circuit shown in Fig. 16. If the temperature is uniformly distributed, the following differential equation can be used as temperature model [16]:

$$S = \frac{T}{R} + C \cdot \frac{dT}{dt} \tag{6}$$

where R=0.0435m^{2}K/W is the thermal resistance and C=15.71·10^{-3}J/m^{2}K is the thermal capacitance.

For each MPPT technique and for each input, the energy supplied by the PV system was calculated over a time interval of 0.5s. The results are shown in Table 3. For each input, the minimum (underlined), maximum (bolded) obtained energy values are indicated. The theoretical energy that a PV system could produce with an ideal MPPT technique is also reported.

From the data in Table 3, we note that the P&O and IC algorithms are superior to the other methods and have very similar performance and energy production. This is confirmed by their widespread use in commercial implementations.

The ICb technique provides the greatest energy supply for eleven of the fourteen inputs considered. In particular, Fig. 17 shows the power generated by the PV system using the ICa and ICb algorithms on the input in Fig. 15c. Note that the output of the ICb method has the same shape as the solar insulation input, the only difference is a small transient from the rapid insulation variation. The same trend is obtained using P&Oa and P&Ob techniques.

Comparing the two different IC techniques for very low irradiance values, it can be observed that the ICb method is more advantageous than the ICa method when the solar insulation has a value less than 300W/m^2 (for the input in Fig. 15j, E_{ICb}(j) is 446.3J while E_{ICa}(j) is 411.6J).

The behavior of the P&Oc technique is very different from that of the other two P&O techniques. Its time trend is the same as in Fig. 17, but its energy supply is lower than those of the other P&O algorithms. This result is explained by the fact that an additional MPPT cycle is needed to choose the perturbation direction so doing the P&Oc is slow respect to the other methods.

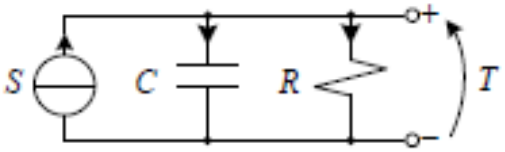

Fig. 16. Equivalent thermal circuit.

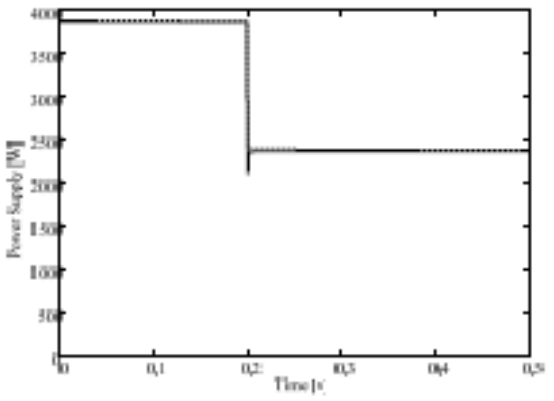

Fig. 17. Power generated by the PV array in the case of input (c): ICa and ICb methods (solid line) and ideal (dashed line) MPPT method.

The OV and SC techniques require an additional static switch, yet they provide low energy supply with respect to the P&O and IC algorithms. This is mainly due to power annulment during electronic switching (see Fig. 18 with the irradiance input of Fig. 15c). Furthermore, the OV and SC algorithms do not follow the instantaneous time trend, because the step in the irradiance variation occurs between two consecutive electronic switching. In fact, these techniques cannot calculate the new MPP, until the new level of solar insulation is measured.

Moreover, for these techniques the choice of sampling period is very critical; if the period is too short, energy production will be very low because of the increased number of electronic switching. If the period is too long, on the other hand, the MPP cannot be closely followed when rapid irradiance variation occurs.

The efficiency of the OV and SC techniques (shown in Fig. 18) could be improved by adding the open circuit or short circuit switch only to few PV panels instead of the complete PV system. On the other hand, this solution is disadvantageous if the selected PV panels are shadowed.

Moreover the presence of an additional switch increase the losses and consequently reduce their performance.

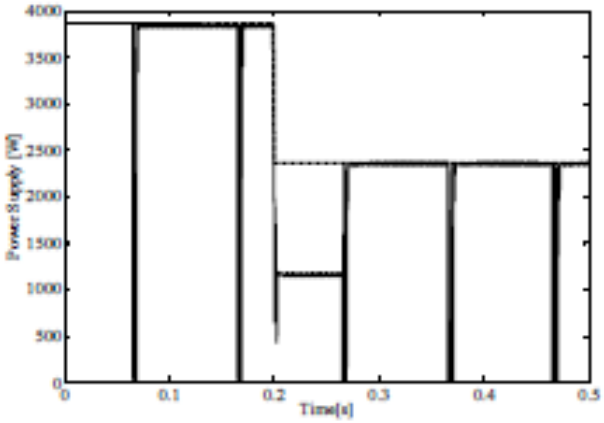

Fig. 18. Power generated by the PV array in the case of input (c): SC (solid line) and ideal (dashed line) MPPT method.

As other MPPT algorithms, which cyclically perturb the system, also the temperature methods continuously calculate and update the voltage reference.

In particular, the TP method provides only slightly less energy than the P&O and IC techniques. Instead, the TG method does not have the same efficiency since equation (4) calculates the open-circuit voltage rather than the actual optimal voltage: the error introduced through the open-circuit voltage calculation (absent in the TP algorithm) must be summed with the error introduced in the voltage reference computation.

Finally, the CV technique is the worst of the ten MPPT methods analyzed here. In fact, this technique does not follow the MPP, but instead fixes the reference voltage to the optimal voltage under STC or to another best fixed voltage, holding it constant under any operating condition. Fig. 19 shows the PV system power supply using the CV technique, with the irradiance input shown in Fig. 15c. With respect to the ICb technique (Fig. 17), very low power is generated. Fig. 20 shows the PV array power supply using the CV technique, with the case input (n). With respect to the instantaneous time trend (Fig. 20), very low power is generated.

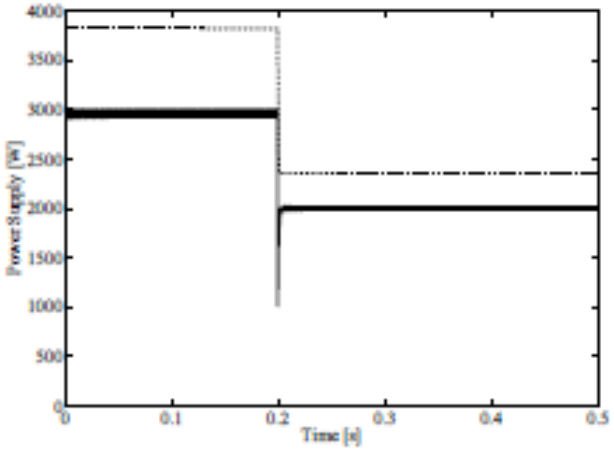

Fig. 19. Power generated by the PV array in the case of input (c): CV (solid line) and ideal (dashed line) MPPT method.

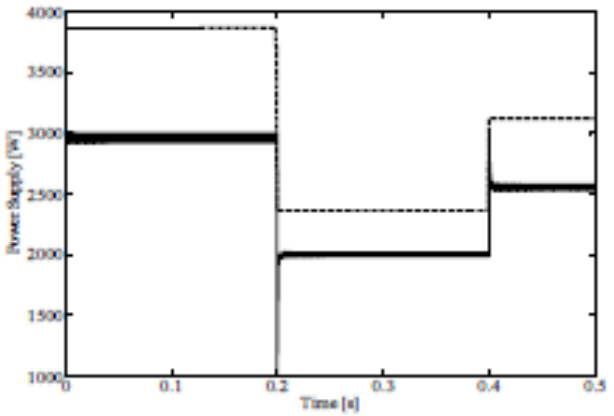

Fig. 20. Power generated by the PV array in the case of input (n): CV (solid line) and ideal (dashed line) MPPT method.

In the last row of Table 3 a ranking is proposed of the different MPPT techniques analyzed based on the sum of the energy generated in the different irradiance conditions. This ranking is only qualitative; in fact the energy contents differ for the various irradiance inputs. Nevertheless, the rankings obtained considering single inputs are substantially comparable to the total energy rankings.

5 Costs Comparison

To complete our analysis a simple discussion about the cost of the MPPT technique is presented [20]. A satisfactory MPPT costs comparison can be carried out by knowing the technique (analogical or digital) adopted in the control device, the number of sensors, and the use of additional power component, considering the other costs (power components, electronic components, boards, etc…) equal for all the devices.

The MPPT implementation typology greatly depends on the end-users' knowledge, with analogical circuit, SC, OV, or CV are good options, otherwise with digital circuit that require the use of microcontroller, P&O, IC, and temperature methods are enough easily to implement. Moreover it is important to underline that analogical implementations are generally cheaper than digital (the microcontroller and relative program are expensive). To make all the cost comparable between them, the computation cost comparison is formulated taking into account the present spread of MPPT methods.

The number of sensors required to implement the MPPT technique also affects the final costs. Most of the time, it is easier and more reliable to measure voltage than current and the current sensors are usually more expensive and bulky. The irradiance or temperature sensors are very expensive and uncommon.

After these considerations, Table 4 proposes a simplified classification considering the costs of sensors, microcontroller and the additional power components.

Table 4. Cost evaluation.
(A=absent, L=low, M=medium, H=high)

	COST			
MPPT	Additional power component	Sensor	Microcontroller computation	Total
CV	A	L	A/L	L
SC	H	M	A/L	M
OV	H	L/M	A/L	L/M
P&Oa	A	M	L	L/M
P&Ob	A	M	L	L/M
P&Oc	A	M	M	M
ICa	A	M	M	M
ICb	A	H	M/H	H
TG	A	M/H	M	M/H
TP	A	H	M/H	H

6 Conclusion

This paper has presented a comparison among ten different Maximum Power Point Tracking techniques in relation to their performance and implementation costs. In particular, fourteen different types of solar insulation are considered, and the energy supplied by a complete PV array is calculated; furthermore, regarding the MPPT implementation costs, a cost comparison is proposed taking into consideration the costs of sensors, microcontroller and additional power components.

A ranking of the ten methods has been proposed. Taking into account the analysis results along with hardware and computational costs, the P&Ob and ICa methods receive the best rankings.

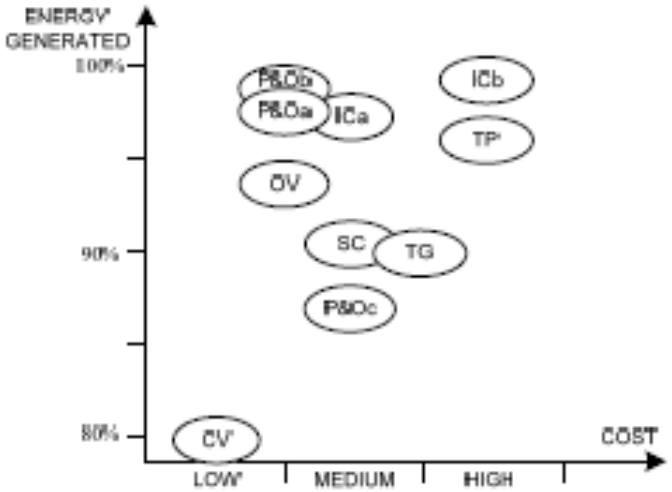

Fig. 21. Synthesis of the result of Tables IV and V.

The results, reassumed in Fig. 21, indicate that the P&O and IC algorithms are in general the most efficient of the analysed MPPT techniques. Furthermore, P&O and ICa methods do not require additional static switches, as opposed to the SC and OV techniques, therefore the relative costs are not high. The P&Oc method, unlike the other P&O methods, has low efficiency because of its lack of speed in tracking the MPP. Although the ICb method has the greatest efficiency, this does not justify the cost of using one more sensor than the ICa method. In fact, the two IC techniques have very similar efficiency but ICb have e higher implementation cost respect to ICa.

Finally, taking into consideration the TP temperature techniques, they present two main inconveniences:

- variations in the Table 2 parameters create errors in the V_{MPP} evaluation;
- the measured temperature may be affected by phenomena unrelated to the solar irradiation.

Further research on this subject should focus on experimental comparisons between these techniques, especially under shadow conditions.

References:

[1] S. Leva, D. Zaninelli, Technical and Financial Analysis for Hybrid Photovoltaic Power Generation Systems, *WSEAS Transactions on Power Systems*, vol.5, no.1, May 2006, pp.831-838

[2] S. Leva, D. Zaninelli, R. Contino, Integrated renewable sources for supplying remote power systems, *WSEAS Transactions on Power Systems*, vol.2, no.2, February 2007, pp.41-48

[3] J.Schaefer, Review of Photovoltaic Power Plant Performance and Economics, *IEEE Trans. Energy Convers.*, vol. EC-5,pp. 232-238, June, 1990.

[4] N.Femia, D.Granozio, G.Petrone, G.Spaguuolo, M.Vitelli, Optimized One-Cycle Control in Photovoltaic Grid Connected Applications, *IEEE Trans. Aerosp. Electron. Syst.*, vol. 2, no 3, July 2006.

[5] W. Wu, N. Pongratananukul, W. Qiu, K. Rustom, T. Kasparis and I. Batarseh, DSP-based Multiple Peack Power Tracking for Expandable Power System, *Proc. APEC*, 2003, pp. 525-530.

[6] C. Hua and C. Shen, Comparative Study of Peak Power Tracking Techniques for Solar Storage System, *Proc. APEC*, 1998, pp. 679-685.

[7] D.P.Hohm and M.E.Ropp, Comparative Study of Maximum Power Point Tracking Algorithms Using an Experimental, Programmable, Maximum Power Point Tracking Test Bed, *Proc. Photovoltaic Specialist Conference*, 2000, pp. 1699-1702.

[8] K.H.Hussein, I.Muta, T.Hoshino and M.osakada Maximum Power Point Tracking: an Algorithm for Rapidly Chancing Atmospheric Conditions, *IEE Proc.-Gener. Transm. Distrib.*, vol. 142, no.1, pp. 59-64, January, 1995.

[9] X.Sun, W.Wu, Xin Li and Q.Zhao, A Research on Photovoltaic Energy Controlling System with Maximum Power Point Tracking, *Power Conversion Conference*, 2002, pp. 822-826.

[10] T.L. Kottas, Y.S.Boutalis and A. D. Karlis, New Maximum Power Point Tracker for PV Arrays Using Fuzzy Controller in Close Cooperation with Fuzzy Cognitive Network, *IEEE Trans. Energy Conv.*, vol.21, no.3, 2006.

[11] A. El Jouni, R. El-Bachtiri and J. Boumhidi, Sliding Mode Controller for the Maximum Power Point Tracking of a Photovoltaic Pumping System, *WSEAS Transactions on Power Systems*, vol.1, no.10, pp. 1675-1680, 2006.

[12] Y.T.Hsiao and C.H.Chen, Maximum Power Tracking for Photovoltaic Power System, *Proc. Industry Application Conference*, 2002, pp. 1035-1040.

[13] G.J.Yu, Y.S.Jung, J.Y.Choi, I.Choy, J.H.Song and G.S.Kim, A Novel Two-Mode MPPT Control Algorithm Based on Comparative Study of Existing Algorithms, *Proc. Photovoltaic Specialists Conference*, 2002, pp. 1531-1534.

[14] T.Noguchi, S.Togashi and R.Nakamoto, Short-Current Pulse-Based Maximum-Power-Point Tracking Method for Multiple Photovoltaic-and-Converter Module System, *IEEE Trans. Ind. Electron.*, vol.49, no.1, pp. 217-223, 2002.

[15] D.Y. Lee, H.J. Noh, D.S. Hyun and I.Choy, An Improved MPPT Converter Using Current Compensation Method for Small Scaled PV-Applications, *Proc. APEC*, 2003, pp.540-545.

[16] M.Park and I.K. Yu, A Study on Optimal Voltage for MPPT Obtained by Surface Temperature of Solar Cell, *Proc. IECON*, 2004, pp. 2040-2045.

[17] F. Castelli Dezza, M. Diforte, R. Faranda, Control strategy for a single phase solution able to improve power quality in DG applications, *Proc. PELINCEC*, 2005

[18] F. Castelli Dezza, M. Diforte, R. Faranda, A solar converter for distributed generation able to improve the power quality supply, *Proc. 18th International Conference on Electricity Distribution*, Turin (Italy), June 2005

[19] O. Wasynczuk, Dynamic behavior of a class of photovoltaic power systems, *IEEE Trans. Power App. Syst.*, vol. 102, no. 9, pp. 3031–3037, Sep. 1983

[20] T. Esram, and P.L. Chapman, Comparison of Photovoltaic Array Maximum Power Point Tracking Techniques, *IEEE Trans. Energy Conv.*, vol.22, no.2, June, 2007, pp.439-449

Available online at www.sciencedirect.com
ScienceDirect
Solar Energy 84 (2010) 79–89
SOLAR ENERGY
www.elsevier.com/locate/solener

A reliable, fast and low cost maximum power point tracker for photovoltaic applications

J.M. Enrique *, J.M. Andújar, M.A. Bohórquez

Departamento de Ingeniería Electrónica, de Sistemas Informáticos y Automática, Universidad de Huelva, Spain

Received 19 February 2009; received in revised form 22 July 2009; accepted 16 October 2009
Available online 14 November 2009

Communicated by: Associate Editor Elias Stefanakos

Abstract

This work presents a new maximum power point tracker system for photovoltaic applications. The developed system is an analog version of the "P&O-oriented" algorithm. It maintains its main advantages: simplicity, reliability and easy practical implementation, and avoids its main disadvantages: inaccurateness and relatively slow response. Additionally, the developed system can be implemented in a practical way at a low cost, which means an added value. The system also shows an excellent behavior for very fast variables in incident radiation levels.

Keywords: Analog system; Efficiency; Low cost; Maximum power point tracker; Photovoltaic array; "P&O" algorithm

1. Introduction

In the specialized literature numerous proposals of MPP tracking systems can be found. Most of them have similar efficiency, which can also be considered acceptable for most applications. As a result, the interest of the authors when implementing this work has focused on achieving a certain added value in the proposed system, which can be found in the accurateness, speed and low cost. This allows its application even to household installations, where investment costs may be the most determining factor for decision making. The developed system presents the advantage of its high speed which also helps to improve the photovoltaic system efficiency.

A photovoltaic (PV) array that functions under uniform radiation and temperature conditions presents an I–V and P–V characteristic as the one shown in Figs. 1(a) and (b), respectively. As can be observed, there is a single point, called "MPP" (Maximum Power Point), where the array provides the maximum power possible for these environmental conditions (radiation and temperature), and so functions with the maximum performance. When a load is connected directly to a PV array (direct coupling), the operation point is defined by the intersection of its I–V characteristics, as shown in Fig. 1(a).

In general, this operation point does not coincide with the MPP. Thus, in direct coupling systems, the array must be over-dimensioned to guarantee the power demand of the load. Obviously, this implies a more expensive system. To solve this problem, a DC/DC (Xiao et al., 2007) converter with an algorithm for the automatic control of its duty cycle "δ" is inserted between the photovoltaic array and the load (see Fig. 2), resulting in what is known as MPPT (Maximum Power Point Tracker) system.

The MPPT must control the voltage or current (through the δ of the converter) of the PV array regardless of the

* Corresponding author. Address: Departamento de Ingeniería Electrónica, de Sistemas Informáticos y Automática, Universidad de Huelva, Huelva, Spain. Tel.: +34 959 217374/7656/7671; fax: +34 959 217348.
E-mail addresses: juanm.enrique@diesia.uhu.es (J.M. Enrique), andujar@diesia.uhu.es (J.M. Andújar), bohorquez@diesia.uhu.es (M.A. Bohórquez).

0038-092X/$ - see front matter © 2009 Elsevier Ltd. All rights reserved.
doi:10.1016/j.solener.2009.10.011

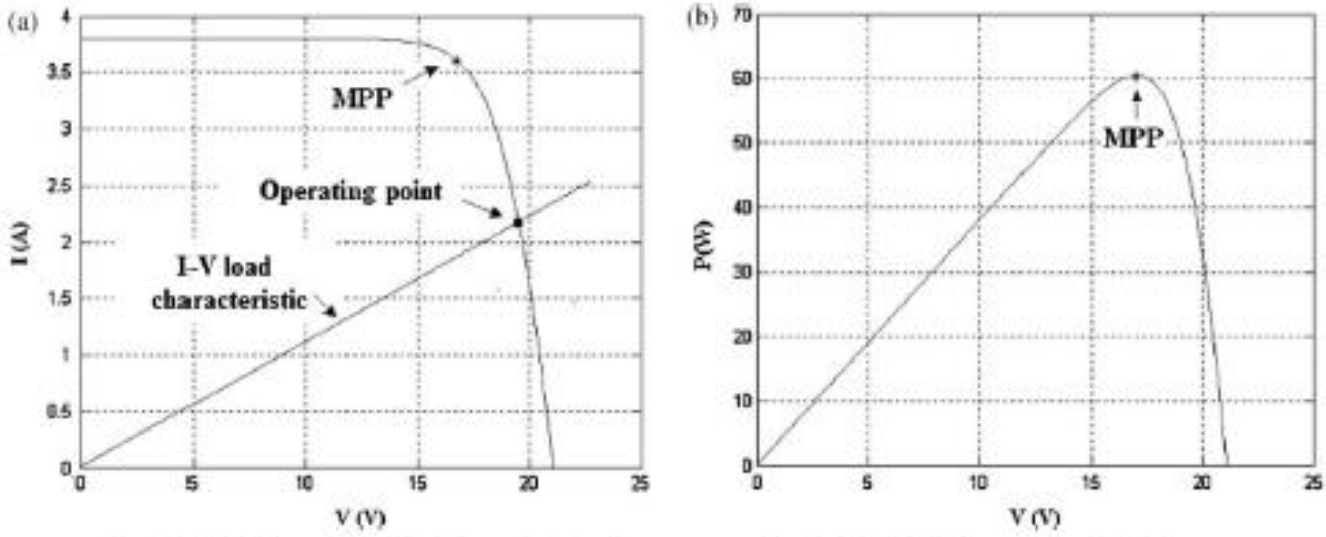

Fig. 1. (a) I–V characteristic of a PV array, MPP and system operation point. (b) P–V characteristic of the PV array.

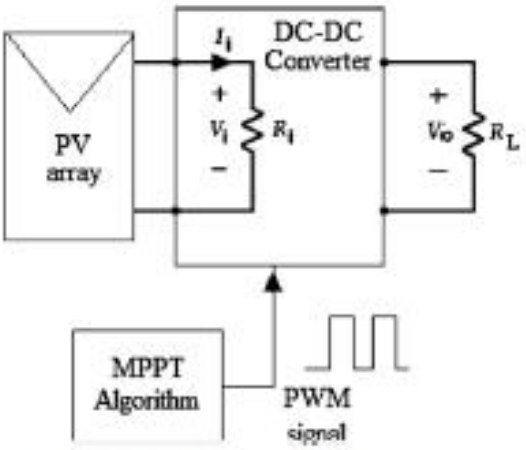

Fig. 2. Basic diagram of an MPPT system.

load, trying to place it in the MPP. The DC/DC converter presents an input impedance (R_i) which depends basically on the load impedance (R_L) and the duty cycle (δ) (Enrique et al., 2005a,b, 2007; Durán et al., 2008, 2009). Therefore, the MPPT must find the optimal δ for the operation point of the PV array to coincide with the maximum power point (MPP).

Although the solution to operating in the MPP may seem immediate, it is not. This is because the location of the MPP in the I–V curve of the PV array is not known *a priori*. This point must be located, either by mathematical calculations over a valid model, or by using some search algorithm. This implies even more difficulty if we consider the fact that the MPP presents non-linear dependencies with temperature and radiation, as observed in Fig. 3.

Fig. 3(a) shows a set of I–V curves for different levels of radiation and constant temperature. In Fig. 3(b), the same set of curves is presented at a higher temperature. Observe the change in the voltage and, especially, in the current of the MPP.

Numerous MPPT algorithms have been proposed and developed in the literature. Among them, the "Perturbation and Observation (P&O)" algorithm is probably the most

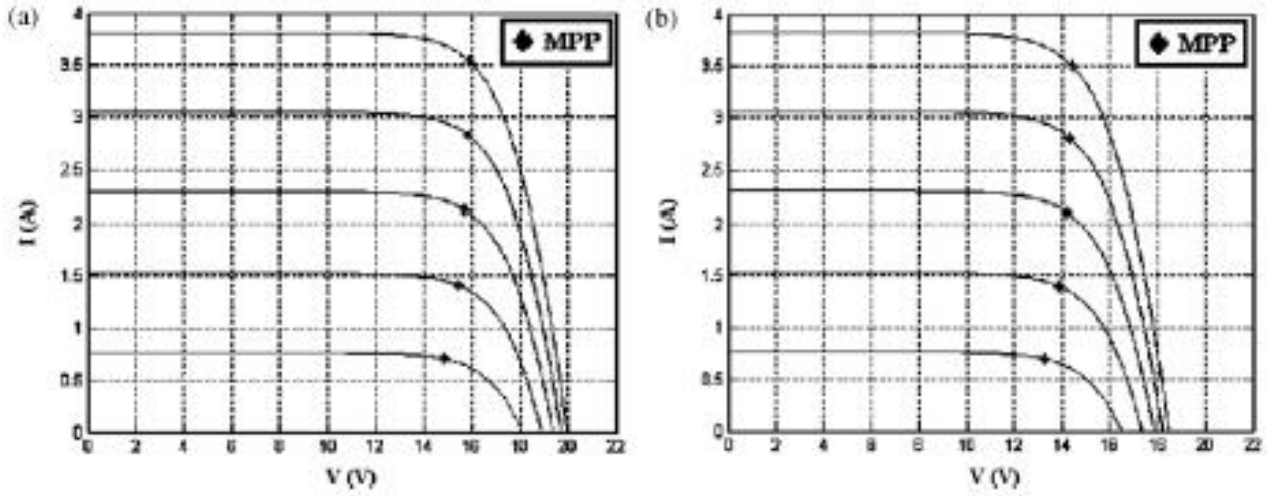

Fig. 3. (a) I–V characteristic of a PV array at 40 °C and different radiation levels (200–400 to 600–800 and 1000 W/m^2). (b) I–V characteristic of a PV array at 60 °C and different radiation levels (200–400 to 600–800 and 1000 W/m^2).

extensively used in commercial MPPT systems. However, there is no clear agreement on which algorithm is best. Hohm and Ropp (2002) presented a study that basically concludes with not very different performances for most of the different algorithms and where the traditional P&O is quite successful.

To establish the quality of a given MPPT system (and to be able to compare it with other systems), it is necessary to define the "*tracking efficiency* (η)", given by Eq. (1) (Hohm and Ropp, 2002):

$$\eta_{MPPT} = \frac{\int_0^t P_{inst}(t)dt}{\int_0^t P_{max}(t)dt} \quad (1)$$

where, for radiation and temperature conditions in the given time period, $P_{inst}(t)$ is the instantaneous power supplied by the MPPT system controlled PV array, and $P_{max}(t)$ is the actual MPP power.

2. Algorithms for MPP tracking

A very short revision of the most usual algorithms for MPP tracking is presented below.

2.1. Perturbation and Observation (P&O)

The Perturbation and Observation (P&O) algorithm is probably the most frequently used in practice, mainly due to its easy implementation (Kim et al., 1996). Its operation is briefly explained as follows: assume that the PV array operates at a given point, which is outside the MPP. The PV array operational voltage is perturbed by a small ΔV, and then the change in the power (ΔP) is measured. If $\Delta P > 0$, the operation point has approached the MPP, and therefore, the next perturbation must take place in the same direction as the previous one (same algebraic sign). If, on the contrary, $\Delta P < 0$, the system has moved away from the MPP and, consequently, the next perturbation must be performed in the opposite direction (opposed algebraic sign).

As stated before, the advantages of this algorithm are its simplicity and easy implementation. However, it has limitations that reduce its tracking efficiency. When the light intensity decreases considerably, the P–V curve becomes very flat. This makes it difficult for the MPPT to locate the MPP, since the changes that take place in the power are small as regards perturbations occurred in the voltage.

Another disadvantage of the "P&O" algorithm is that it cannot determine when it has exactly reached the MPP. Thus, it remains oscillating around it, changing the sign of the perturbation for each ΔP measured. It has also been observed that this algorithm can show misbehavior under fast changes in the radiation levels (Kawamura et al., 1997).

Several improvements in the "P&O" algorithm have been proposed (Enslin et al., 1997; Andujar et al., 2005; Xiao et al., 2007). One of them is the addition of a waiting time if the system identifies a series of alternate signs in the perturbation, meaning that it is very close to the MPP. This allows reducing the oscillation around the MPP and improves the algorithm efficiency under constant radiation conditions. However, this algorithm causes the MPPT to be very slow, making its misbehavior more noticeable in partly cloudy days.

Other modifications to the "P&O" algorithm, as the ones detailed below, directly affect the perturbation sign according to whether certain conditions are given.

2.1.1. "P&O" oriented algorithm

The "P&O" oriented algorithm (Andujar et al., 2005) is able to distinguish with certain accuracy whether the system is operating to the right or left of the MPP and act consequently, so increasing tracking efficiency. However, it is observed that whenever there is a sudden variation in the incident radiation (caused, for example, by the passing of a cloud) and, therefore, in the power supplied by the photovoltaic generator, the system is unable to distinguish instantaneously the appropriate direction of the change in δ (Hohm and Ropp, 2002). This algorithm is discussed in detailed in Section 3.

2.1.2. "P&O" modified algorithm

To correct the defect caused by sudden radiation variations in the previous algorithm, a slight variation has been proposed (Andujar et al., 2005). As already known, variations in the light radiation have an effect mainly and directly on the current supplied by the photovoltaic array (Alonso, 1998). Thus, an increase in radiation will cause a rise in the value of the MPP current (see Fig. 3). When the algorithm detects a variation in radiation over a certain threshold, its response is an immediate increase in δ. In this way, the DC/DC converter decreases its input impedance R_i, and so obliges the photovoltaic generator to move to higher current points close to the MPP. An advantage of this algorithm is that it does not require precise measurements of radiation (this would remarkably increase the price of its practical implementation), since it only needs the sign of the radiation increase within an interval of measures. A simple photodiode can be useful for this purpose.

2.2. Constant voltage and current

The "Constant Voltage (CV)" algorithm (Hohm and Ropp, 2002; Koizumi et al., 2006) is based on the fact that in the I–V curves of a PV array the ratio between the maximum power point voltage and that of the open circuit is roughly constant (something similar occurs with the ratio between the current of the maximum power point and that of the short circuit) (Noguchi et al., 2002; Mutoh et al., 2006; Mutoh and Inoue, 2007), that is:

$$\frac{V_{MPP}}{V_{OC}} \cong K < 1 \quad (2)$$

where V_{MPP} is the maximum power point voltage and V_{OC} is the open circuit voltage. The PV array is temporarily isolated by the MPPT system to measure V_{OC}. Next, the MPPT calculates the correct operation point using Eq. (2) and adjusts the voltage of the PV array until it reaches the MPP. This operation is repeated periodically to track the MPP.

Although this method is simple, choosing the optimal K value, which, on the other hand, is not totally constant, may be difficult. The literature indicates good values for K within the range 0.73–0.80 (Andersen and Alvsten, 1995; van der Merwe and van der Merwe, 1998; Abou El Ela and Roger, 1984).

This method can be implemented in a relatively easy way using analog software. However, its efficiency is lower than that of other methods (Hohm and Ropp, 2002). The main reasons are:

(I) Errors in the K value.
(II) The measure of V_{OC} (I_{SC}) requires the momentary interruption of the power supplied by the array.

2.3. Incremental conductance

The so called "incremental conductance" method (Hohm and Ropp, 2002) derives directly from the power equation, which will be given in the MPP by:

$$\left.\frac{dP}{dV}\right|_{MPP} = \left.\frac{d(V\cdot I)}{dV}\right|_{MPP} = 0 \Rightarrow -\frac{I}{V} = \frac{dI}{dV} \tag{3}$$

If instantaneous conductance g_L, and increasing conductance g_P, are defined as:

$$g_L = -\frac{I}{V}; \quad g_P = \frac{dI}{dV} \tag{4}$$

Then, expression (3) can be re-written in the form of:

$$\left.\frac{dP}{dV}\right|_{MPP} = 0 \Rightarrow g_L = g_P \tag{5}$$

The previous equation indicates that in the MPP the instantaneous and incremental conductance must be equal. If the operation point does not coincide with the MPP, then a series of inequations directly derived from expression (5) (Hohm and Ropp, 2002; Koizumi et al., 2006) allow us to know whether the operation voltage is higher or lower than V_{MPP}, and so to act consequently.

Once the MPP has been reached, every time a change occurs in the radiation on the array the MPPT will tend to increase or decrease the operation voltage to follow the MPP.

The disadvantage of this method is that it needs a precise calculation of g_L and g_P, which makes the MPPT more difficult and relatively slow.

2.4. Parasitic capacity

This algorithm is similar to the previous one, except that in this algorithm the effect of the parasitic capacity of the junction p–n is included. This effect can be modeled (Brambilla et al., 1998) as a condenser connected between the terminals of each cell. By connecting cells in parallel the parasitic capacity observed by the MPP will increase. As a result, the differences between the tracking efficiencies of the MPP between "Increasing Conductance" and "Parasitic Capacity" algorithms are more outstanding in high power arrays, where there are numerous modules connected in parallel.

The practical implementation of this algorithm is complex, especially for the difficulty entailed by the calculation of increasing conductance g_P. A detailed study of this algorithm is shown in Brambilla et al. (1998).

2.5. Model-based algorithms

If a suitable model is available for a cell or photovoltaic array and there are precise radiation and temperature measures available (which implies a significant increase in the price of the system, although there have recently been developed sensors of temperature and radiation at a low cost (Martínez and Andújar, 2009; Martínez et al., 2009), the MPP voltage and current may be directly calculated by solving equation $dP/dV = 0$ (for example, using a numeric method). Then, the MPPT would just have to adjust voltage and current values to those calculated ones (Xiao et al., 2006).

Even so, the model-based MPPTs are not practical, since the values for the cell parameters are not known with accuracy and, in fact, can vary significantly between cells from the same production series. Moreover, only the cost of a precise light radiation sensor (pyranometer) can cause this MPPT system to be non-viable in practice.

Having revised the most usual algorithms and methods for MPP tracking, it seems that the P&O algorithm and, more specifically, its "oriented" variant, is the one with the best ratio efficiency/easiness of practical implementation. This is mainly due to its proper operation, simplicity and low cost (note that it needs no radiation and temperature sensors). Nonetheless, as already mentioned, it has the disadvantage of its instantaneous confusion when facing sudden variations in the incident radiation. This disadvantage could be overcome with a system fast enough to make its reaction speed higher than the speed of the incident radiation change – which is the main reason in the MPP movement. To achieve this without losing the advantages of the *P&O-oriented* algorithm, the authors have developed a system which is described below.

3. P&O oriented analog system

A completely analog system able to implement the algorithm for MPP tracking, known as "P&O-oriented" algorithm, is presented in this section (Andujar et al., 2005).

3.1. Operation of the P&O-oriented algorithm

Consider Fig. 4, where the P–V characteristic of a photovoltaic array at a given temperature and radiation is

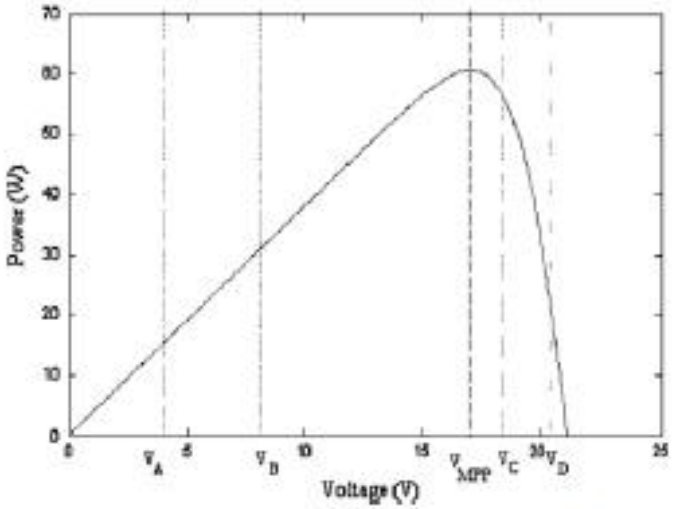

Fig. 4. *P–V* characteristic of a photovoltaic array. The developed MPPT algorithm is able to distinguish whether the system is operating to the right or left of the MPP and act consequently.

shown. Assume that, due to a modification in the duty cycle (δ) of the converter, the system evolves from V_A to V_B ($\Delta V > 0$ and $\Delta P > 0$). As observed in Fig. 4, the MPP voltage, V_{MPP}, is higher than V_B, and therefore, the output voltage must keep increasing. Now assume that the perturbation has moved the operation point from V_B to V_A. In this case, the voltage of the array must increase again to approach V_{MPP}. All possible combinations are shown in Table 1.

The only variable to which the control system can access is the duty cycle (δ). Any increase in δ implies a decrease in the input resistance R_i of the DC–DC converter (and subsequently, a decrease in the operation voltage of the photovoltaic generator) and vice versa (Enrique et al., 2005a,b, 2007; Durán et al., 2008, 2009). The system starts from an initial value (for example $\delta = 0.5$) that varies at constant increase ($\Delta\delta$) according to expressions (6) and (7).

$$b_i = -sign[(\Delta V) \cdot (\Delta P)] \tag{6}$$

$$\delta_i = \delta_{i-1} + b_i \cdot \Delta\delta \tag{7}$$

In each iteration "i", ΔP and ΔV measures are obtained. Next, the value of δ is adjusted to approach it to the MPP. Note that no temperature and solar radiation measures are needed to do the tracking, which reduces the price of the control system. The flow chart diagram of this algorithm is shown in Fig. 5.

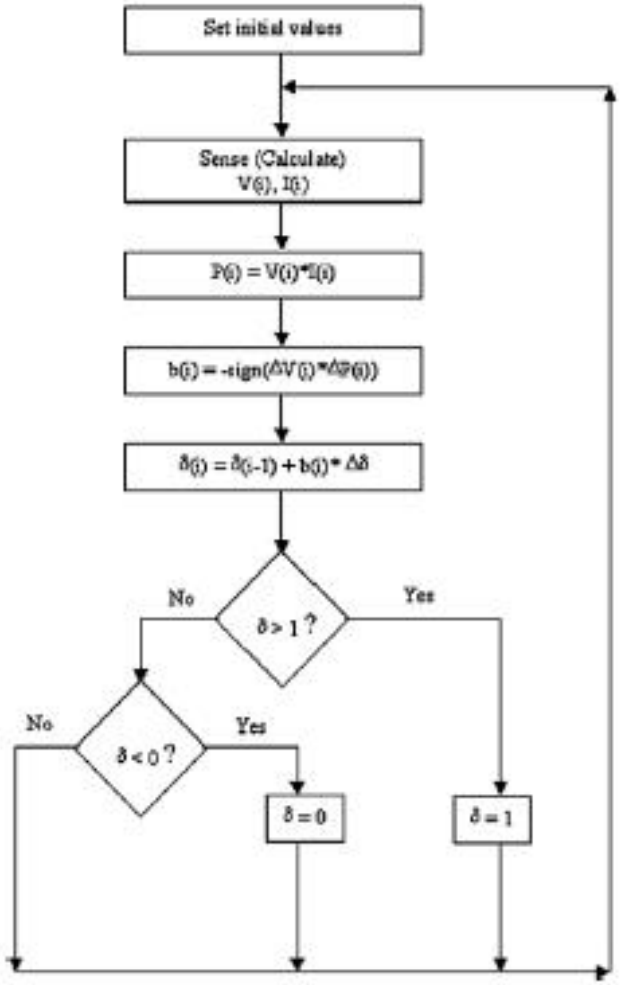

Fig. 5. Flow chart of the MPPT P&O-oriented algorithm.

3.2. The developed system

The whole developed system is shown in Fig. 11. To explain its operation, the system will be analyzed by blocks. Fig. 6 shows the circuit that, from the voltage and current measures at the PV array output, generates a reference signal, V_{ref}, which will then be used in another block to generate a PWM signal.

From the voltage and current measures at the array output (V, I), the variable power, P, is generated by using the multiplier "Mult. 1". Two differentiators followed by two comparators generate the value of the functions *sign*(dV) and *sign*(dP). These two signals are multiplied and compared again to generate the analog equivalent of the bit

Table 1
Possible cases and control law to enable the photovoltaic system follow the MPP.

Case	System evolution			Control law ($V \rightarrow V_{MPP}$)		
	sign(ΔV)	*sign*(ΔP)	$b_i = -sign((\Delta V) \cdot (\Delta P))$	V	*sign*(ΔV)	δ
$V_A \rightarrow V_B$	+1	+1	−1	↑	+1	↓
$V_B \rightarrow V_A$	−1	−1	−1	↑	+1	↓
$V_C \rightarrow V_D$	+1	−1	+1	↓	−1	↑
$V_D \rightarrow V_C$	−1	+1	+1	↓	−1	↑

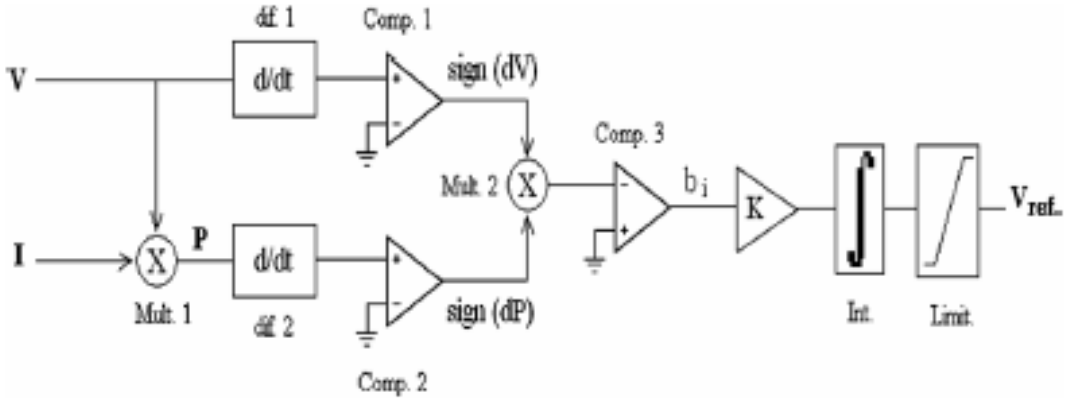

Fig. 6. System generating the reference signal.

"b_i". The iterations of expression (3) are formed by integrating the subsequent b_i. Finally, the output signal is limited in order to maintain it within the appropriate range, generating V_{ref}. This signal can be used as control signal of a PWM generating system (Enrique et al., 2005a,b).

To perform the practical implementation of the developed system, the chip AD633J has been selected as multiplier block. For the comparators, the cheap (approx. 0.5 $) and extensively used op-amp TL082 has been selected. The integrator and differentiator blocks are shown in Fig 7. Both structures are basic in analog electronics. The op-amp TL082 has also been used for their implementation.

A lowpass RC filter has been inserted before each differentiator block to remove part of the harmonic content of the input signals. The output signal, V_{ref}, of the system in Fig. 6 is used as reference voltage for a PWM generator (see Fig. 8), so that its duty cycle can be adjusted.

The output PWM signal of the circuit in Fig. 8 allows controlling the behavior of the DC/DC converter. This converter (boost-type, in this case) is shown in Fig. 9 connected to a 25 Ω load.

To reduce the price of the sensors, the voltage input is taken from the photovoltaic array using a high impedance voltage divider with a voltage follower. The measurement of the current variable is performed by measuring the voltage fall in a very low value resistance, located at one of the PV array terminals. This measure must be amplified before reaching the multiplier. For this purpose, a very low offset voltage precision op-amp OP27 has been used (see Fig. 10).

Fig. 11 shows the diagram of the whole developed MPPT system.

4. Simulations

The developed system has been verified using PSpice®. The photovoltaic generator has been implemented using ABM blocks (*Analog Behavioral Modeling*). The parameters of the generator model correspond to the "BP Saturno" module ($ns = 60$ and $np = 1$) (CIEMAT, 2000).

Fig. 12 presents the model and I–V and P–V curves of the module used at 21 °C and 1000 W/m^2. Table 2 shows the MPP power and current (P_{MPP} and I_{MPP}, respectively) for different levels of radiation and constant temperature.

To verify the correct operation of the system, fast variations in the incident radiation have been applied to it (see Fig. 13). Observe that during start-up, an initial rise of 688.7 W/m^2 in the incident radiation ($P_{MPP} = 55.2$ W) is reached by the system in approximately 10 ms. Once the maximum power point has been reached, the system maintains it even for variations higher than 5×10^3 W/m^2/s, much higher than those present in nature. Additionally, it can be observed that the system presents a high precision, since the actual trajectory of the MPP and the one intended do not have practically noticeable differences. Fig. 14 shows the current obtained with the tracker system.

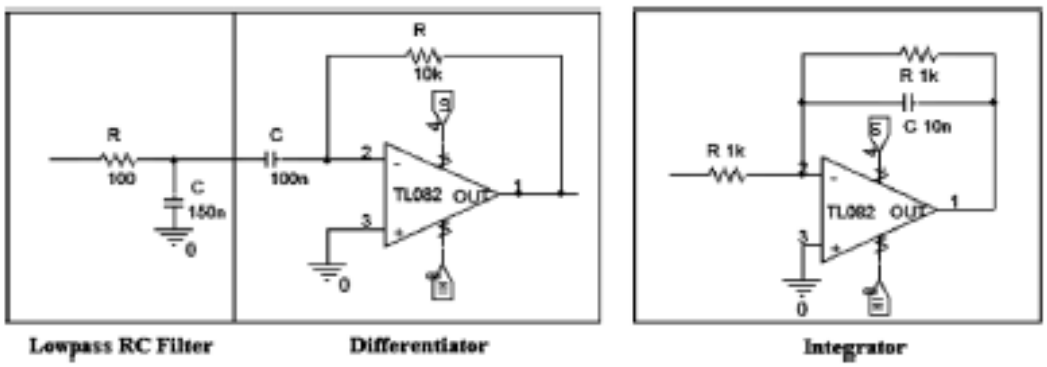

Fig. 7. Differentiator and integrator blocks used.

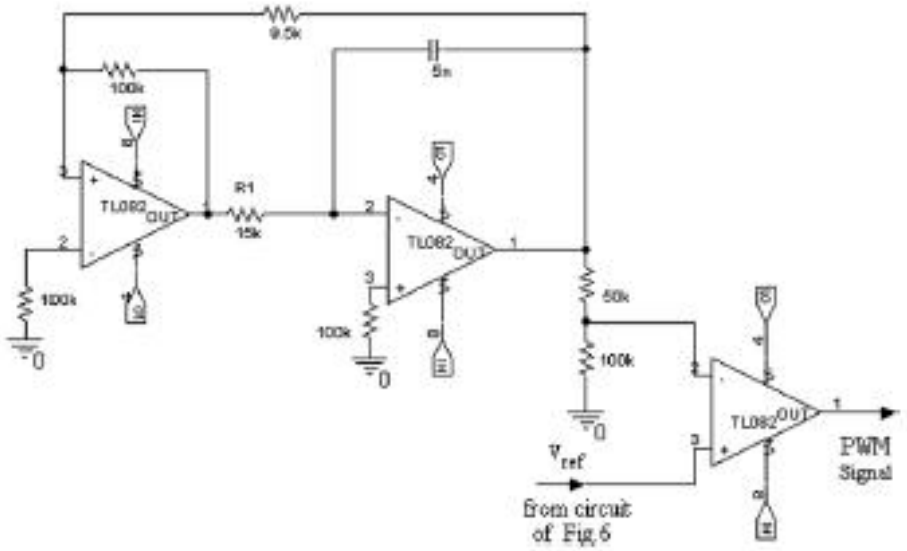

Fig. 8. System generating the PWM signal.

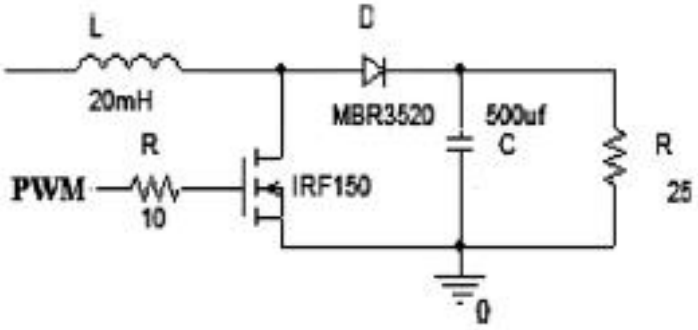

Fig. 9. Boost converter used.

With this sudden start-up, the tracking system is able to obtain efficiencies superior to 97.2% in the first 100 ms. Once the MPP has been reached (during the first milliseconds of the start-up) the system presents a tracking efficiency η higher than 99% (99.99%), even for variations in the incident radiation as fast and extreme as those shown in Fig. 13. This efficiency is superior to 81–85% of a classical "P&O" system (*Perturb and Observed*), superior to 88–89% of an "InC" system (*Incremental Conductance*) and to 73–85% of a "CV" system (*Constant Voltage*) (Hohm and Ropp, 2002). In Fig. 15, note how the system is able to adjust automatically the duty cycle of the PWM signal.

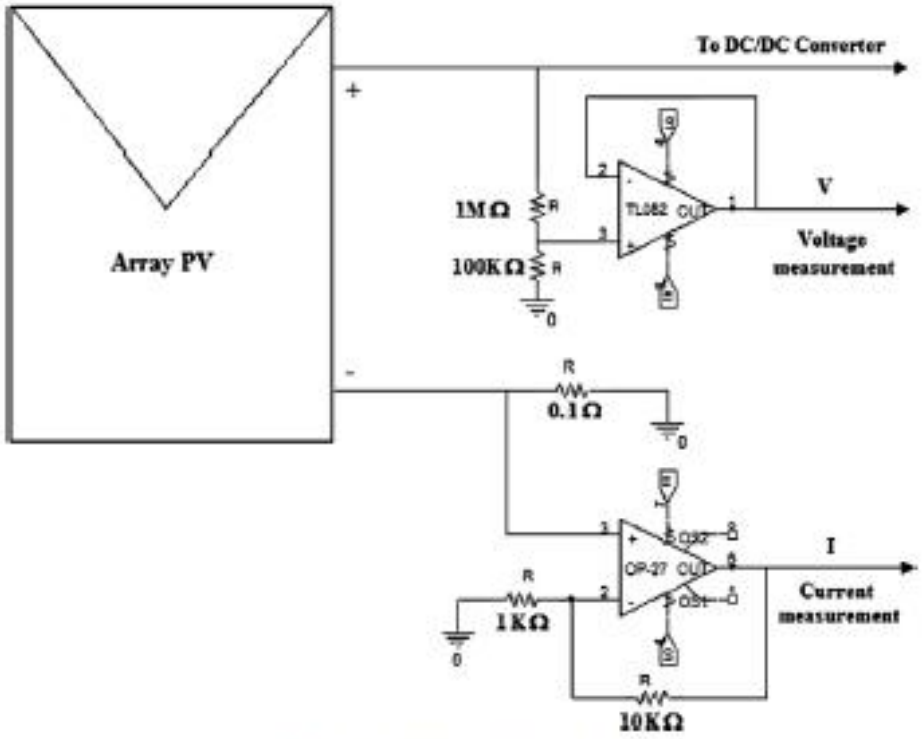

Fig. 10. Measure of variables V and I.

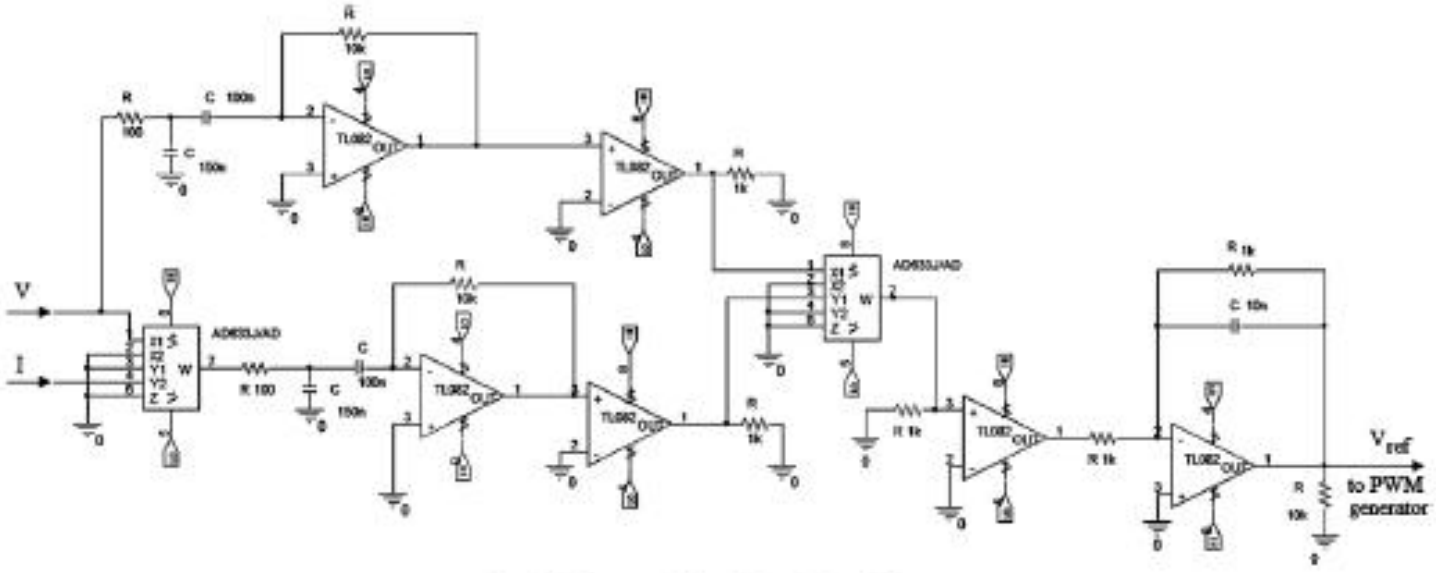

Fig. 11. Diagram of the whole developed system.

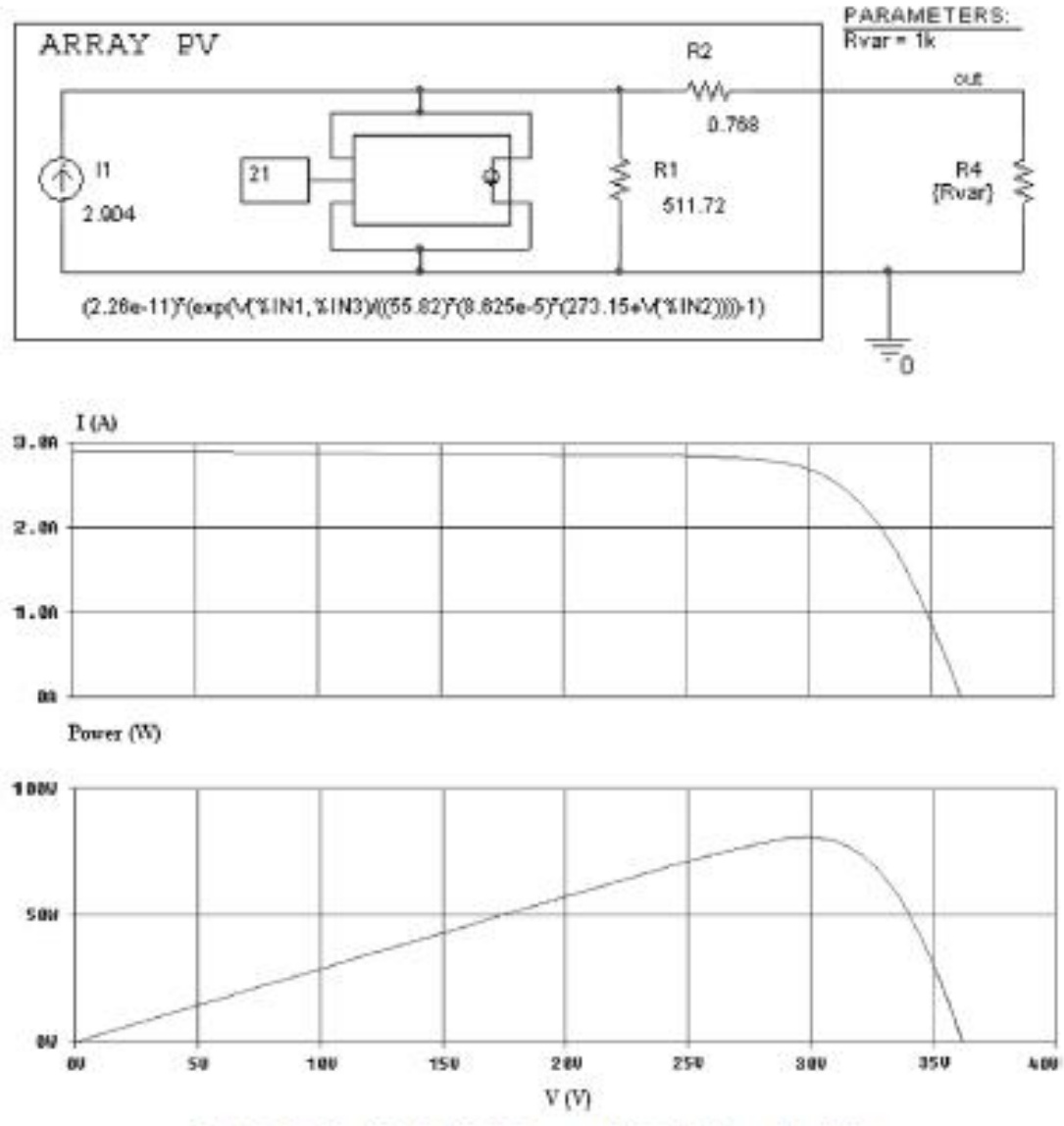

Fig. 12. Model and I–V and P–V curves of the "BP Saturno" module.

Table 2
P_{MPP} and I_{MPP} for different levels of radiation and constant temperature corresponding to the "BP Saturno" generator.

Temperature (°C)	Radiation (W/m²)	P_{MPP} (W)	I_{MPP} (A)
21	688.7	55.2	1.86
21	1000	80.6	2.71
21	1721.8	136.2	4.76

5. Conclusions

In this work, the design of a new maximum power point (MPP) tracking system for photovoltaic systems has been developed. The system is an analog version of the tracking "P&O-oriented" algorithm. From the results obtained by simulation, it can be concluded that the developed system presents an excellent precision and speed in the MPP track-

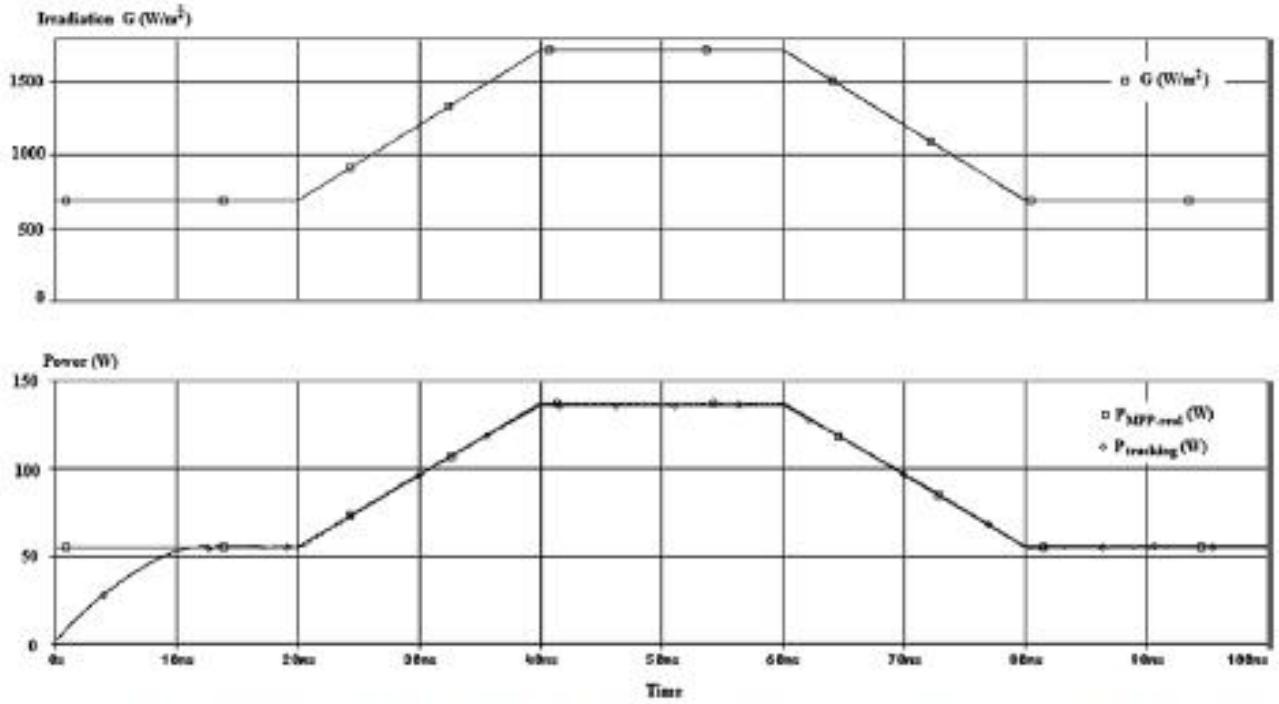

Fig. 13. Top chart: applied variations in the incident radiation. Bottom chart: comparative between the actual trajectory of the MPP and that followed by the developed system for variations in the incident radiation.

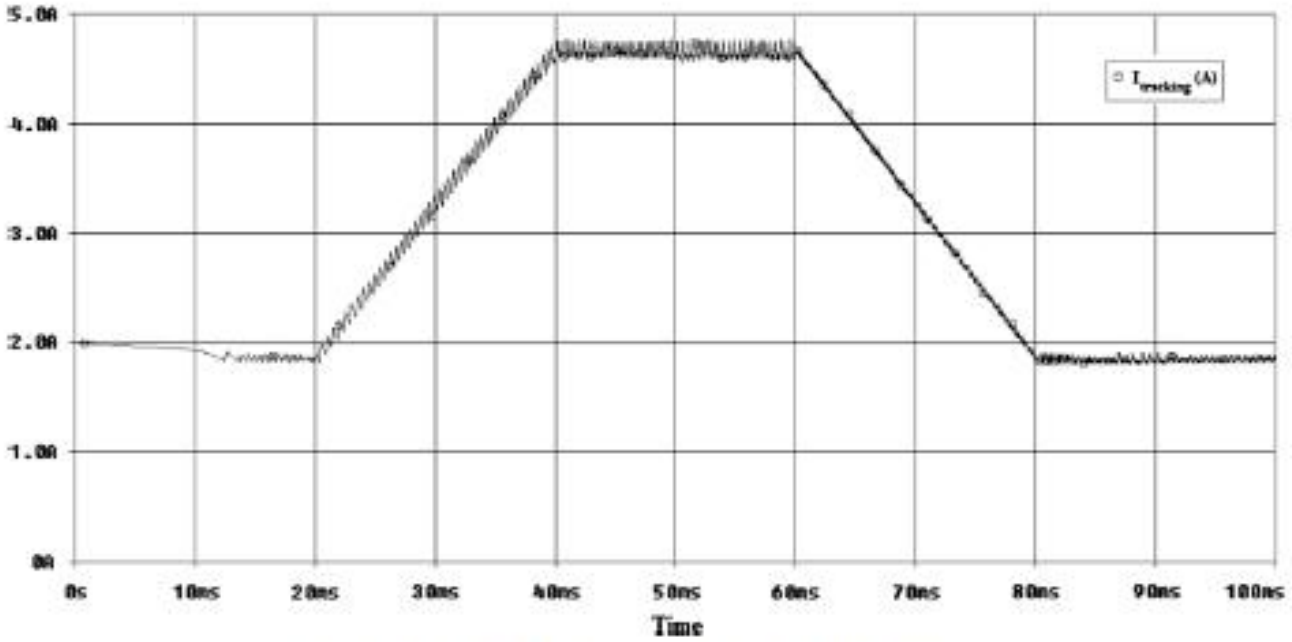

Fig. 14. Current supplied by the system for variations in the incident radiation.

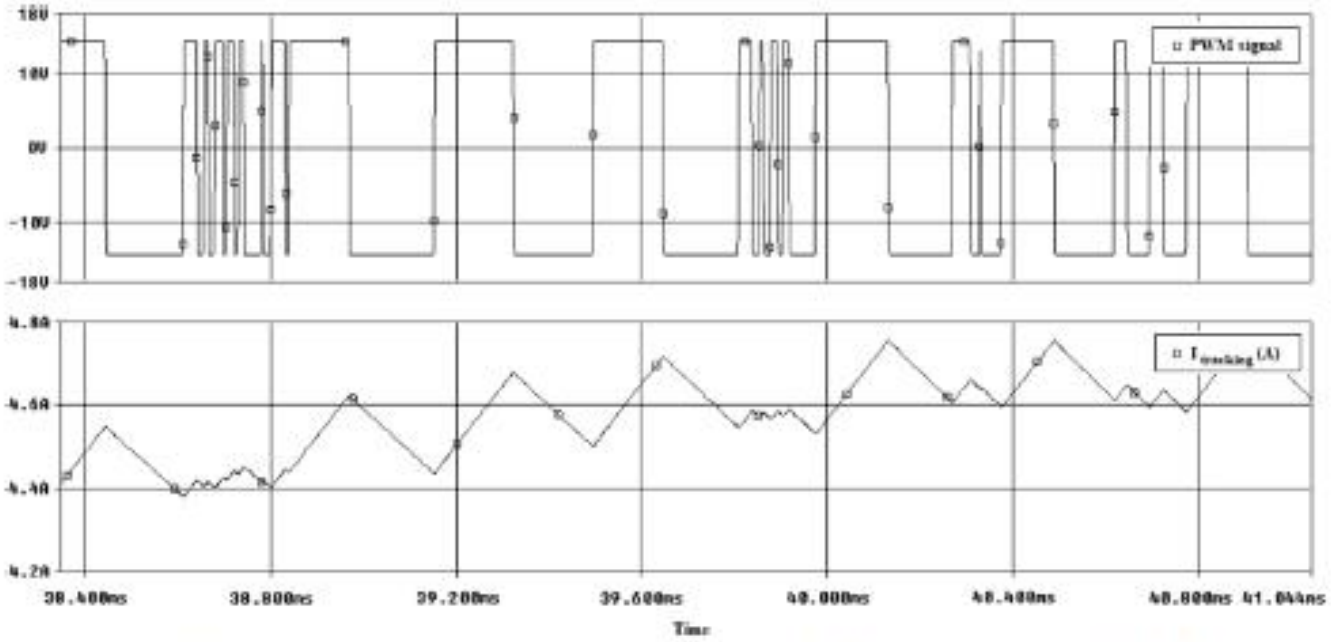

Fig. 15. Top chart: PWM signal generated by the developed system during a certain interval. Bottom chart: current supplied by the system during the time interval.

ing, even for very sudden variations in the levels of incident radiation, so increasing the total energy performance of the installation. The system is able to reach the MPP in the first 10 ms, getting high efficiency values practically from the start-up. Once the system has reached the MPP, the efficiency is superior to 99%, improving the ones obtained by other methods ("P&O", "InC", "CV"). This quality, along with its high simplicity and low price, makes the proposed system highly suitable for use in any kind of photovoltaic installation.

Acknowledgment

The present work is a contribution of the DPI2007 62336/project, funded by The Spanish Ministry of Education.

References

Abou El Ela, M., Roger, J., 1984. Optimization of the function of a photovoltaic array using a feedback control system. Solar Cells: Their Science, Technology, Applications and Economics 13 (2), 185–195.

Alonso, G.M.C., 1998. El Generador Fotovoltaico. CIEMAT, Serie de Ponencias, Editorial CIEMAT, Madrid.

Andersen, M., Alvsten, B., 1995. 200 W low cost module integrated utility interface for modular photovoltaic energy systems. In: IECON: Proceedings of the 1995 IEEE 21st International Conference on Industrial Electronics, Control and Instrumentation, vol. 1, no. 1, pp. 572–577.

Andujar, J.M., Enrique, J.M., Bohórquez, M.A.M., Durán, E., 2005. Sistema de Control de Bajo Costo para el Seguimiento del punto de Máxima Potencia en Sistemas Fotovoltaicos. In: Proc. De las XXVI Jornadas de Automática, Alicante, España. ISBN: 84-689-0730-8.

Brambilla, A., et al., 1998. New approach to photovoltaic arrays maximum power point tracking. In: Proceedings of the 30th IEEE Power Electronics Conference, pp. 632–637.

CIEMAT: Fundamentos, dimensionado y aplicaciones de la energía solar fotovoltaica, Cap. 11, Editorial CIEMAT, Madrid 2000.

Durán, E., Galán, J., Andújar, J.M., Sidrach-de-Cardona, M., 2008. A new method to obtain *I–V* characteristics curves of photovoltaic modules based on SEPIC and Cuk converters. EPE Journal 18 (2), 5–15.

Durán, E, Andújar, J.M., Galán, J., Sidrach-de-Cardona, M., 2009. Methodology and experimental system for measuring and displaying *I–V* characteristic curves of PV facilities. Progress in Photovoltaics. Available from: <http://dx.doi.org/10.1002/pip.909/>.

Enrique, J.M., Durán, E., Sidrach, M., Andújar, J.M., 2005a. A new approach to obtain *I–V* and *P–V* curves of PV panels by using DC–DC converters. In: 31st IEEE Photovoltaic Specialists Conference, January 3–7, 2005.

Enrique, J.M., Sidrach-de-Cardona M., Durán E., Bohórquez M.A, Carretero, J.E., Andújar J.M., 2005. An optimum configuration of DC/DC converters to use in photovoltaics facilities. In: 20th European Photovoltaic Solar Energy Conference and Exhibition, EUPVSEC 2005, Barcelona, Junio 2005.

Enrique, J.M., Durán, E., Sidrach-de-Cardona, M., Andujar, J.M., 2007. Theoretical assessment of the maximum power point tracking efficiency of photovoltaic facilities with different converter topologies. Solar Energy 81 (1), 31–38.

Enslin, J.H.R., Wolf, M., Swiegers, W., 1997. Integrated photovoltaic maximum power point tracking converter. IEEE Transactions on Industrial Electronics 44 (6), 769–773.

Hohm, D.P., Ropp, M.E., 2002. Comparative study of maximum power point tracking algorithms. Progress in Photovoltaics: Research and Applications.

Kawamura, T., et al., 1997. Analysis of MPPT characteristics in photovoltaic power systems. Solar energy materials and solar cells. In: Proceedings of the 1996 9th International Photovoltaic Science and Engineering Conference, PVSEC-9 1997, vol. 47, no. 14, pp. 155–165.

Kim, Y., Jo, H., Kim, D., 1996. A new peak power tracker for cost-effective photovoltaic power systems. IEEE Proceedings 3 (1), 1673–1678.

Koizumi, H., Mizuno, T., Kaito, T., Noda, Y., Goshima, N., Kawasaki, M., Nagasaka, K., Kurokawa, K., 2006. A novel microcontroller for grid-connected photovoltaic systems. IEEE Transactions on Industrial Electronics 53 (6), 1889–1897. doi:10.1109/TIE.2006.885526.

Martínez, M.A., Andújar, J.M., 2009. A new and inexpensive temperature measuring system. Application to photovoltaic solar facilities. Solar Energy 83 (6), 883–890.

Martínez, M.A., Andújar, J.M., Enrique, J.M., 2009. A new and inexpensive pyranometer for the visible spectral range. Sensors-Basel 9 (6), 4615–4634.

Mutoh, N., Inoue, T., 2007. A control method to charge series-connected ultraelectric double-layer capacitors suitable for photovoltaic generation systems combining MPPT control method. IEEE Transactions on Industrial Electronics 54 (1), 374–383. doi:10.1109/TIE.2006.885149.

Mutoh, N., Ohno, M., Inoue, T., 2006. A method for MPPT control while searching for parameters corresponding to weather conditions for PV generation systems. IEEE Transactions on Industrial Electronics 53 (4), 1055–1065. doi:10.1109/TIE.2006.878328.

Noguchi, T., Togashi, S., Nakamoto, R., 2002. Short-current pulse-based maximum-power-point tracking method for multiple photovoltaic-and-converter module system. IEEE Transactions on Industrial Electronics 49 (1), 217–223. doi:10.1109/41.982265.

van der Merwe, L., van der Merwe, G., 1998. Maximum power point tracking – implementation strategies. In: Proceedings of the IEEE International Symposium on Industrial Electronics, vol. 1, no. 1, 214–217.

Xiao, W., Lind, M.G.J., Dunford, W.G., Capel, A., 2006. Real-time identification of optimal operating points in photovoltaic power systems. IEEE Transactions on Industrial Electronics 53 (4), 1017–1026. doi:10.1109/TIE.2006.878355.

Xiao, Weidong, Ozog, N., Dunford, W.G., 2007. Topology study of photovoltaic interface for maximum power point tracking. IEEE Transactions on Industrial Electronics 54 (3), 1696–1704. doi:10.1109/TIE.2007.894732.

Xiao, W., Dunford, W.G., Palmer, P.R., Capel, A., 2007. Application of centered differentiation and steepest descent to maximum power point tracking. IEEE Transactions on Industrial Electronics 54 (5), 2539–2549. doi:10.1109/TIE.2007.899922.

A Fuzzy Logical MPPT Control Strategy for PMSG Wind Generation Systems

Xing-Peng Li, Wen-Lu Fu, Qing-Jun Shi, Jian-Bing Xu, and Quan-Yuan Jiang

Abstract—**Making full use of wind power is one of the main purposes of the wind turbine generator control. Conventional hill climbing search (HCS) method can realize the maximum power point tracking (MPPT). However, the step size of HCS method is constant so that it cannot consider both steady-state response and dynamic response. A fuzzy logical control (FLC) algorithm is proposed to solve this problem in this paper, which can track the maximum power point (MPP) quickly and smoothly. To evaluate MPPT algorithms, four performance indices are also proposed in this paper. They are the energy captured by wind turbine, the maximum power-point tracking time when wind speed changes slowly, the fluctuation magnitude of real power during steady state, and the energy captured by wind turbine when wind speed changes fast. Three cases are designed and simulated in MATLAB/Simulink respectively. The comparison of the three MPPT strategies concludes that the proposed fuzzy logical control algorithm is more superior to the conventional HCS algorithms.**

Index Terms—**Fuzzy logical control, hill climbing search, maximum power point tracking, permanent magnet synchronous generator, wind generation system.**

1. Introduction

Wind turbine is an essential portion in wind generation systems. The amount of mechanical energy that can be extracted from wind is not only depending on wind speed, but also depending on the wind turbine rotational speed. The wind turbine rotational speed can be adjusted as the wind speed changes to tracking the maximum power point.

Currently, researchers have developed many maximum power point tracking (MPPT) strategies. There are three common MPPT algorithms[1],[2]: a) hill climbing search (HCS) or perturbation and observation (P&O)[3],[4], b) wind speed measurement (WSM)[5], c) power signal feedback (PSK). There are also other MPPT algorithms introduced in [6]–[11].

In comparison, the HCS algorithm is popular[12] due to its simplicity and independence of system characteristics and it can avoid using wind speed. However, the step size of HCS algorithm is constant[13]. Choosing an appropriate step size is not an easy task, where large step size means faster response and less steady-state efficiency while small step size improves steady-state efficiency but slows down the convergence speed [8]. The conventional HCS algorithm cannot combine rapidity and efficiency, which means the algorithm cannot adapt well both in the situation that wind speed changes quickly and in the situation that wind speed is constant.

In this paper, a fuzzy-logical-controller based MPPT strategy for wind generation system is proposed, which can realize variable step-size control. The strategy is independent of the turbine's characteristics. Compared with conventional HCS algorithms with a big step size and a small step size respectively, the proposed algorithm is validated superiorly in MATLAB/Simulink environment. The simulation results indicate the proposed MPPT algorithm has three advantages: a) tracking MPP fast, b) the fluctuation magnitude of real power is small during steady state, and c) the wind energy captured is the most among the three MPPT algorithms.

This paper is organized as follows: Section 2 gives a brief introduction to the wind turbine characteristics and to the wind generation system. Section 3 presents an introduction to the conventional HCS algorithm. In Section 4, we discuss the proposed fuzzy logical control (FLC) strategy and its advantages compared with conventional HCS strategy. Case studies are presented in detail in Section 5. Conclusions are finally made in Section 6.

2. System Overview

2.1 Wind Turbine Characteristics

Depending on the aerodynamic characteristics, the wind

Manuscript received July 15, 2012; revised October 9, 2013. This work was supported by the National High Technology Research and Development Program of China under Grant No. 2011AA05S113, Major State Basic Research Development Program under Grant No. 2012CB215106, Science and Technology Plan Program in Zhejiang Province under Grant No. 2009C34013, National Science and Technology Supporting Plan Project under Grant No. 2009BAG12A09.

X.-P. Li is with the College of Electrical Engineering, Zhejiang University, Hangzhou 310027, China (Corresponding author e-mail: lixingpeng818@163.com).

W.-L. Fu, J.-B. Xu, and Q.-Y. Jiang are with the College of Electrical Engineering, Zhejiang University, Hangzhou 310027, China (e-mail: fwl19920416@163.com; jqy@zju.edu.cn).

Q.-J. Shi is with Chongqing Changshou Power Supply Bureau, Chongqing 401220, China (e-mail: shi583031882@126.com).

Digital Object Identifier: 10.3969/j.issn.1674-862X.2013.01.013.

power captured by the wind turbine can be expressed as

$$P = \frac{1}{2} C_p(\lambda, \beta) \rho \pi R^2 V^3 \quad (1)$$

where $C_p(\lambda, \beta)$ is the wind turbine power coefficient which is a function of λ and β, ρ is the air density, R is the radius of wind turbine blade, V is the wind speed, β is the blade pitch angle, and λ is the tip speed ratio:

$$\lambda = \frac{wR}{V} \quad (2)$$

where w is the wind turbine rotational speed. There exits an optimal tip speed ratio λ_{opt} that can maximize C_p and P. Then, the maximum wind power P_{max} captured by wind turbine can be described as

$$P_{max} = \frac{1}{2} \rho \pi R^5 \frac{C_{p,max}}{\lambda_{opt}^3} w^3. \quad (3)$$

The output mechanical power versus rotational speed characteristic of wind turbine for different wind speeds is shown in Fig. 1, in which the dotted line shows the maximum power points for different wind turbine rotational speed w and different wind speed V. Each P–w curve is characterized by a unique turbine speed corresponding to the maximum power point for that wind velocity[14]. The peak power points in the P–w curves correspond to $dP/dw = 0$ [15].

A direct driven permanent magnet synchronous generator (PMSG) connected to a utility grid is selected in this paper. The specifications of the simulated PMSG generation system are listed in Table 1.

2.2 Wind Generation System

Direct driven PMSG wind generator can connect a utility grid through various converter topologies[16], where double PWM converters are a common topology for PMSG wind generation systems. The double PWM converters own a flexible structure for different control methods and can be used to adjust the motor speed and control the power injected into a utility grid. In this paper, the configuration of the imitation platform for the PMSG wind generation system is shown in Fig. 2.

In the operation control process, two PWM converters play different roles. The grid-side converter uses vector control technology based on decoupling control of active power and reactive power, which can smooth the output active power and provide reactive power support for the utility grid. Another task of the grid-side converter is to maintain the stability of the DC bus voltage. The turbine-side converter controls PMSG using vector control technology based on rotor flux oriented control. Then, the rotational speed can be adjusted to maintain the best tip speed ratio and to achieve the maximum wind power tracking when wind speed changes. The simulation model diagram of turbine-side converter control is shown in Fig. 3. From Fig. 3, we can see that the turbine is operated in the rotational speed control mode. The reference rotational speed is dynamically modified as the wind speed changes.

2.3 Issues with MPPT

To maintain the best tip speed ratio and to achieve MPPT control, the rotational speed needs to be adjusted as the wind speed changes in practical operation. The issue with MPPT is how to determine the optimal rotational speed for different wind speed.

Many MPPT algorithms have already been proposed. Among them, the HCS method is popularly applied for the method is simple, fast and it can operate independently from predefined wind turbine characteristic.

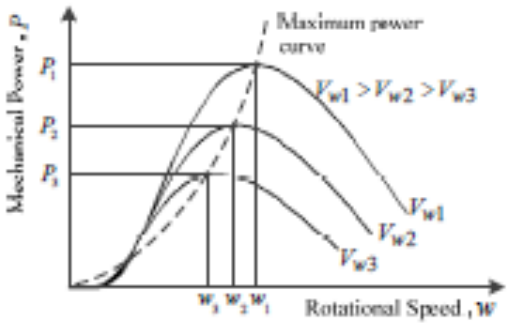

Fig. 1. Wind turbine P–w characteristics and maximum power curve.

Table 1: Parameters of PMSG

Parameters	value
Nominal wind speed (m/s)	11
Nominal turbine rotational speed (r/min)	240
Number of rotor poles	13
Diameter of wind turbine (m)	2.8

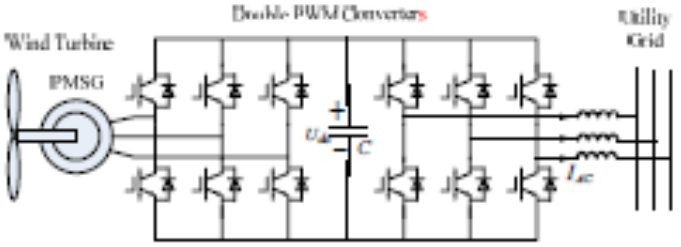

Fig. 2. PMSG wind generation system with double PWM converters.

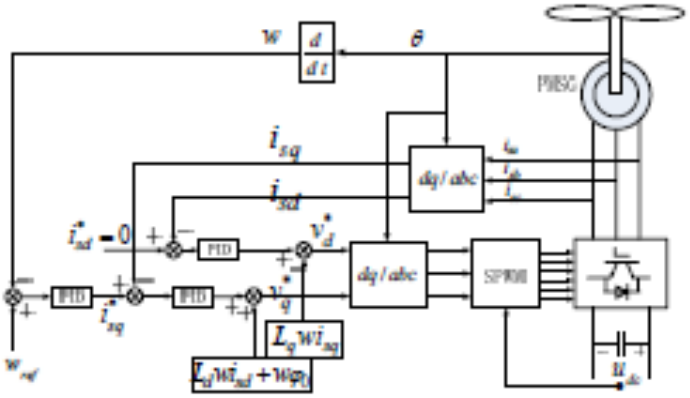

Fig. 3. Turbine-side converter control model for simulation.

Fig. 4. Control block of FLC algorithm.

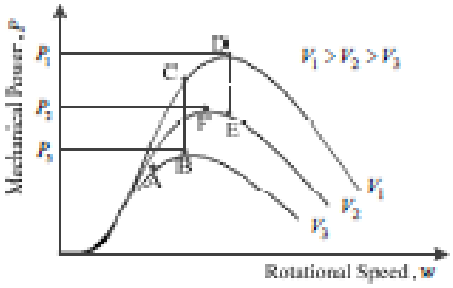

Fig. 5. Principle illustration of HCS control algorithm.

However, the step size of the conventional HCS algorithm is constant and it cannot change suitably as the environment changes. This paper presents a fuzzy logical control algorithm to determine the reference rotational speed which can realize variable step-size control as wind speed changes. As shown in Fig. 4, the input variables of fuzzy logical control algorithm are rotational speed w and mechanical power P. The reference rotational speed w_{ref} can be calculated through fuzzy logic rules. The proposed FLC algorithm is described in detail in Section 4.

3. Basic Principle of HCS Algorithm

The process of the conventional hill climbing searching algorithm used for the maximum power point tracking can be explained using Fig. 5. The basic principle of the HCS algorithm is: if the previous increment of rotational speed Δw results in an increase of mechanical power ΔP, the search of Δw continues in the same direction; otherwise, the search reverses its direction. The algorithm is described in detail as follows.

Assume that the wind turbine is operating at point A in the characteristic curve shown in Fig. 5. The wind turbine rotational speed is increased and the corresponding mechanical power is detected. If the power is increased compared with that in the earlier step, the search process is in the correct direction, and the wind turbine rotational speed is increased again. If the power is decreased compared with that in the earlier step, the search will be in the opposite direction. This process is continued until the powers slope becomes zero, indicating that the HCS algorithm succeeds to reach the maximum power point, which corresponds to point B.

If the wind speed changes from v_3 to v_1, the turbine operating-point will jump to point C from point B instantly. Then P–w slope is positive and the turbine rotational speed is increased. The slope is observed until it becomes zero. Then the wind turbine can track the maximum power point, i.e., it will operate at point D. Now if there is a decrease in wind speed from v_1 to v_2, the operating-point could eventually shift from point D to point F, depending on the same principle.

The flow chart of conventional HCS algorithm is illustrated in Fig. 6.

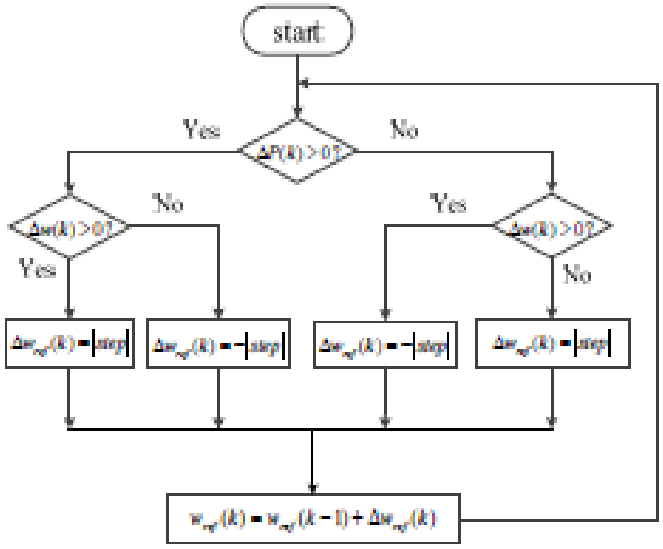

Fig. 6. Flow chart of HCS algorithm.

4. Introduction to FLC Algorithm

The conventional HCS algorithm implementation is simple and is independent of turbine characteristics[12], but there still exist issues like the selection of step size. A big step size can track the MPP fast but at the same time it can result in severe oscillations around the maximum power point. Reducing the perturbation step size can minimize the oscillations around MPP. However, a small step size can slow down the MPPT process especially when wind speed varies fast. To give a solution to this conflicting situation, a fuzzy logical control algorithm which has a variable perturbation step size is proposed in this paper. The FLC algorithm can effectively track the MPP fast and smoothly.

In the part of setting reference wind turbine rotational speed, the conventional HCS algorithm is replaced by the proposed FLC algorithm, which can realize variable step-size control. Through fuzzy control, the step size can be large when the operating point is far away from the MPP while the step size can become small when the operating point comes close to the MPP. Therefore, the FLC algorithm can dynamically change its step size, depending on the turbine operation condition.

The set of the fuzzy logical controller is described as follows: the input variables are $\Delta P(k)$ and $\Delta w(k)$, while the output variable is $\Delta w_{ref}(k)$. $\Delta P(k)$ and $\Delta w(k)$ can be obtained by

$$\Delta P(k) = P(k) - P(k-1) \tag{4}$$

$$\Delta w(k) = w(k) - w(k-1). \tag{5}$$

The member function of input variables of fuzzy logical controller with MATLAB is defined as follows: there are seven member functions of input variable $\Delta P(k)$: PB (positive big), PM (positive medium), PS (positive small), ZE (zero), NS (negative small), NM (negative medium), and NB (negative big), respectively, as shown in Fig. 7; the member functions of input variable $\Delta w(k)$ are P (positive), Z (zero), and N (negative), respectively.

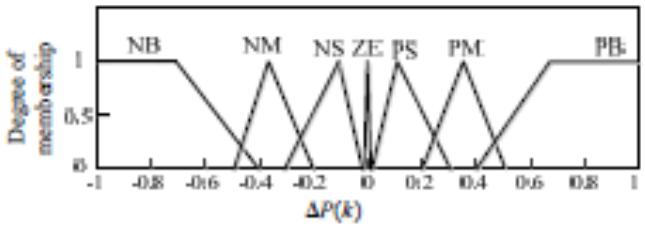

Fig. 7. Member functions of input variables $\Delta P(k)$.

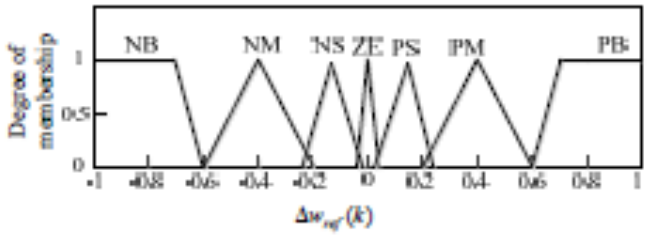

Fig. 8. Member functions of output variable $\Delta w_{ref}(k)$.

Table 2: Rules for the fuzzy logical controller

$\Delta w(k)$	$\Delta P(k)$						
	NB	NM	NS	ZE	PS	PM	PB
N	PB	PM	PS	NS	NS	NM	NB
Z	NM	NS	NS	ZE	PS	PS	PM
P	NB	NM	NS	PS	PS	PM	PB

The member functions of output variable $\Delta w_{ref}(k)$, which are similar to $\Delta P(k)$, are PB, PM, PS, ZE, NS, NM, NB, respectively. The detail information can be viewed from Fig. 8.

The relationship between turbine mechanical power and turbine rotational speed can be expressed in (6) to (8) depending on the P–w curve.

$$dP/dw > 0, \quad (w < w_{mpp}) \tag{6}$$

$$dP/dw = 0, \quad (w = w_{mpp}) \tag{7}$$

$$dP/dw < 0, \quad (w > w_{mpp}) \tag{8}$$

where w_{mpp} denotes the turbine rotational speed corresponding to the MPP.

The fuzzy logical control rules are based on the properties of wind turbine, as shown in Table 2. Then the newly setting reference rotational speed can be updated by

$$w_{ref}(k) = w_{ref}(k-1) + \Delta w_{ref}(k). \tag{9}$$

5. Case Studies

Case studies on the proposed MPPT control strategy and two conventional HCS algorithms with different size steps have been conducted to validate the proposed MPPT strategy.

Four performance indices for MPPT in a grid-connected wind generation system are also proposed in this paper. They are the wind energy captured by wind turbine, the maximum power point tracking time when the wind speed changes slowly, the fluctuation magnitude of real power during steady-state, and the wind energy captured by wind turbine when the wind speed changes fast.

Table 3: Results of case 1

MPPT strategy	Performance indices			
	T_1 (s)	T_2 (s)	ΔP (W)	W (J)
HCS (step size: 0.08 r/min)	0.095	0.086	0.6	6918
HCS (step size: 0.04 r/min)	0.124	0.169	0.2	6970.5
FLC (variable step-size)	**0.029**	**0.055**	**0.25**	**7010**

Table 4: Results of case 2

MPPT Strategy	Performance indices			
	T_1 (s)	T_2 (s)	ΔP (W)	W (J)
HCS (step size: 0.08 r/min)	0.115	0.088	0.5	6852
HCS (step size: 0.04 r/min)	0.224	0.173	0.15	6788.5
FLC (variable step size)	**0.073**	**0.057**	**0.25**	**6879**

Three cases are designed, and three MPPT control strategies are simulated in the environment of MATLAB/ Simulink respectively. The three MPPT control strategies are: a) HCS algorithm with a big perturbation step size, b) HCS algorithm with a small perturbation step size, and c) FLC algorithm with variable perturbation step size.

Initial conditions of the three cases are the same: the wind speed is 7 m/s, and the wind turbine operates at the optimal point, i.e. MPP.

5.1 Case 1

Case 1: Wind speed rises to 11 m/s linearly from 0.9 s to 1.0 s. The time used for tracking the MPP is T_1 after the first change of wind speed. From 1.9 s to 2.0 s, wind speed drops to 8 m/s linearly. The time used for tracking the MPP is T_2 after the second change of wind speed. The symbol ΔP denotes the fluctuation magnitude of real power during steady state, while the symbol W denotes the wind energy captured by the wind turbine from 0.9 s to 3.0 s. The result of case 1 is shown in Table 3.

5.2 Case 2

Case 2: The wind speed is up to 11 m/s in step change at time 1.0 s while down to 8 m/s in step change at time 2.0 s. The result of Case 2 is shown in Table 4. The symbols T_1, T_2, and ΔP of Table 4 have the same meaning as defined in Case 1. Here W denotes the wind energy captured by the wind turbine from 1.0 s to 3.0 s.

The output mechanical power curves (1.0 s to 1.5 s) of three different MPPT strategies after the first change of wind speed are given in Fig. 9 in order to compare the performance of the three MPPT strategies more easily. Fig. 10 shows variable perturbation step size of the proposed FLC algorithm. Through Fig. 10, it can be concluded that the step size controlled by the FLC algorithm can be changed suitably depending on the system operation condition. At time 1.073 s, the step size becomes small which can indicate the system operating point is very close to MPP or it is the MPP itself.

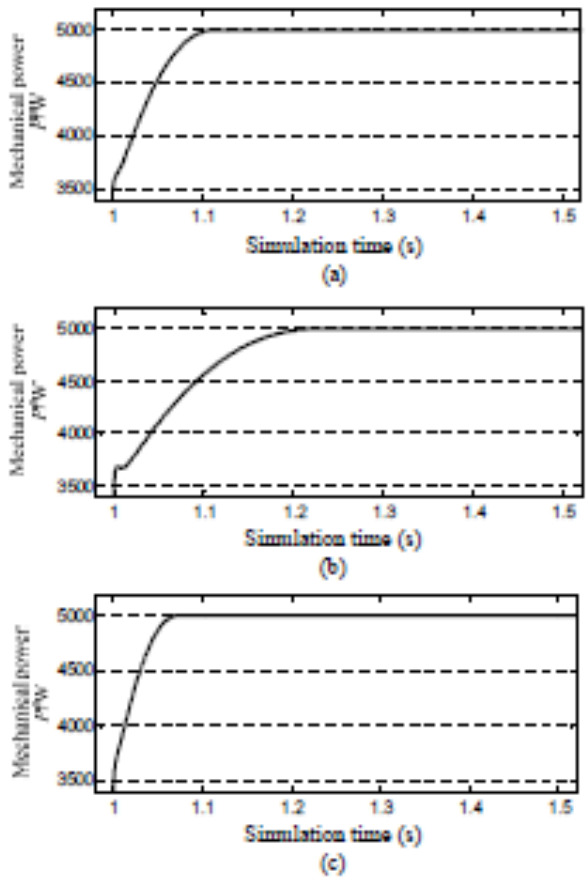

Fig. 9. Output power curves of three MPPT strategies: (a) HCS algorithm (step size: 0.08 r/min), (b) HCS algorithm (step size: 0.04 r/min), and (c) FLC algorithm (variable step size).

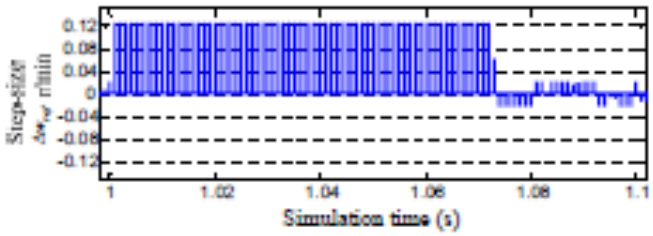

Fig. 10. Variable step size of FLC algorithm.

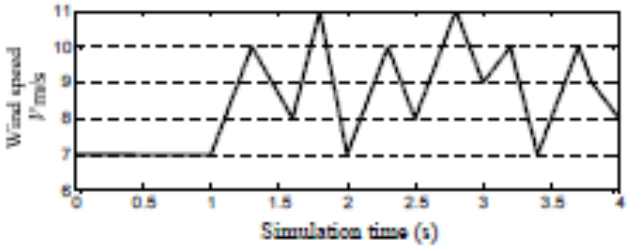

Fig. 11. Curve of wind speed.

Table 5: Results of case 3

MPPT Strategy	Case3: W (J)
HCS (step size: 0.08r/min)	7137.0
HCS (step size: 0.04r/min)	6867.5
FLC (variable step size)	7404.0

5.3 Case 3

Case 3: The wind speed changes fast and irregularly from 1.0s to 4.0s. The curve of wind speed is shown in Fig. 11. The wind energies captured by turbines from 1.0 s to 4.0 s through three different MPPT algorithms are listed in Table 5.

Through the above three cases, we can see that the system can always operate at its optimal points for a certain wind speed by using any of the three MPPT strategies. But the emphasis is when the wind speed changes, the FLC algorithm shows good performances than the conventional HCS algorithm no matter its step size is large or small. FLC algorithm can track the MPP much faster than the other two methods. At the same time, the fluctuation magnitude of real power of FLC algorithm is small during steady state. Case studies also show that the wind energy captured by FLC algorithm is the most among the three MPPT strategies both in the situation of wind speed changing slowly and in the situation of wind speed changing fiercely. All these results can validate that the proposed MPPT algorithm is highly efficient than the conventional HCS algorithms.

Generally speaking, compared with the conventional HCS control approaches, the proposed algorithm reflects significant advantages no matter in the aspect of tracking speed or in the aspect of the fluctuation magnitude of real power.

6. Conclusions

This paper proposes a fuzzy-logical-controller based MPPT strategy with variable step size, which can consider both tracking speed and steady-state efficiency. The proposed algorithm can change its perturbation step size dynamically depending on the change of wind speed, which enables the turbine to track the MPP quickly and smoothly.

Three MPPT algorithms and three cases were developed in this paper. The effectiveness of the proposed algorithm is verified in MATLAB/Simulink environment with SimPowerSystems and Fuzzy Logical Toolbox. The simulation results indicate that the proposed fuzzy-logical-controller based MPPT algorithm shows good performance. The wind turbine could track the optimum operating point swiftly using the proposed algorithm and the steady-state power would not fluctuate fiercely. In general, the proposed FLC MPPT algorithm can enhance the efficiency of wind turbine operation compared with the conventional HCS strategy.

References

[1] A. Soetedjo, A. Lomi, and W. P. Mulayanto, "Modeling of wind energy system with MPPT control," presented at Int. Conf. on Electrical Engineering and Informatics, Bandung, Jul. 2011.

[2] S. M. Barakati, "Modeling and controller design of a wind energy conversion system including a matrix converter," Ph.D. dissertation, University of Waterloo, Canada, 2008.

[3] E. Koutroulis and K. Kalaitzakis, "Design of a maximum power tracking system for wind-energy-conversion applications," *IEEE Trans. on Industrial Electronics*, vol. 53, no. 2, pp. 486–494, Apr., 2006.

[4] Q. Wang and L. Chang, "An intelligent maximum power extraction algorithm for inverter-based variable speed wind turbine systems," *IEEE Trans. Power Electronics*, vol. 19, no. 5, pp. 1242–1249, Sep. 2004.

[5] A. M. Eltamaly, "Modeling of wind turbine driving permanent magnet generator with maximum power point tracking system," *Journal of King Saud University, Engineering Science*, vol. 19, no. 2, pp. 223–237, 2007.

[6] C. Patsios, A. Chaniotis, M. Rotas, and A. G. Kladas, "A comparison of maximum-power-point tracking control techniques for low-power variable-speed wind generators," presented at 2009 8th Int. Symposium on Advanced Electromechanical Motion Systems & Electric Drives Joint Symposium, Lille, Jul. 2009.

[7] M. Shirazi, A. H. Viki, and O. Babayi, "A comparative study of maximum power extraction strategies in PMSG wind turbine system," in *Proc. of 2009 IEEE Electrical Power & Energy Conf.*, Montreal, 2009, pp. 1–6.

[8] M. A. Abdullah, A. H. M. Yatim, and C. W. Tan, "A study of maximum power point tracking algorithms for wind energy system," in *Proc. of 2011 IEEE First Conf. on Clean Energy and Technology*, Kuala Lumpur, 2011, pp. 321–326.

[9] S. M. Raza Kazmi, H. Goto, H.-J. Guo, and O. Ichinokura, "Review and critical analysis of the research papers published till date on maximum power point tracking in wind energy conversion system," in *Proc. of 2010 IEEE Energy Conversion Congress and Exposition*, Atlanta, 2010, pp. 4075–4082.

[10] R. Vepa, "Nonlinear, optimal control of a wind turbine generator," *IEEE Trans. Energy Conversion*, vol. 26, no. 2, pp. 468–478, Jun. 2011.

[11] M. Pucci and M. Cirrincione, "Neural MPPT control of wind generators with induction machines without speed sensors," *IEEE Trans. Industrial Electronics*, vol. 58, no. 1, pp. 37–47, Jan. 2011.

[12] S. Musunuri and H. L. Ginn III, "A fast maximum power extraction algorithm for wind energy systems," in *Proc. of 2011 IEEE Power and Energy Society General Meeting*, Detroit, Jul. 2011, pp. 1–7.

[13] M. G. Molina and P. E. Mercado, "A new control strategy of variable speed wind turbine generator for three-phase grid-connected applications," in *2008 IEEE/PES Transmission and Distribution Conf. and Exposition*, Chicago, Aug. 2008, pp. 1–8.

[14] V. Agarwal, R. K. Aggarwal, P. Patidar, and C. Patki, "A novel scheme for rapid tracking of maximum power point in wind energy generation systems," *IEEE Trans. Energy Conversion*, vol. 25, no. 1, pp. 228–236, Mar. 2010.

[15] R. Datta and V. T. Ranganathan, "A method of tracking the peak power points for a variable speed wind energy conversion system," *IEEE Trans. Energy Conversion*, vol. 18, no. 1, pp. 163–168, Mar. 2003.

[16] J. A. Baroudi, V. Dinavahi, and A. M. Knight, "A review of power converter topologies for wind generators," *Renewable Energy*, vol. 32, no. 14, pp. 2369–2385, Nov. 2007.

Xing-Peng Li was born in Shandong, China in 1989. He received the B.S. degree from the College of Electrical Engineering, Shandong University, Jinan, China in 2010. He is currently pursuing the master degree with the College of Electrical and Engineering, Zhejiang University, Hangzhou, China. His research interests include distributed generation, microgrid power energy management, and fault location.

Wen-Lu Fu was born in Jiangxi, China in 1992. She is currently pursuing the B.S. degree from the College of Electrical and Engineering, Zhejiang University, Hangzhou, China. Her research interests include distributed generation, and power management for microgrid with CHP.

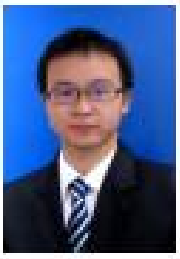

Qing-Jun Shi was born in Sichuan, China in 1987. He received his B.S. degree from Hefei University of Technology, Hefei, China in 2009 and the M.S. degree from Zhejiang University, Hangzhou, China in 2012, both from electrical engineering. Currently, he is with the Chongqing Changshou Power Supply Bureau, Chongqing, China. His research interests are distributed generation control, microgrid energy management, and coordination control.

Jian-Bing Xu was born in Shandong, China in 1989. He received his B.S. degree from the College of Electrical Engineering from Shandong University, Jinan, China in 2010. Currently, he is pursuing the master degree with the College of Electrical Engineering, Zhejiang University, Hangzhou, China. His research interest includes low voltage ride through performance of wind turbine generators.

Quan-Yuan Jiang was born in Hubei, China in 1975. He received his B.S., M.S., and Ph.D. degrees from the College of Electrical and Electronic Engineering, Huazhong University of Science & Technology, Wuhan, China in 1997, 2000, and 2003, respectively. Now, He works with Zhejiang University as a full professor. His research interests include power system stability, control and optimization.